Sub-millimetre Spectroscopy for AMSUTRAN. Part One: The Theoretical Basis

Emma Turner, Roger Saunders

Met Office, UK

This documentation was developed within the context of the EUMETSAT Satellite Application Facility on Numerical Weather Prediction (NWP SAF), under the Cooperation Agreement dated 7 December 2016, between EUMETSAT and the Met Office, UK, by one or more partners within the NWP SAF. The partners in the NWP SAF are the Met Office, ECMWF, DWD and Météo France.

Change record			
Version	Date	Author / changed by	Remarks
v0.1	14/10/2019	E. Turner	first draft
v0.2	17/10/2019	S. Fox	comments
v0.3	12/11/2019	R. Saunders	comments
v0.4	18/11/2019	P. Rayer	comments
v0.5	20/11/2019	P. Rayer	further comments
v1.0	10/12/2019	E. Turner	final draft

Abstract

A review of the recent research surrounding sub-millimetre spectroscopy is presented, with the aim of updating AMSUTRAN - the Met Office microwave line-by-line model used for generating RTTOV coefficients - motivated by the forthcoming ICI satellite instrument, which will uniquely sense the previously unexplored region between 200 and 664 GHz, requiring the underlying clear-sky characteristics to be improved and verified. The three principle molecules relevant to the spectral region: water vapour, ozone and oxygen, are analysed in turn.

Water vapour lines from three major line databases: HITRAN, AER and GEISA, are compared to the current MPM89 based configuration. They produce less overall absorption, which is surprising given the much greater number of lines included, and is traced to the 750 GHz cutoff applied. TOA brightness temperatures derived from AER 3.5 lines deviate from GEISA 2015 and two versions of HITRAN (2012 and 2016) by up to 0.3 K at higher frequencies due to an $\sim$5% increase in the values of air-broadened half-width for its 556.94 and 752.03 GHz lines. The range of results are compared for nine different parameterisations of the water vapour continuum, derived both in-situ and in the laboratory, and differences are found to be up to 3 K in window regions, though no single study was undertaken using the full range of spectral and atmospheric conditions that will be experienced by ICI. The inseparable nature of lines and continua is proven by an unconvincing attempt at re-regression, restricting the choice to those concurrently derived, and resulting in a recommendation of the MT-CKD 3.0 continuum with AER 3.5 lines. This is consistent with the infrared counterpart to AMSUTRAN operated by Météo-France. It is vital that ozone lines are added to AMSUTRAN beyond their current limit of 300 GHz as their omission would lead to errors of several kelvin. It was recently discovered that in 2004, HITRAN intensities originally derived from JPL values were inadvertently scaled down by $\sim$3–4% based on a study that centred on the infrared and have remained so ever since. A new line list provided directly by JPL, containing modified 2005 values, which is reduced in this analysis to a subset that matches the AER 'fast' database, leaving around 10% of the lines, is recommended for implementation. For oxygen, retaining the original MPM89 formulation for the most intense 44 lines is advised, primarily because of the complexity involved in incorporating a new line mixing parameterisation, which contains considerable uncertainty in itself. However, it would be wise to add minor oxygen lines from the HITRAN database beyond 200 GHz, as at least two are located close to ICI channels, but it is not thought that any of these lines peak high enough to be subject to Zeeman splitting.

The effect of incorporating all of these changes in ICI channels, with respect to the current spectroscopy, is up to $\sim$0.2 K due to the new water vapour parameters (an increase apart from the window channels), and up to $\sim$1.6 K due to the addition of ozone (a decrease which acts to cancel some of the changes due to water vapour). Validation against RTTOV reveals a slight improvement of statistics for the new spectroscopy, with verification against an independent profile set resulting in maximum biases of 0.05 $\pm$0.18 K. This combination will be taken forward for evaluation in the Met Office OPS system using the current suite of satellite instruments, and performances will be inferred via correlations between microwave and sub-millimetre frequencies (Part Two).

Contents

1 Introduction and Motivation

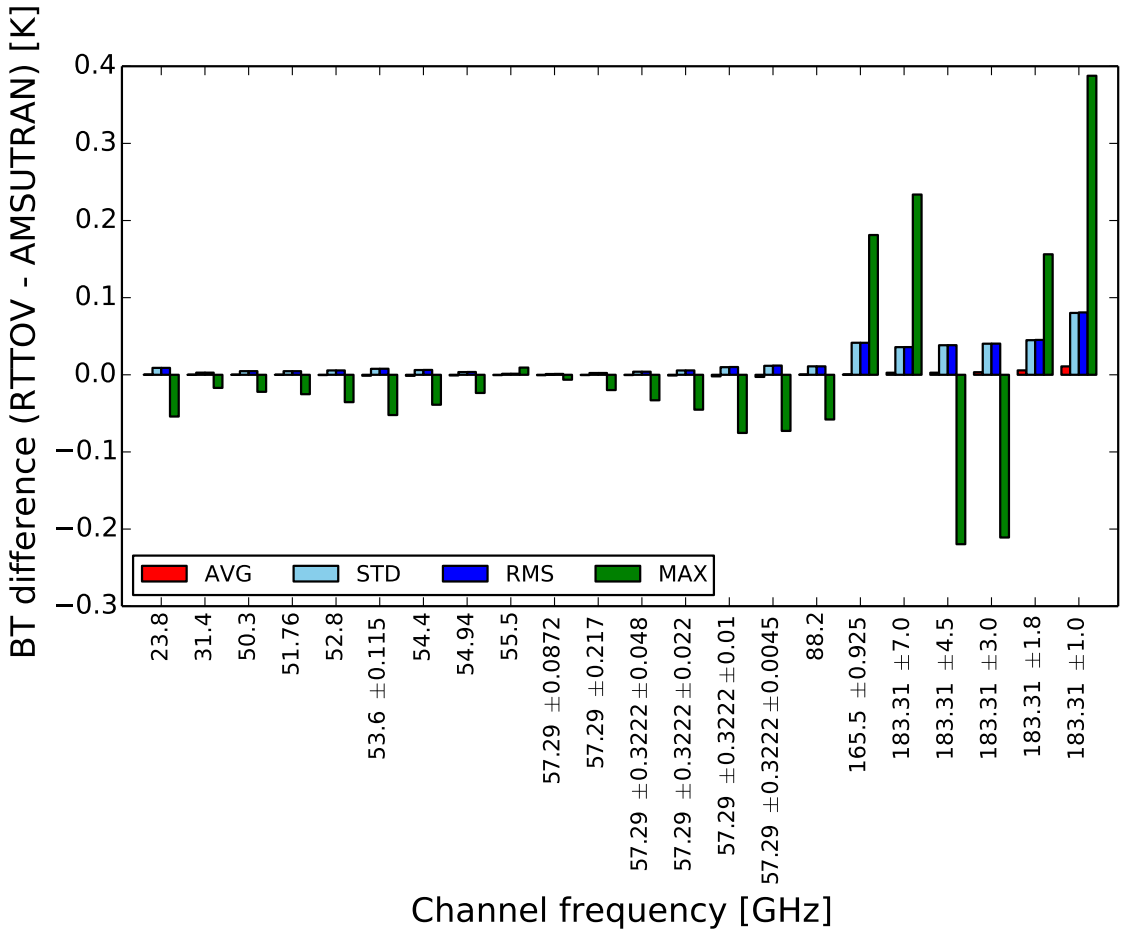

Figure 1: ATMS Validation statistics of RTTOV with respect to the line-by-line model (AMSUTRAN) over a set of 83 diverse profiles and 6 scan angles. Profiles are on 54 levels and make up the 'dependent' set, which is used to calculated all RTTOV coefficients. TOA brightness temperature differences are between ATMS channel integrated radiances from AMSUTRAN, and radiances calculated with RTTOV coefficients and predictors. The spectroscopic configuration is the 16 May 2016 control from section 2.1. Ozone is included up to 300 GHz in the mixed gases. AVG is the mean, STD is the standard deviation, RMS is the root mean squared error, and MAX is the maximum difference.

The skill of fast radiative transfer models, such as RTTOV (Radiative Transfer for TOVS) (Saunders et al., 2018), in reproducing the results of their underlying line-by-line codes is such that the difference between them is often negligible compared to the spread of results produced by alternate spectroscopic parameters and formulations. Top Of Atmosphere (TOA) brightness temperature differences between RTTOV and AMSUTRAN, the line-by-line code it is trained upon for the microwave, is shown in Figure 1 for the channels of the Advanced Technology Microwave Sounder (ATMS) (Kim et al., 2014) over a diverse set of 83 profiles (see Appendix A). For this instrument, mean differences do not exceed 0.01 ± 0.08 K (for channel 22 which is closest to the centre of the 183.31 GHz water vapour spectral line), but maximum differences can be much larger, up to 0.4 K in this case. Albeit small, this error in the fast parameterisation intrinsically places an upper limit on how effective improvements to the line-by-line code can be.

In an ideal world highly accurate theoretical descriptions and parameters would exist to render the difference between observations and simulations close to zero (assuming all other forms of biases, such as those directly from observations, are also non-existent). Even in a non-ideal world, such as the one we live in, some of the 'well-behaved' biases can be removed by bias correction methods, whether 'static' (Harris and Kelly, 2001) or variational (VarBC) (Cameron and Bell, 2016; Auligné et al., 2007), for use in NWP. However, these methods do not remove all biases as they depend on the accuracy of the NWP model, and furthermore such bias correction is not used in other scientific areas such as climate simulations. The problem is complicated by the fact that biases from different sources can compensate, meaning that if one element, such as the spectroscopy, is improved the overall result could potentially appear worse, but this should not be seen as an obstacle for progress. The value of improving upon the existing configuration depends upon the intended use, and as the primary purpose of AMSUTRAN is to produce channel averaged transmittances the motivating factor is satellite instrument requirements, remaining aware that much of the spectroscopic detail may be lost in the smoothing process.

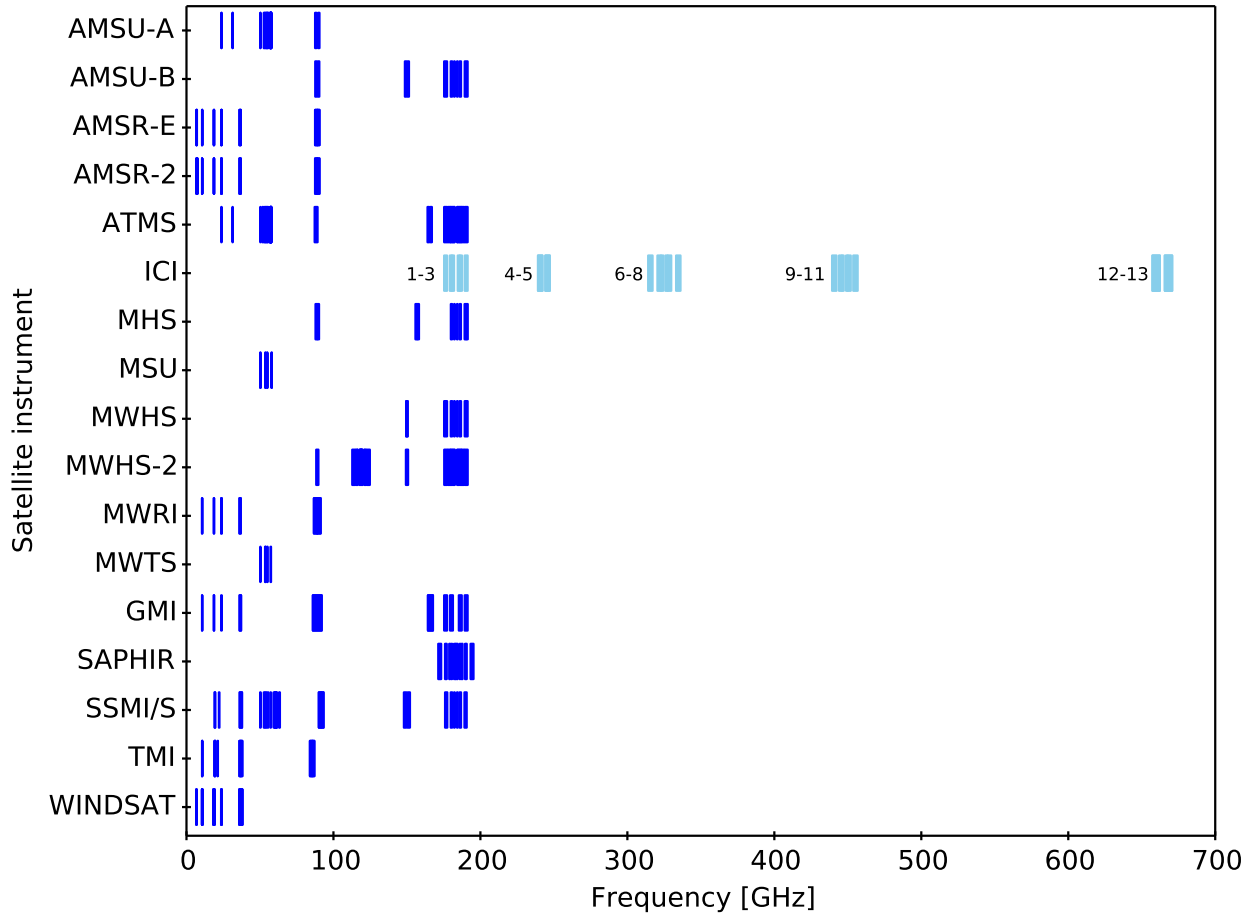

Figure 2: Spectral coverage of channels in the current suite of microwave satellite instruments currently assimilated in the Met Office NWP system. The forthcoming ICI instrument is highlighted in sky blue and its channels labeled.

1.1 Ice Cloud Imager (ICI)

Past improvements have focused on improving the region below 200 GHz as, apart from a handful of exceptions (see Frisk et al., 2003; Kikuchi et al., 2010; Froidevaux et al., 2006), this has traditionally been the upper spectral limit of atmospheric microwave radiometers (in contrast with those built for astronomical purposes, see Turner et al., 2016). However, this is due to change with the launch of the EUMETSAT Polar System - Second Generation (EPS-SG) B satellite, which is currently planned for 2022 and will carry the Ice Cloud Imager (ICI) as part of its payload, which will measure the 183–664 GHz range (Bergadá et al., 2016; Thomas et al., 2014). ICI channel characteristics are listed in Table 1 and the relative spectral coverage of ICI channels are shown in Figure 2 alongside the other microwave satellite instruments currently assimilated by the Met Office.

ICI will fill an observational gap by sensing different altitudes of cloud depending on frequency and estimate cloud ice water path and mean ice particle size (Wang et al., 2017). The treatment of clouds is handled by RTTOV but AMSUTRAN will provide the preliminary information for simulating the clear-sky, where particular attention must be paid to absorption by water vapour (H_2O) and oxygen (O_2) which dominates at sub-millimetre (sub-mm) wavelengths. This region has been untouched (apart from a modification of parameters that was applied to all oxygen lines, including the six above 200 GHz) since AMSUTRAN was first created in the mid 1990's.

Table 1: ICI channel definitions. Resolution specifies the grid of frequencies at which line-by-line calculations are made before averaging over the channel.

Channel number	Centre frequency (GHz)	Frequency offset (GHz)	Bandwidth (GHz)	Resolution (MHz)	Polarisation at 53.1° downwards view	Feature
1	183.31	±7.0	2.0	50	V	H_2O
2	183.31	±3.4	1.5	10	V	H_2O
3	183.31	±2.0	1.5	10	V	H_2O
4*	243.2	±2.5	3.0	100	V	window
5*	243.2	±2.5	3.0	100	H	window
6	325.15	±9.5	3.0	100	V	H_2O
7	325.15	±3.5	2.4	100	V	H_2O
8	325.15	±1.5	1.6	50	V	H_2O
9	448.0	±7.2	3.0	50	V	H_2O
10	448.0	±3.0	2.0	10	V	H_2O
11	448.0	±1.4	1.2	10	V	H_2O
12*	664.0	±4.2	5.0	100	V	window
13*	664.0	±4.2	5.0	100	H	window

* RTTOV defines channels with dual polarisation (V & H) as two channels in contrast to some other sources as they require separate simulation. Hence channel '4' at 243.2 GHz is here split into 4 and 5, channels 6-11 are shifted one channel higher with respect to other sources and the channel at 664.0 GHz is labeled 12 and 13.

1.2 Sub-millimetre spectrum

Figure 3 presents an overview of the microwave (<300 GHz) and sub-millimetre (>300 GHz) spectrum, using three different measures of radiative transfer typically associated with TOA geometry: transmittance, optical depth and brightness temperature. There is a considerable amount of variation in these quantities between atmospheric profiles (grey lines), but in general beyond 200 GHz the atmospheric transmittance from surface

to space falls off rapidly, due primarily to strong water vapour absorption from pure rotational transitions. Even with a dry atmosphere there will be little transmittance from the surface at frequencies higher than 500 GHz, however, there are two 'partial' windows centred around 650 and 850 GHz that transmit a small amount (around 10%) in very low humidity conditions. The five bands of ICI channels are strategically positioned to take advantage of the varying absorption of water vapour, with three bands straddling strong lines at 183.31, 325.15 and 448.00 GHz, and two bands centered over window regions at 243 and 664 GHz, the latter of which will be affected by strong neighbouring lines at 556.94 and 752.03, and both will be affected by the water vapour continuum.

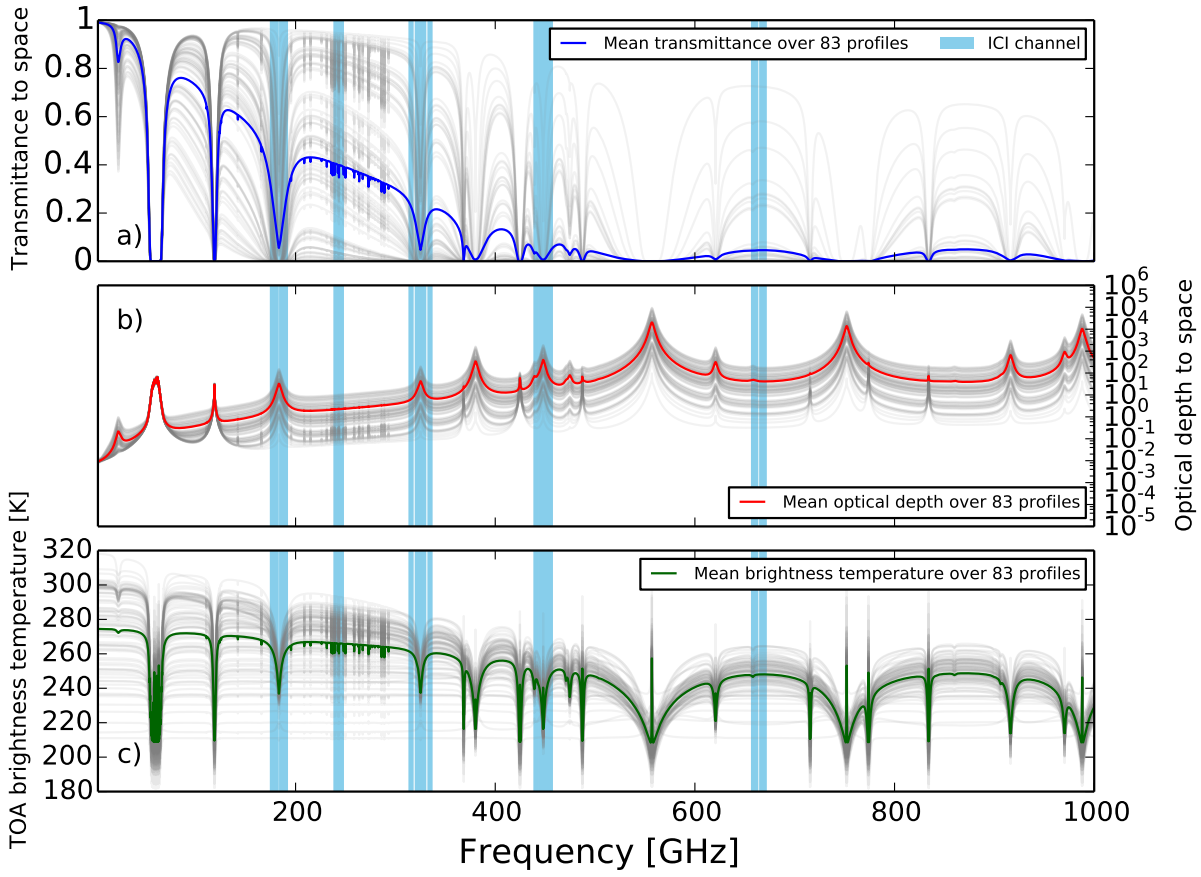

Figure 3: Total surface to space: a) transmittance, b) optical depth and, c) brightness temperature for 83 diverse atmospheric profiles (grey lines) and their mean (bold lines) simulated by AMSUTRAN using the current spectroscopic configuration described in section 2.1. The passbands of ICI channels are shaded in light blue.

This report considers the theoretical basis and also the practical applicability of implementing more up-to-date sub-millimetre, and by association, microwave, spectroscopy in AMSUTRAN, which may not be the same thing. The spectrum does not need to be simulated to the accuracy required by, for example, laser spectroscopy, which would necessitate great computational expense. Ultimately the configuration which gives results that consistently minimises statistical differences between simulated radiances and observations will be favoured

though this is beyond the scope of the current part of this report. Although there is a lack of satellite data covering the sub-millimetre region, observations with which to test the new configuration may be sought elsewhere, or performance inferred from spectroscopic parameterisations shared with the neighbouring microwave region. Recently Fox et al. (2017b) compared simulations made with a variety of spectroscopic combinations, including the AMSUTRAN configuration, available in the Atmospheric Radiative Transfer Simulator (ARTS) with measurements from the airborne instrument International SubMillimetre Airborne Radiometer (ISMAR) (Fox et al., 2017a), which is a demonstrator built to inform decisions on the design of ICI. A fairly recent review of the current state of sub-millimetre atmospheric observations from TOA and ground vantage points can be found in Turner et al. (2016).

What follows is an intensive review of the spectroscopy relevant to AMSUTRAN, comparing the current configuration with the results of more recent research, and making recommendations for what to use in the future. Whilst the primary focus are the spectral regions covered by ICI channels the whole of the microwave/sub-mm region up to 1000 GHz is likely to be affected. A subsequent study (Part Two) will test the new spectroscopy using impact trials in the Met Office NWP system by modifying RTTOV coefficients for current microwave satellite instruments.

2 AMSUTRAN

AMSUTRAN is a line-by-line transmittance model with TOA down-looking geometry that has been developed and maintained by the Met Office for over 20 years, with the primary purpose of producing a set of satellite instrument specific channel-averaged transmittances for a standardised range of atmospheric profiles. Some of AMSUTRAN's parameters were derived over 40 years ago and in the interim time more sophisticated spectroscopy has been developed, such as improved values for the line coupling coefficients and other line parameters, but there have only been a handful of modifications. Spectroscopy extends to 1000 GHz yet the focus of verification has remained below 200 GHz, being the domain of the current suite of space-borne atmospheric instruments (Figure 2). The code can also generate monochromatic output, which is primarily used for its own development. Full details of the current configuration of AMSUTRAN, and the subsequently re-organised structure, can be found in Turner et al. (2019). An overview of the key features are given below.

2.1 17 May 2016 Spectroscopic Configuration

The core of the code was originally based on the Millimeter Propogation Model (MPM) (Liebe and Layton, 1987) with line and continuum parameters from Liebe (1989). The molecules considered in MPM are water vapour, oxygen and nitrogen. Atmospheric attenuation of radiation is modeled as complex refractivity $N(\nu)$ where the imaginary part $N''(\nu)$ represents power attenuation in the form of extinction and is measured by the absorption co-efficient $\alpha(\nu)$ measured in dB/km:

$$\alpha(\nu) = 0.1820\nu N''(\nu) \tag{1}$$

which is calculated for a frequency ν.
The resonant part of $N''(\nu)$ is given by the sum of the product of line strengths S_i and line shapes $F_i(\nu)$ for each spectral line i in the frequency range considered:

$$N''(\nu) = \sum_{i=1}^{nlines} S_i F_i(\nu) \tag{2}$$

where $nlines$ equals 44 for oxygen and 30 for water vapour. The line shape function $F(\nu)$, is the Van Vleck-Weisskopf (Van Vleck and Weisskopf, 1945) as modified by Rosenkranz (1988) which is judged to be appropriate for use in the microwave where Doppler broadening is not significant. This is not strictly the case for the high peaking lines in the 60 GHz oxygen complex where there are Doppler and Zeeman effects and these are addressed in section 5. The lineshape function used in AMSUTRAN is:

$$F(\nu) = \frac{\nu}{\nu_i}\left[\frac{\gamma_i + \delta_i(\nu - \nu_i)}{(\nu - \nu_i)^2 + \gamma_i^2} + \frac{\gamma_i - \delta_i(\nu + \nu_i)}{(\nu + \nu_i)^2 + \gamma_i^2}\right] \tag{3}$$

where γ_i is the pressure broadened width and δ_i is the pressure induced interference. Equations for S_i and γ_i for each spectral line are given in terms of the atmospheric state (pressure and temperature) and predefined line parameters. For oxygen:

$$S_i = a_1 10^{-6} p\theta^3 exp[a_2(1-\theta)] \tag{4}$$

$$\gamma_i = a_3 10^{-3}(p\theta^{0.8-a_4} + 1.1e\theta) \tag{5}$$

$$\delta_i = (a_5 + a_6\theta)10^{-3}p\theta^{0.8} \tag{6}$$

where θ is the relative inverse temperature $\theta = 300/T$, p_{dry} and e are the partial pressures of dry air and water vapour respectively, in units of kPa. a_1 to a_6 are line specific constants that relate to, in turn; a_1, line strength in kHz/kPa; a_2, temperature dependence of line strength (dimensionless); a_3, air-broadened half width in MHz/kPa; a_4, temperature dependence of air-broadened half width (unit less); a_5 and a_6, parameters for line coupling in kPa^{-1}. For molecules where line mixing is not included, such as for water vapour and ozone, this function reduces to the original VVW:

$$F(\nu) = \frac{\nu}{\nu_i}\left[\frac{\gamma_i}{(\nu-\nu_i)^2+\gamma_i^2} + \frac{\gamma_i}{(\nu+\nu_i)^2+\gamma_i^2}\right] \tag{7}$$

For water vapour where $\delta_i = 0$:

$$S_i = b_1 e\theta^{3.5} exp[b_2(1-\theta)] \tag{8}$$

$$\gamma_i = b_3 10^{-3}(p\theta^{b_4} + b_5 e\theta^{b6}) \tag{9}$$

where b_1 to b_4 have the same definitions as the corresponding factors a_1 to a_4, b_5 is the ratio of self-broadened to air-broadened half width (unit less), and b_6 is the temperature dependence of the self-broadened half width (unit less). Non-resonant absorption is also modeled for three molecules, the oxygen and nitrogen constitute what is sometimes called the dry continua. However, the most important contribution comes from water vapour which is represented as below:

$$\alpha(\nu) = 0.1820\nu N''_{wv}(\nu) \tag{10}$$

$$N''_{wv}(\nu) = (b_s p_{wv} + b_f p_{dry})10^{-5}\nu p_{wv}\theta^3 \tag{11}$$

where b_s = $3.57\theta^{7.5}$ is the self continuum coefficient and b_f = 0.113 is the foreign continuum coefficient from Liebe and Layton (1987). The four traditionally defined continuum parameters are C_s^{300K} = 6.5 and C_f^{300K} = 0.206 in units of (dB/km)/(GHz^{2}hPa^2) (x10^{-8}), and coefficients of temperature dependence, n_s = 7.5 and n_f = 0.0. These parameters were determined from controlled laboratory experiments at 137.8 GHz where, over a range of temperatures, pressures and humidities, the continuum was derived as a residual of the total absorption and the theoretical line absorption.

Over time the following modifications have been made to the spectroscopic parameters based on more recent research.

- All oxygen line parameters, a_1 to a_6, have been replaced with those given in Table 5 of (Tretyakov et al., 2005). a_6 parameters are taken from Liebe et al. (1992).
- The oxygen continuum parameterisation has been replaced by that given in Liebe et al. (1992).
- The nitrogen continuum has been replaced by that given in Liebe et al. (1993).
- The b_3 value for the 22.235 GHz water vapour line has been replaced by the equivalent quantity in the HITRAN 2000 line database (Rothman et al., 2003), based on the endorsement by (Liljegren et al., 2005).

Table 2: Gaussian-cgs (HITRAN) and radio engineering (MPM) units for the relevant spectroscopic parameters for calculating the absorption co-efficient α. atm is the atmospheric unit, where 1 atm = 101.325 kPa. HITRAN catalogues do not include temperature exponents for self-broadened half-widths or define a model for calculating absorption coefficients.

Parameter	Symbol	HITRAN Units	MPM Units
Frequency	ν	cm^{-1}	GHz
Line intensity	S	cm^{-1}/(molecule/cm^2)	kHz
Lineshape	F	1/cm^{-1}	GHz^{-1}
Air-broadened half-width	γ_{air}, a_3, b_3	cm^{-1}/atm	MHz/kPa
Self-broadened half-width	$\gamma_{self}, b_5 \times b_3$	cm^{-1}/atm	MHz/kPa
Temperature exponent of air-broadened half-width	n_{air}, a_4, b_4	dimensionless	dimensionless
Temperature exponent of self-broadened half-width	n_{self}, b_6	–	dimensionless
Absorption coefficient	α	–	dB/km

- The b_3 and b_4 values for the 183.31 GHz water vapour line have been replaced by those derived by Payne et al. (2008). The paper presents two values for b_3; the one adopted by AMSUTRAN is theoretically derived from the complex implementation of the Robert-Bonamy (CRB) theory (Robert and Bonamy, 1979).
- The 35 most intense ozone lines below 300 GHz have been incorporated using line parameters from HITRAN 2000, necessitating a new routine for converting corresponding quantities in the line database to the radio engineering units appropriate to the MPM formulations (Table 2).

The above configuration and listed modifications constitute the spectroscopy that was ‘frozen’ on 17 May 2016 and has since remained un-changed. In the following comparisons this configuration is referred to as AMSUTRAN version 1 (v1).

3 Water vapour

In its broadest sense water vapour can be separated into resonant (spectral lines) and non-resonant (continuum) absorption. Non-resonant absorption can be separated further into self and foreign-broadened components. Figure 4 gives an overview of the range of spectral absorption by these different components, and the percentage each aspect contributes to the total (in the self and foreign cases this is relative to the total continuum). Most of the sub-millimetre spectrum is dominated by line absorption, with the exception of frequencies around 880 GHz where in some atmospheric conditions the continuum contributes up to 55% of the absorption. The ICI channels around 664 GHz, which is considered to be a window, are still on average 75% influenced by surrounding lines: specifically those at 556.94 and 752.03 GHz. Below 300 GHz the continuum dominates by up to 85% apart from in the two regions directly surrounding the 22.235 and 183.31 GHz lines. The relative contribution of foreign and self to the total continuum is spectrally invariant with an average ratio of 3:1, however, within the possible range of atmospheric profiles it could be as much as 100% foreign in very dry conditions, or up to 53% self when it is very humid. This partition will be specific to the MPM89 continuum used in this analysis and could be different for other models.

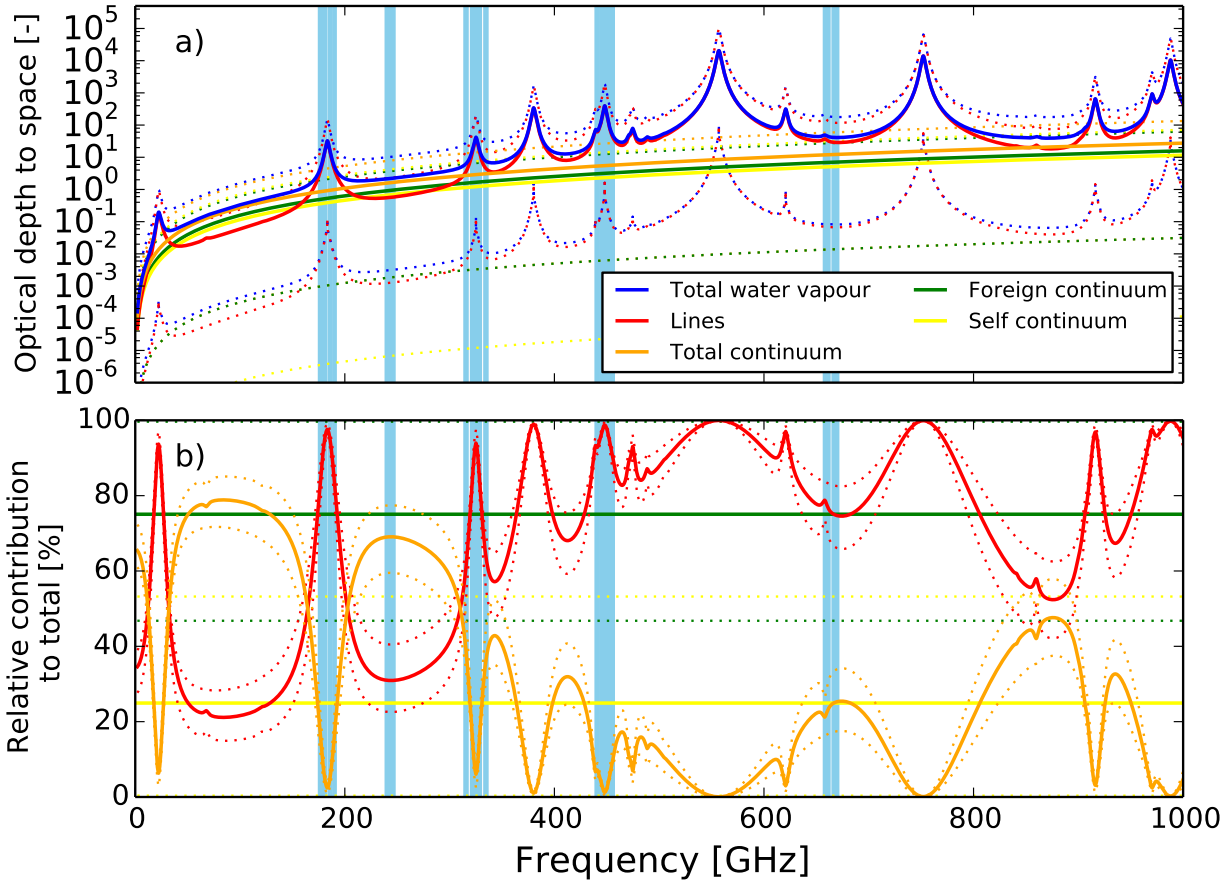

Figure 4: Resonant and non-resonant components of water vapour absorption. a) Surface-to-space optical depths. b) Percentage contribution of each component: lines and total continuum to total water vapour, or self and foreign continuum to total continuum. Bold lines show the mean of 83 diverse profiles and dotted lines of corresponding colour are the maximum and minimum values of that component at each frequency. The passbands of ICI channels are shaded in sky blue.

3.1 Water vapour lines

Figure 5a shows the location and intensity of the 30 water vapour lines included in AMSUTRAN v1. Intensities are converted from units of kHz to $cm^{-1}/[molecules/cm^2]$ for comparison with other larger line databases such as HITRAN. For the conversion algorithm see Appendix A of Turner et al. (2019). By comparison of the transmittance and optical depth with those in Figure 3 it is clear that most of the total absorption beyond 200 GHz is due to water vapour.

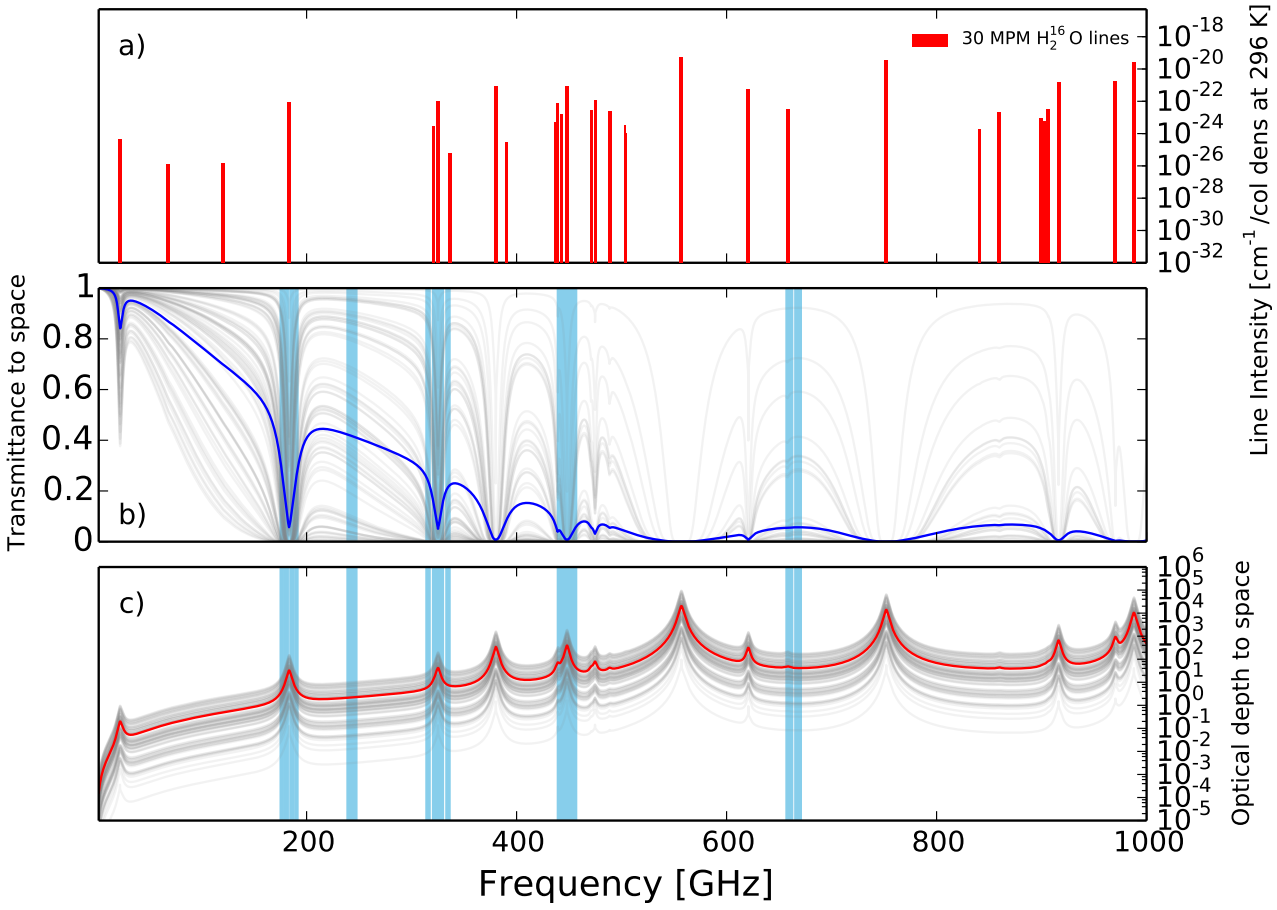

Figure 5: a) Location, log of intensity and to-scale halfwidth at 296 K of the 30 water vapour lines in the v1 configuration of AMSUTRAN. b) Surface-to-space transmittance and c) surface-to-space optical depth for water vapour only, for 83 diverse atmospheric profiles (grey lines) and their mean (bold line). The passbands of ICI channels are shaded in light blue.

Below 200 GHz many satellite instruments make use of the high intensity 183.31 GHz water vapour line, and to a lesser extent the 22.235 GHz line, hence why these were isolated for improvement in the prior version of AMSUTRAN. As water vapour heavily influences all ICI channels, it is pertinent to review all major sources of water vapour spectroscopy and potential alternatives.

An extensive compilation of spectral lines can readily be found in one of the continually evolving spectroscopic databases that are publically available. These are lists of parameters that are maintained and incrementally refined based on a variety of evaluation techniques and new data that has emerged since the last incarna-

tion. The most well-known example is possibly HITRAN (HIgh-resolution TRANsmission molecular absorption database), that has been re-released approximately every four years since the early 1970's (Gordon et al., 2017; McClatchey et al., 1973). Alternatively, Atmospheric and Environmental Research (AER) produces a line database based on a recent version of HITRAN with modifications to significant lines resulting from dedicated atmospheric closure experiments, e.g. Turner et al. (2012). The radiative transfer models developed at AER are used extensively by the atmospheric science community, including the counterpart to AMSUTRAN in the infrared, LBLRTM (Clough et al., 2005). Following a similar philosophy, the developers of the GEISA database (Gestion et Etude des Informations Spectroscopiques Atmosphriques: Management and Study of Atmospheric Spectroscopic Information) (Jacquinet-Husson et al., 2016) have recently produced a Spectroscopic Parameters And Radiative Transfer Evaluation (SPARTE) tool in order to screen candidate spectroscopy based on comparisons with a wide range of observations, such as radiosondes (Armante et al., 2016).

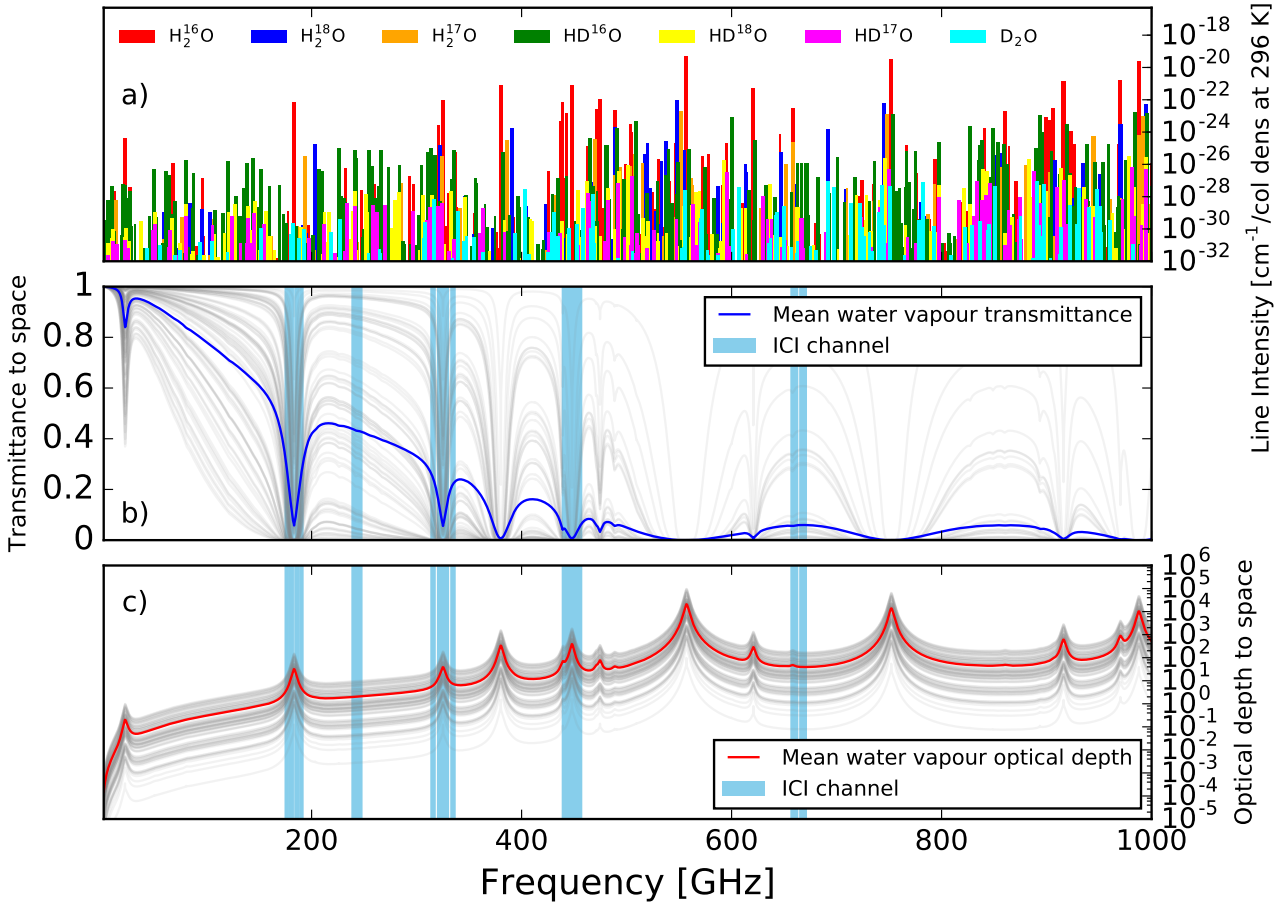

Figure 6: a) Location, log of intensity and to-scale halfwidth at 296 K of 1668 water vapour lines (between 1 and 1000 GHz) in the HITRAN 2016 database. b) Surface-to-space transmittance and c) surface-to-space optical depth, for 83 diverse atmospheric profiles (grey lines) and their mean (bold line) for water vapour lines only. The passbands of ICI channels are shaded in sky blue.

These databases contain numerous lines in the microwave region totaling hundreds, if not thousands, when all isotopologues are included. However, it is not expected that a complete replacement of all lines in AMSU-

TRAN would result in dramatic differences, as the latter represents the vast majority of resonant absorption. Furthermore, the continua of the corresponding species is empirically defined by the residual of these lines and hence accounts for the additional absorption. As the lines are inextricably tied to continua, it is therefore inappropriate to replace one without ensuring consistency with the other. This is particularly true with the lines in AMSUTRAN as the MPM formulation does not apply a frequency cutoff to the lines which is common in many line-by-line models, particularly those that include large line databases that are incrementally updated. Defining a cutoff prevents remote line alterations from perturbing local frequencies and a value of 750 GHz has commonly been adopted.

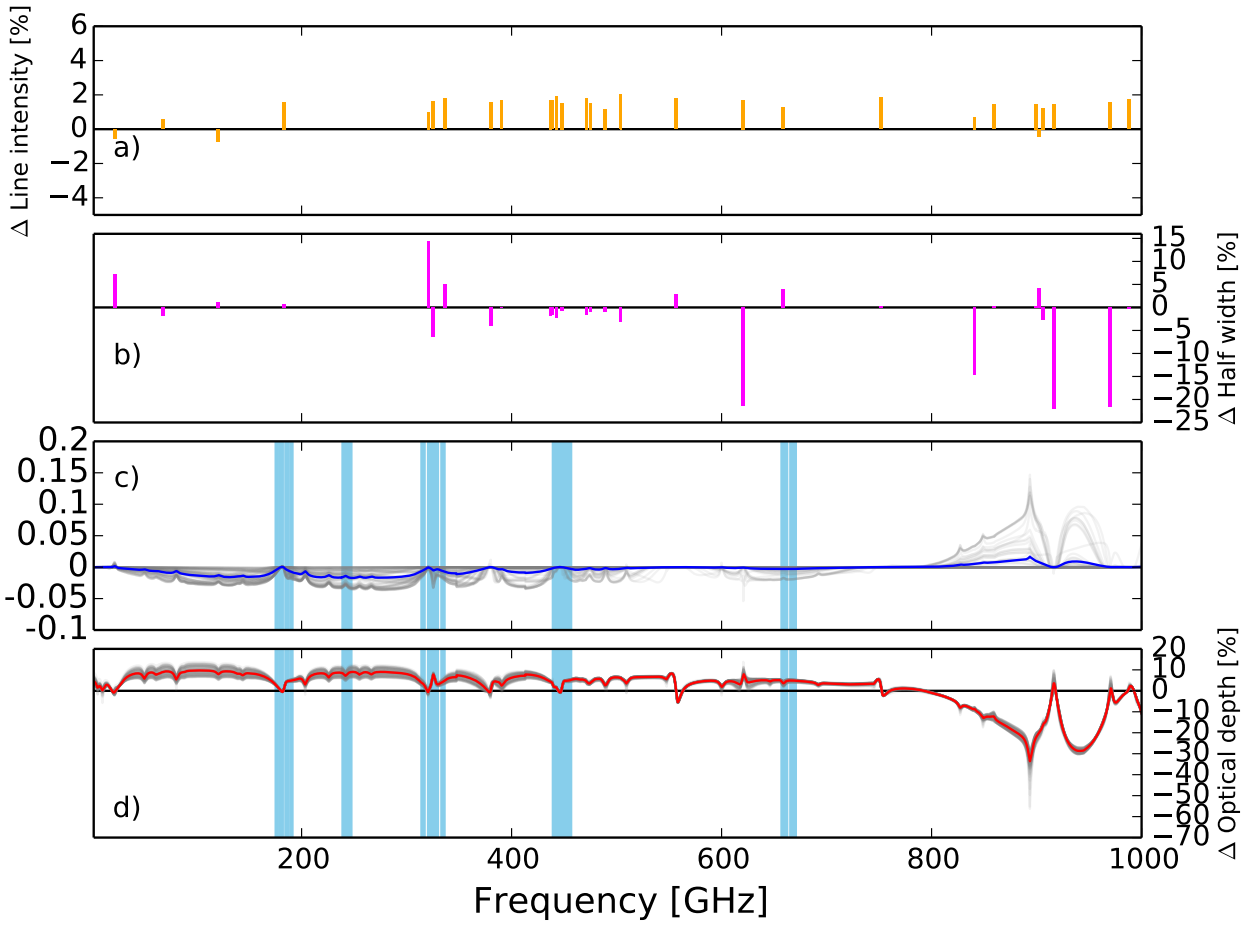

Figure 7: Differences between the AMSUTRAN v1 spectroscopic configuration of water vapour lines and those from the HITRAN 2016 database (AMSUTRAN - HITRAN). a) Percentage difference in line intensity for the 30 lines included in AMSUTRAN v1 at 296 K; b) percentage difference in total halfwidth; c) surface-to-space transmittance differences for 83 diverse atmospheric profiles (grey lines) and their mean (bold line) for water vapour only; d) percentage surface-to-space optical depth differences for 83 diverse atmospheric profiles (grey lines) and their mean (bold line) for water vapour lines only. The passbands of ICI channels are shaded in sky blue.

3.1.1 HITRAN 2016

Figure 6 is the equivalent of Figure 5 but the water vapour line parameters are from the HITRAN 2016 database. The difference between the two sets of lines are shown in Figure 7. For 27 of 30 lines, AMSUTRAN v1 intensities are between 0.5 and 2 % higher than HITRAN's, which aligns with the possibility they are in a sense representing absorption from all other lines not included. Only 10 of AMSUTRAN's lines have a greater halfwidth than HITRAN's, which somewhat compensates for the larger intensities. As the two quantities are difficult to separate when the line is measured this is not unexpected. The sharp spike in residual optical depth at 893 GHz is due to an absent water vapour line in the MPM models that appears to be significant at higher frequencies. Even though there are now 1668 lines from seven different isotopologues of water vapour included below 1000 GHz (2966 below 1750 GHz with influence; specified by the 750 GHz cutoff), the difference in the transmittance/optical depth is not significant as expected. In fact, for most of the spectrum there are higher transmittances and lower optical depths attributed to the HITRAN lines, which counter-intuitively results in less absorption overall for the larger line database.

In order to identify the dominant factors responsible for these differences, Figure 8 shows Figure 7d split by spectroscopic parameter. There are around 10 out of the 30 lines included in AMSUTRAN v1 whose parameters cause significant differences in the optical depth. Air-broadening parameters have far more of an effect than self-broadening and for most of the spectrum the broadening and intensity line shape parameters alone are responsible for less absorption when using HITRAN, particularly above 300 GHz. At frequencies below this it is clear that most of the excess optical depth is due to the absence of a cutoff, as when a threshold of 750 GHz is applied to AMSUTRAN there is a 10% difference away from line centres, which almost entirely closes the gap between the two. It is clear that the far wings of the few lines above 750 GHz are have a significant effect on optical depths in these window regions. The remaining lines in the HITRAN 2016 catalogue do not change the overall envelope of this perturbation, and they make little difference in ICI channels (apart from those at 664 GHz) indicating their less significant effect. The slightly different line centre frequencies and, more importantly, the pressure shift values included in the HITRAN catalogue create the oscillatory shaped difference with opposite signs either side of the major line centres which can have a large effect at individual frequencies but tends to average out over the width of a band.

3.1.2 AER 3.5

AER is an experimental research centre that adopts an empirical philosophy for validating atmospheric spectroscopy, based on the results of atmospheric campaigns such as RHUBC-II (Mlawer et al., 2019). The base line parameters for its custom catalogue are generally taken from HITRAN and key lines are adjusted. Ten water vapour lines have been modified in the 0–1000 GHz range for the update to version 3.5. The intensities of the 22.23, 183.31, 325.15 and 380.19 GHz lines have been reduced by 1–2% and the air-broadened half widths of the 22.23, 183.31, 556.93, 620.70, 752.03, 916.17 and 987.92 GHz lines have been increased by between 2-6 %. A subset of the database known as the 'fast' version is also available, which retains only those lines that contribute significantly to the total absorption, whilst reducing computational expense. There are 338 water vapour lines that contribute to the 0-1000 GHz region (located up to 1750 GHz) from this modified list

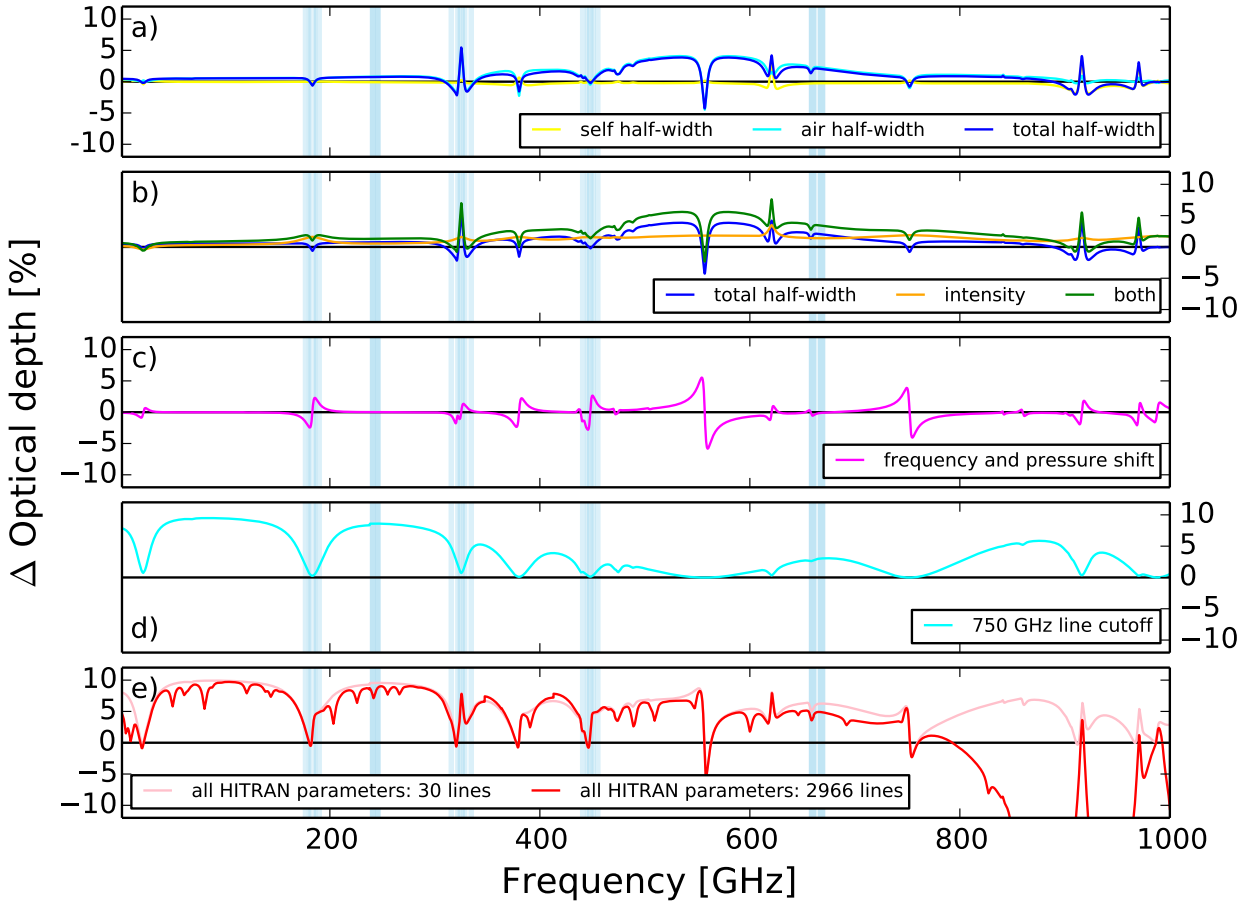

Figure 8: Figure 7d broken down by spectroscopic parameter, by substituting each one for the corresponding HITRAN values in turn for the just the 30 lines included in AMSUTRAN v1. a) Half-width parameters. b) Line intensity and half-width. c) Line centre frequency and pressure shift d) Applying a cutoff to absorption 750 GHz away from each line centre. e) All HITRAN parameters replacing the 30 lines in AMSUTRAN (pink line), and then including the total number of lines in the HITRAN database (2966 up to 1750 GHz: red line). Only the means of 83 profiles are shown for clarity.

(184 located between 1-1000 GHz), which around one fifth of the original 1600 from the parent HITRAN 2012 catalogue. Calculations confirm the difference between the two is negligible and hence the fast database is used in the subsequent simulations.

3.1.3 GEISA 2015

The GEISA spectroscopic database has been developed at the Laboratoire de Météorologie Dynamique (LMD) in France since the early 1970's, and there have been six releases, the latest of which is GEISA 2015 (Jacquinet-Husson et al., 2016). One way in which it differs from HITRAN in that it considers symmetry properties of isotopologues independently and uses radiative closure studies to evaluate data before accepting it into the database, though this technique has thus far been restricted to the infrared. GEISA 2015 contains updates to the water vapour line position and intensity parameters from 321 GHz onwards based on Coudert et al. (2014). Broadening parameters take the same values as those in the HITRAN 2016 catalogue. There

are 827 water vapour lines in the 1 – 1750 GHz region that have an influence on absorption within the 1 – 1000 GHz region, which itself contains 364 of these lines.

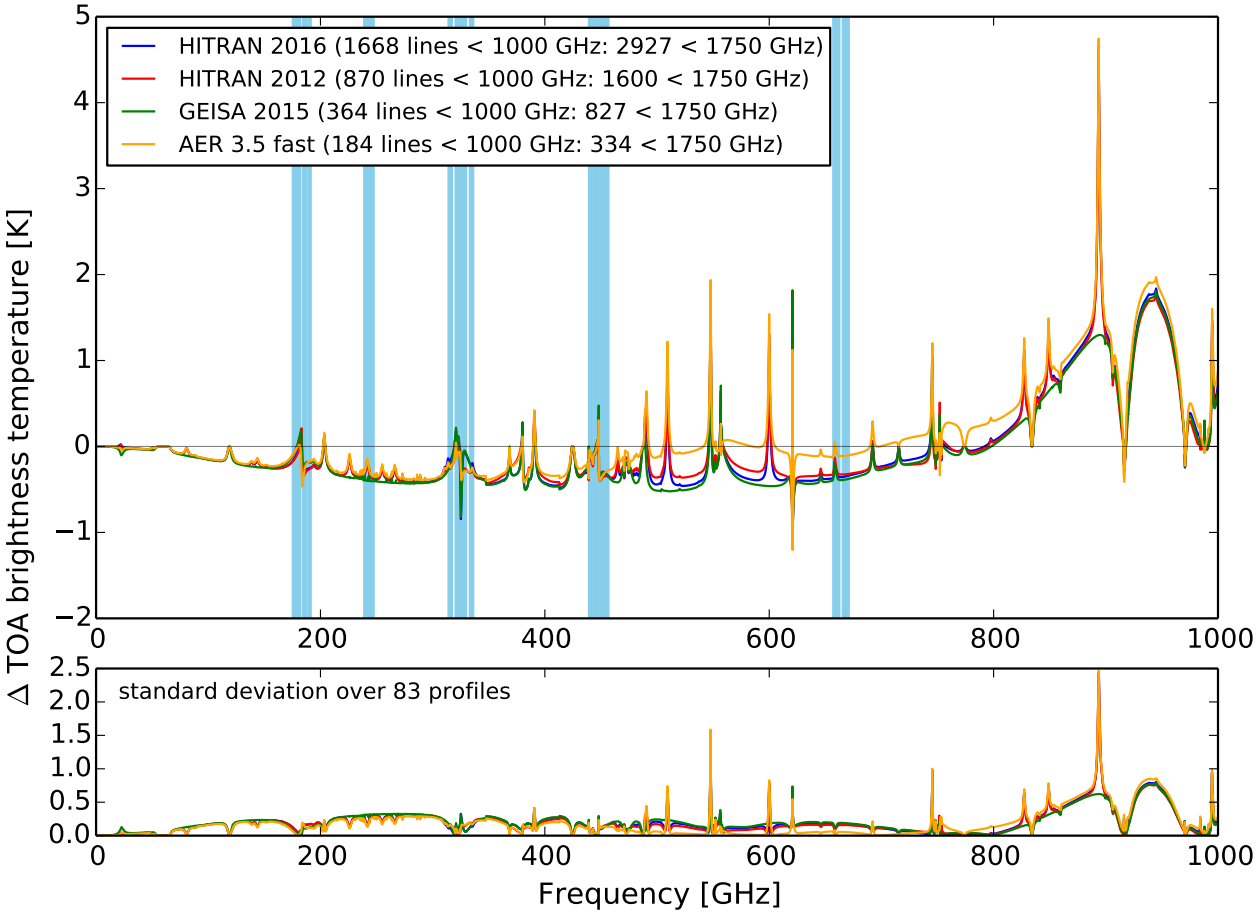

Figure 9: TOA brightness temperature differences between simulations using AMSUTRAN v1 (30 lines) as the baseline and larger line databases (AMSUTRAN - other). Only the mean (top) and standard deviation (bottom) over 83 profiles are shown. The MPM89 water vapour continuum is used for all simulations.

Table 3: Spectroscopic parameters of key water vapour lines for ICI. MPM89 values of S (intensity), γ_{air} (air-broadened half-width) and γ_{self} (self-broadened half-width) have been adjusted from their reference temperature of 300 K to 296 K for comparison with the other databases. Unless otherwise indicated AMSUTRAN v1 parameters take the same values as MPM89. n_{self} (temperature dependence of self-broadened half-width) is not specified in HITRAN, GEISA or AER so it is set to the same value as n_{air} (temperature dependence of air-broadened half-width). Sources for the data are listed in the footnotes.

Parameter	ν	S	γ_{air}	n_{air}	γ_{self}	n_{self}	δ
units	GHz	$\frac{cm^{-1}}{(molecules \times cm^2)}$	$\frac{cm^{-1}}{atm}$	-	$\frac{cm^{-1}}{atm}$	-	$\frac{cm^{-1}}{atm}$
183.31 GHz							
AMSUTRAN v1	183.310074	7.861e-23	0.0997[a†]	0.77[a†]	0.510	0.85	-
MPM89	183.310074	7.861e-23	0.0959	0.64	0.510	0.85	-
HITRAN 2016	183.310107[b]	7.736e-23[c]	0.0992[a]	0.76[a]	0.519[d]	0.76	-0.002689[a]
GEISA 2015	183.310197[j]	7.860e-23[j]	0.0992[a]	0.76[a]	0.519[d]	0.76	-0.002689[a]
HITRAN 2012	183.310107[b]	7.785e-23[m]	0.0992[a]	0.68[f]	0.519[d]	0.68	-0.0027
AER 3.5	183.310107[b]	7.691e-23[g]	0.1025[g]	0.71[g]	0.519[d]	0.71	-0.0027
325.15 GHz							
MPM89	325.152919	9.227e-23	0.0949	0.68	0.461	0.74	-
HITRAN 2016	325.153101[b]	9.077e-23[c]	0.1002[h]	0.74[i]	0.507[d]	0.74	-0.001679[i]
GEISA 2015	325.153161[j]	9.102e-23[j]	0.1002[h]	0.74[i]	0.508[d]	0.74	-0.001679[i]
HITRAN 2012	325.153101[b]	9.089e-23[e]	0.0944[k]	0.73[i]	0.507[d]	0.73	-0.002
AER 3.5	325.153101[b]	9.012e-23[g]	0.0944[k]	0.73	0.507[d]	0.73	-0.002
448.00 GHz							
MPM89	448.001075	8.767e-22	0.0897	0.66	0.434	0.67	-
HITRAN 2016	448.001185[b]	8.633e-22[c]	0.0888[f]	0.70[i]	0.467[l]	0.70	-0.002819[i]
GEISA 2015	448.001215[j]	8.640e-22[j]	0.0888[f]	0.70[i]	0.467[l]	0.70	-0.002819[i]
HITRAN 2012	448.001185[b]	8.625e-22[e]	0.0889[k]	0.65[f]	0.467[l]	0.65	-0.0031
AER 3.5	448.001185[b]	8.625e-22[e]	0.0889[k]	0.65[f]	0.467[l]	0.65	-0.0031
556.94 GHz							
MPM89	556.936002	5.333e-20	0.1095	0.69	0.452	1.00	-
HITRAN 2016	556.935991[b]	5.238e-20[c]	0.1039[d]	0.75[i]	0.486[l]	0.75	0.00652[i]
GEISA 2015	556.936021[j]	5.205e-20[j]	0.1039[d]	0.75[i]	0.487[l]	0.75	0.00652[i]
HITRAN 2012	556.935991[b]	5.238e-20[c]	0.1039[d]	0.75[i]	0.486[l]	0.75	0.00652[i]
AER 3.5	556.935991[b]	5.207e-20[g]	0.1103[g]	0.75[i]	0.487[l]	0.75	0.0068
752.03 GHz							
MPM89	752.033227	3.518e-20	0.1044	0.68	0.428	0.84	-
HITRAN 2016	752.033098[b]	3.454e-20[c]	0.1022[d]	0.77[i]	0.463[l]	0.77	0.00435[i]
GEISA 2015	752.033098[j]	3.431e-20[j]	0.1022[d]	0.77[i]	0.463[l]	0.77	0.00435[i]
HITRAN 2012	752.033098[b]	3.454e-20[c]	0.1022[d]	0.77[i]	0.463[l]	0.77	0.00435[i]
AER 3.5	752.033098[b]	3.433e-20[g]	0.1072[g]	0.77[i]	0.463[l]	0.77	0.0085

[a†] Payne et al. (2008) values from the complex implementation of the Robert-Bonamy (CRB) theory
[a] Payne et al. (2008) values from experimental constraints
[b] Lanquetin et al. (2001)
[c] Lodi et al. (2011)
[d] Gamache and Hartmann (2004)
[e] Martin et al. (2013)
[f] Birk and Wagner (2012)
[g] Mlawer et al. (2019)
[h] Ryadov and Furashov (1966)
[i] Gamache and Laraia (2009)
[j] Coudert et al. (2014)
[k] Jacquemart et al. (2005)
[l] Cazzoli et al. (2008)
[m] Coudert (1999)

3.1.4 Line comparison

Figure 9 presents the difference between these four sets of lines and the v1 configuration of AMSUTRAN calculated in terms of brightness temperature from a satellite vantage point, looking directly downwards. There can be large differences of up to 2 $\pm$1.5 K at line centre locations due to the different spectroscopic parameters (primarily intensity). The peak at 893 GHz is due to an absent line in the MPM model, and the GEISA database. As previously identified the oscillation of differences around lines such as those at 183.31 and 325.15 GHz lines is due to the pressure shift parameters in the larger line databases that are absent in the MPM model, which shift everything to lower frequencies. At frequencies below 400 GHz the differences between the larger databases are small away from line centres, however, at higher frequencies AER deviates away from the others. To examine further. the intra-database differences are enhanced in Figure 10 where HITRAN 2012 is now the baseline. The difference between AER and its base set of lines (HITRAN 2012) reaches 0.3 K, which is attributed primarily to the increased air-broadened half-widths of the 556.93, 620.70 and 752.03 GHz lines. As the parameters for these lines are identical in both versions of HITRAN this does not explain the 0.1 K difference between them, which is possibly due to extra far wing absorption from the near double amount of minor lines in HITRAN 2016. The negative spikes in the GEISA entry are due to some absent lines in the catalogue, which would have a noticeable effect on the 243 GHz ICI channels of potentially 0.3 K.

3.1.5 Water vapour lines summary

Line parameters from the aforementioned databases are compared in Table 3 for the five lines most important to ICI: 183.31, 325.15, 448.0 GHz, 556.94 and 752.03 GHz. The source of their values are referenced where possible.

For these five lines the following conclusions can be drawn:

- GEISA 2015 and HITRAN 2016 adopt the same parameter values, apart from GEISA uses Coudert et al. (2014) instead of Lodi et al. (2011) to derive intensity for frequencies above 300 GHz. The source of slightly different values of line location above 4 decimal places ($<$1 kHz) is unknown.
- AER 3.5 use HITRAN 2012 values apart from where empirical adjustments have been made as described in Mlawer et al. (2019), which is the case in four of the five lines excepting 448 GHz, resulting in differences of up to 0.3 K.
- Nearly all parameters were modified between HITRAN 2012 and HITRAN 2016, apart from the line shape parameters of the 556 and 752 GHz lines.
- The HITRAN 2016 air-broadened half-width (γ_{air}) for the 325 GHz line was modified from the HITRAN 2012 value to one derived from a study originating from 1966 (Ryadov and Furashov, 1966). This is a direct result of a new 'Diet' recently applied to HITRAN, where a theoretical value is accepted when there is no experimental one available (Gordon et al., 2007). The HITRAN 2012 value was based on the the Robert-Bonamy (CRB) theory, which contradicts the Diet so they reverted to the earlier value (personal communication, I. Gordon, Harvard CfA, 2019).

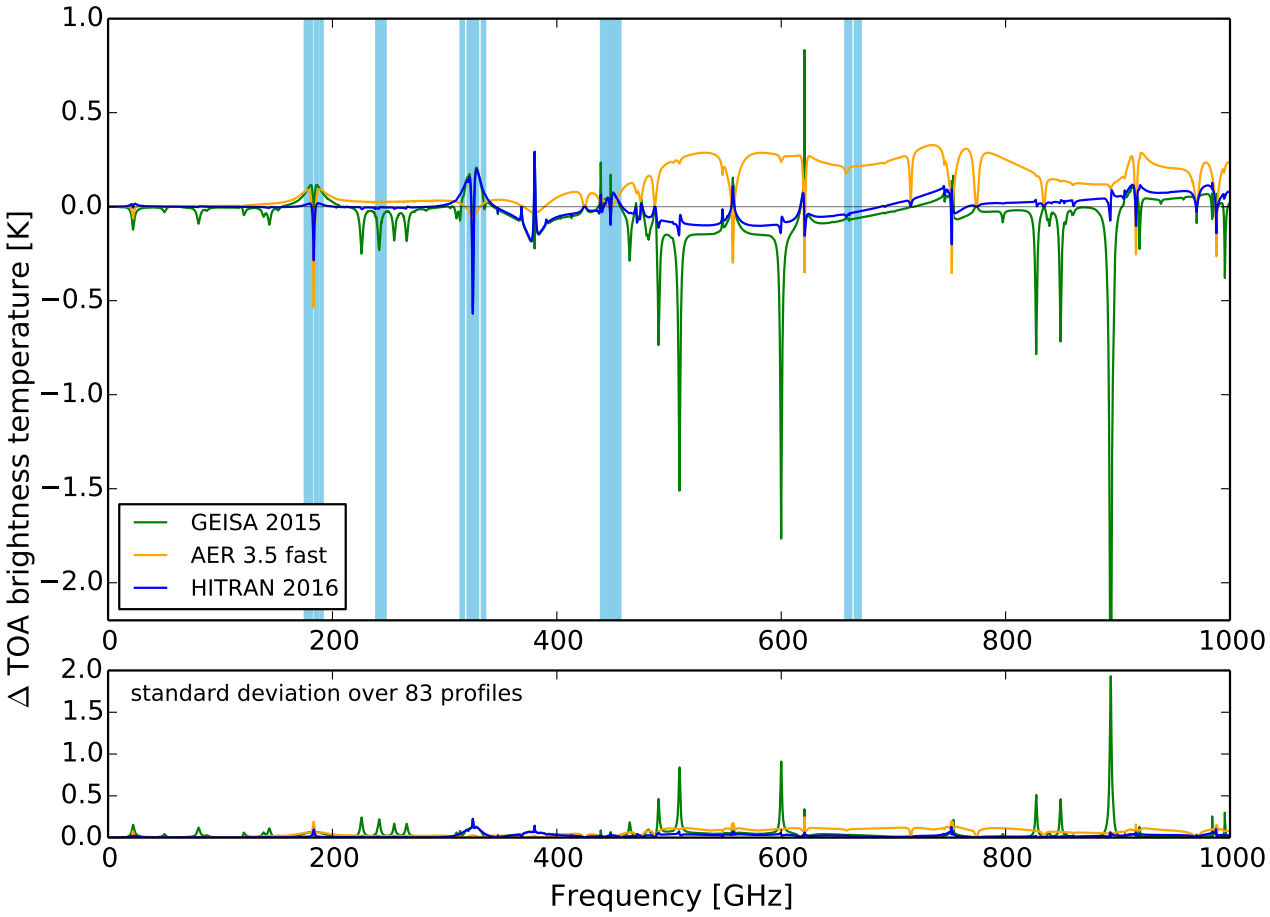

Figure 10: TOA brightness temperature differences between simulations using HITRAN 2012 as the baseline and HITRAN 2016, AER 3.5 'fast' lines and GEISA 2015. Only the mean (top) and standard deviation (bottom) over 83 profiles are shown. The MPM89 water vapour continuum is used for all simulations.

- The all-important 183.31 GHz line has undergone significant recent updates to all of its parameters:
  - HITRAN 2016 and GEISA 2015 have adopted the air-broadened parameters γ_{air}, n_{air} and δ derived empirically by Payne et al. (2008) specifically for the line in question.
  - AMSUTRAN v1 also uses γ_{air} and n_{air} values from Payne et al. (2008) but they are the alternate ones theoretically derived from the complex implementation of the CRB theory, hence the slightly different values.
  - Personal communication with Iouli Gordon (Harvard CfA) suggest the CRB theory contradicts the 'Diet' developed for HITRAN parameters.
  - AER has subsequently modified these parameters and the intensity based on measurements from the RHUBC-II campaign (Mlawer et al., 2019).
  - The intensity increased between GEISA 2011 and GEISA 2015 to a value nearly equivalent to the one used in AMSUTRAN v1, yet the source of the data is currently unknown.

3.2 Water vapour continuum

Despite various theories surrounding the far wings of lines (Clough et al., 1989), dimers and collision-induced absorption, there is still no complete physical based description for the continuum contribution of water vapour absorption that has been observed (Rubens and Aschkinass, 1898; Shine et al., 2012). Hence, models rely on parameters determined empirically with a focus on a spectral region of interest, which in the microwave and sub-mm is a relatively small number of studies. These tend to be either laboratory-based experiments or atmospheric campaigns that make in-situ measurements to quantify (or modify) all, or some of, the self and foreign continuum coefficients, C_s^T and C_f^T, and their temperature dependencies, n^s and n^f, defined in section 2.1.

In AMSUTRAN v1 the continuum follows the empirical derivation of Liebe and Layton (1987) without attributing a specific mechanism. The body of work dedicated to resolving the elusive water vapour dimer has made advances in recent years and it has been suggested that the largest fraction of continuum absorption at millimetre wavelengths and room temperatures can be attributed to dimers (Tretyakov et al., 2013). The dimer is a state associated with a pair of molecules, in this case water vapour monomers, $(H_2O)_2$, which can be either bound, quasi-bound or free-pairs (Serov et al., 2017). The latter two require evaluation of the dimer lifetime but the first in principle does not differ from any usual molecule and produces a characteristic spectrum. Serov et al. (2014) present resolved spectra for measured and ab initio derived dimers at warm temperatures between 280 – 322 K in the 188 – 258 GHz range, to which six almost equally spaced peaks every 12 GHz are attributed. Though interesting, this work is not considered as a candidate for inclusion in AMSUTRAN at this point due to the complexity of the models and the still-evolving nature of the theory.

3.2.1 Continuum models

When considering the best choice of continuum parameters it is important to consider whether the experimental conditions fit requirements from a satellite vantage point. Therefore, preference is given to studies which use atmospheric air as the broadening parameter to calculate the foreign component, those that sample the full range of temperatures characteristic of the atmosphere from the warm tropical surface to the very cold stratosphere, and those that measure at frequencies that overlap with ICI channels, whilst retaining applicability to the microwave. If the quadratic frequency dependence (Equation 11), which has been experimentally observed in other regions such as the microwave (Koshelev et al., 2011), remains valid in the sub-millimetre range considered, however, this relaxes the measurement frequency requirement.

A short-list of candidate studies that have been identified as potentially suitable are listed in Table 4 alongside their experimental conditions. The associated coefficient values are given in Table 5. Only those that can be practically used are included, which unfortunately disqualifies some of the more sub-millimetre focused studies which provide only a limited number of the parameters, as this would necessitate mixing seperately derived coefficients, which as shown in section 3.2.4 is not recommended. This applies to Pardo et al. (2001) and Slocum et al. (2013) who derive only a foreign continuum coefficient, or Yang et al. (2014) who provides both self and foreign but no temperature dependences. This is particularly problematic for the self component whose

Table 4: Water vapour continuum studies experimental conditions

Model	**Frequency** (GHz)	**Temperature** (K)	**Foreign** (species)	**Lines**	**Cutoff** (750 GHz)	**Ref T** (K)
MPM89	137.8	281–316	air (in lab)	MPM89	no	300
PWR98	many	many	air/N_2	PWR98	yes	300
Kuhn 2002	350.3	306–356	N_2	PWR98	yes	300
Podobedov 2008	300.0-2700.0	293–333	N_2	HITRAN 2004	yes	300
Turner 2009	150.0	atmosphere	atmosphere	MPM89	no	300
Koshelev 2011	107.7–143.3	261–328	N_2	PWR98 (adj)	yes	300
Wentz 2016	19–89	atmosphere	atmosphere	PWR98	yes	300
MT-CKD 2.4	0.0–infrared	atmosphere	atmosphere	AER 2.4	yes	296
MT-CKD 3.0	0.0–infrared	atmosphere	atmosphere	AER 3.5	yes	296

Table 5: Water vapour continuum parameters

Model	$\mathbf{C}_s^T$	$\mathbf{C}_f^T$	$\mathbf{n}_s$	$\mathbf{n}_f$
	(dB/km)/(GHz^{2}hPa^2) [x10^{-8}]		–	–
MPM89	6.5	0.206	7.50	0.0
PWR98	7.8	0.236	4.50	0.0
Kuhn 2002	9.11	0.268*	5.10	1.34
Podobedov 2008	4.00	0.206*	5.50	1.80
Turner 2009	5.2	0.225	7.5	0.0
Koshelev 2011	7.96	0.256*	5.24	0.91
Wentz 2016	$3.32\nu^{0.1}$	0.259	4.50	0.0
MT-CKD 2.4	varies every ∼300 GHz			
MT-CKD 3.0	varies every ∼300 GHz			

* adjustment from N_2 to air applied to published values: $G_{N_2}/G_{air} \simeq 1.12$

temperature dependence is strongly negetive - as the temperature increases the self continuum decreases - whereas for the foreign component has little-to-no dependence on temperature. Experiments whose results have subsequently been amalgamated into a further study such as Bauer et al. (1995, 1993) and Godon et al. (1992), which are included in Kuhn et al. (2002), are also omitted. Earlier versions of the MPM model (Liebe and Layton, 1987), are considered to be superceded by MPMP89 (Liebe, 1989). Similarly, MT-CKD (Mlawer-Tobin-Clough-Kneizys-Davies) and CKD models prior to MT-CKD 2.4 are also considered redundant. MPM93 (Liebe et al., 1993) is omitted because it is an outlier in terms of its 'pseudo-line' formulation and has been found to be in-consistent with various atmospheric observations (Turner et al., 2009; Hewison et al., 2006).

From a theoretical point of view there is no single study that fulfills all the specificied requirements for ICI. The existing MPM89 continuum has the advantage of using air as the broadening component, however the temperature range begins at 281 K, which exceeds most of the atmosphere, and the experiments were carried out at a single frequency of 137.8 GHz. The PWR98 model (Rosenkranz, 1998), combines the foreign component from MPM89 so is subject to the same caveats, and the self component from MPM93, which has the advantage of influence from several frequencies below 800 GHz but has been individually excluded for the aforementioned reasons. Both original components have been increased for use with a line cutoff of 750 GHz. Kuhn et al. (2002) and Podobedov et al. (2008) were both performed at sub-millimetre frequencies which is preferential, however, the minimum temperature was 293 K and they both used pure N_2 as the broadening component

which necessitates a manual adjustment in the foreign coefficient to make it applicable for atmospheric air. The dividing factor G_{N_2}/G_{air} is commonly taken to be 0.627/0.558 $\simeq$ 1.12, from the work of Liebe and Layton (1987), which was measured at 303 K and 138 GHz. As a simplication of a complex absorption calculation these results should be used with caution. Koshelev et al. (2011) also used N_2 as the foreign component and the frequencies were low (107.7–143.3 GHz), however, the temperature range was suitably wide (261–328 K). Turner et al. (2009) apply empirical constraints from a set of ground based radiometer measurements to modify a handful of absorption models including MPM89, which has the advantage of being measured in-situ, even though there was only a single measurement frequency of 150 GHz. Following a similer methodology Wentz and Meissner (2016) refine the PWR98 continuum model based on measurements taken by the Global Precipitation Measurement Microwave Imager (GMI) satellite instrument at five frequencies between 10.7 and 89.0 GHz, which is an ideal vantage point for the present study albeit measured at low frequencies.

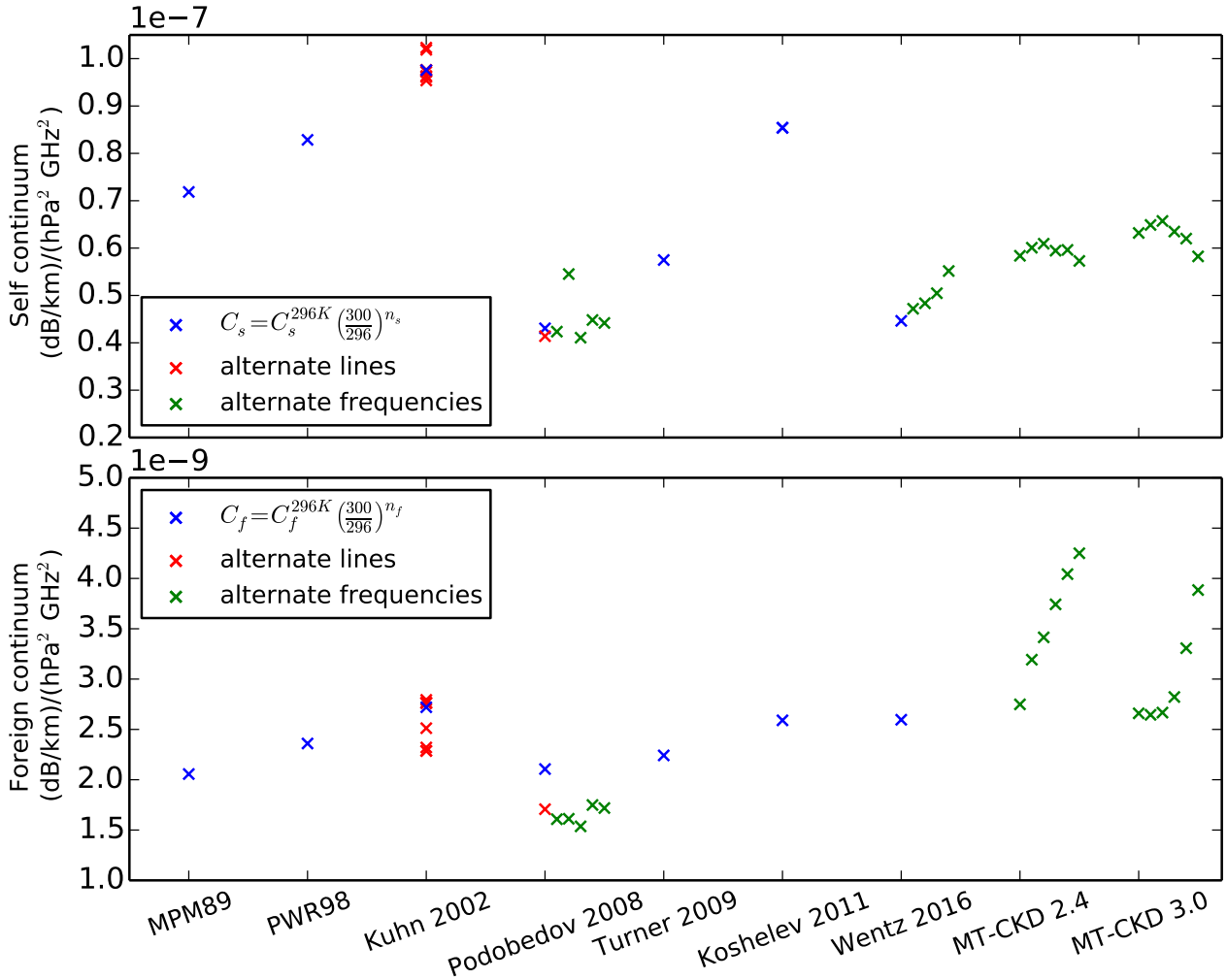

Figure 11: Continuum coefficients at a temperature of 296 K, adjusting all apart from MT-CKD from their nominal temperature of 300 K (blue crosses). Some studies provide values derived with an alternate set of underlying lines (red crosses) and some provide values derived at different frequencies (offset green crosses).

3.2.2 MT-CKD

MT-CKD (Mlawer-Tobin-Clough-Kneizys-Davies) is a more complex form of continuum model developed at AER alongside its line databases. It covers the entire atmospheric spectrum with a different set of continuum coefficients specificied every 10 cm^{-1} (300 GHz), which are interpolated to the required frequency (Mlawer et al., 2012). The model has evolved incrementally since its initial release in 2003 in response to various atmospheric campaigns. MT-CKD 2.4, released June 2009, was constrained in the microwave and sub-millimetre based on data from ARM ground-based radiometers that took measurements at 23.8, 31.4, 150 and 170 GHz (Payne et al., 2011). MT-CKD 3.0 was released in December 2016 with further adjustments made based on the RHUBC-II campaign (Mlawer et al., 2019). The update combined the results of radiative closure studies from six different instruments, including the SAO FTS (Smithsonian Astrophysical Observatory submillimeter Fourier Transform Spectrometer) that measures between 450–1800 GHz, and resulted in a reduction of the foreign continuum, and a slight increase in the self continuum in this region. Foreign coefficients at even lower frequencies were also lowered to allow a smooth continuation of the function, and the self continuum was increased slightly to maintain consistency with Payne et al. (2011).

3.2.3 Continuum and line comparison

As the continuum is defined as a residual between the total absorption and the lines, there is an inextricably link between the two. There is a great deal of variation in the lines used in each of the studies in Table 4, with four choosing a 'reduced' set (either 30 MPM or 15 PWR lines) and three using the HITRAN databases or derivatives thereof (AER). All apply a VVW lineshape apart from AER which uses the Van Vleck Huber (VVH) with a Voigt approximation, which in the low frequency limit approximates the VVW. A common source of confusion surrounding the VVW lineshape is the pre-factor which can either appear as quadratic (ν^2/ν_0^2), or linear (ν/ν_0) in frequency, which can lead to the erroneous assumption that there are two forms of the lineshape (i.e. see Yang et al., 2014). The different definitions actually arise from the interdependence between lineshape and line strength, where the latter can be defined with or without encompassed frequency factors. For example, in the MPM models the prefactor to the lineshape appears linear (Equation 3) as the definition of the absorption coefficient contains an explicit frequency factor ν (Equation 1) and a ν_i is embedded within the leading a_1 and b_1 coefficients. Alternatively, the HITRAN definition of line strength contains a ν_i^2 but no ν factors, hence the appropriate form of the VVW pre-factor is quadratic (e.g. Rosenkranz, 1998). Kuhn et al. (2002) and Podobedov et al. (2008) both use HITRAN line strengths (Kuhn et al. (2002) by way of the Rosenkranz (1998) formalism), however, the respective documentation for each study presents the VVW lineshape with a linear pre-factor so it is unclear whether the quadratic formalism was fully implemented. For the present work it is assumed that it was. All models use the customary line cut-off of $\sim$750 GHz (25 cm^{-1}), apart from MPM89 and its derivative Turner et al. (2009) which don't use one at all.

All experiments were performed at a reference temperature of 300 K apart from MT-CKD, which is performed at 296 K. Figure 11 compares the self and foreign coefficients at a temperature of 296 K which brings them all in line with MT-CKD as the temperature adjustment is less straight-forward for this model. Two of the stud-

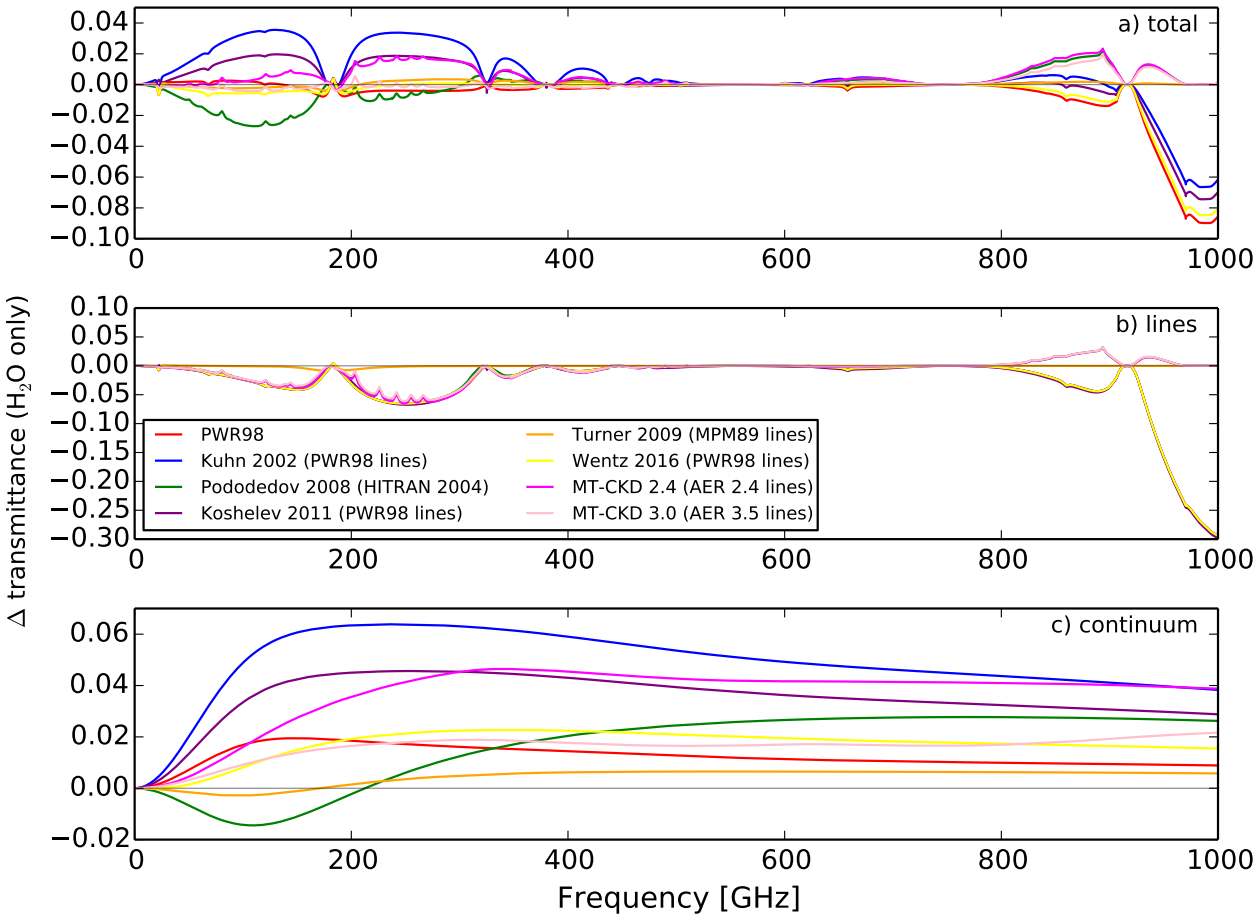

Figure 12: TOA transmittance differences between AMSUTRAN v1 and other water vapour absorption models a) total water vapour, b) water vapour lines and c) water vapour continuum. The mean of 83 diverse atmospheric profiles is shown.

ies derive the coefficients for more than one set of lines (Kuhn et al. 2002 and Podobedov et al. 2008), and two perform the experiment at more than one set of frequencies (Podobedov et al. 2008 and MT-CKD). The study-to-study difference tends to dominate over these intra-experiment variations, except perhaps for the foreign component of MT-CKD which shows a strong frequency dependence between 0–1500 GHz. However, there does not in general appear to be a strong correlation between frequency and continuum strength as two studies, Kuhn et al. (2002) and Podobedov et al. (2008), which both measure at high frequencies (>300 GHz) show quite extreme values with respect to one another.

Continuum transmittances produced by the different models are lower (equating to stronger absorption) than the MPM89 configuration currently used by AMSUTRAN v1 in all cases, apart from for Podobedov et al. (2008) and Turner et al. (2009) below 200 GHz (Figure 12c). Kuhn et al. (2002) absorbs most strongly, which is unsuprising given the coefficient values, and Turner et al. (2009) is most similer to AMSUTRAN v1 (<0.01), which is again unsuprising as it is a modified version of the MPM89 continuum. There is far less transmittance variation between different line databases than between those with or without a cutoff (Figure 12b), as previ-

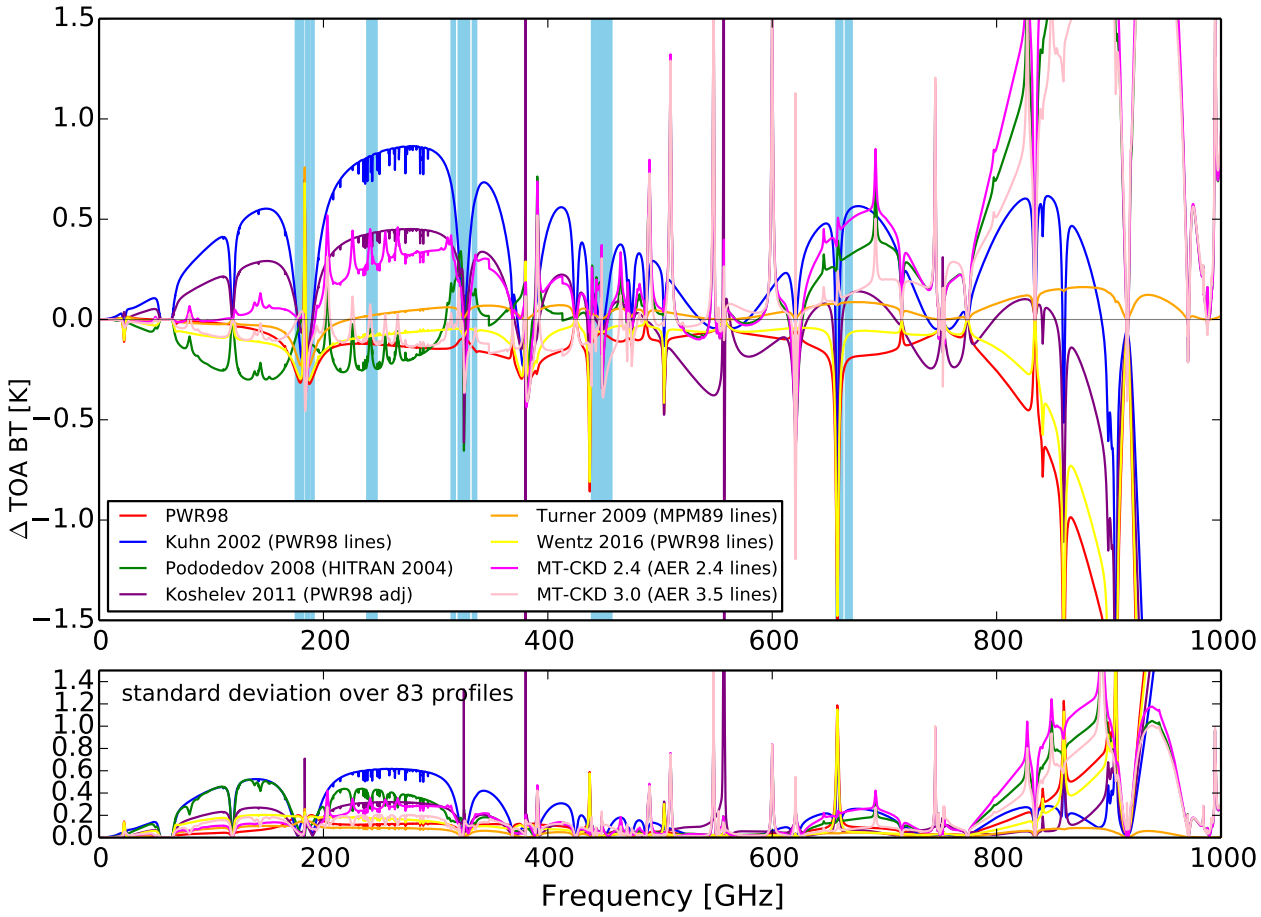

Figure 13: TOA brightness temperature differences between AMSUTRAN v1 and other water vapour absorption models a) total water vapour, b) water vapour lines and c) water vapour continuum. The mean (upper panel) of 83 diverse atmospheric profiles and the standard deviation (lower panel) are shown. Differences due to continuum model are enhanced at the expense of the full coverage due to lines.

ously identified in section 3.1.1. The transmittance differences in the lines and the continuum compensates in some cases such as PWR98, Wentz and Meissner (2016) and MT-CKD 3.0 to bring the overall differences to near zero (Figure 12a). In terms of TOA brightness temperatures these minimal differences correspond to a slight change of around 0.2 K with respect to AMSUTRAN v1 in window regions away from strong lines (Figure 13). Other models can reach up to 0.9 K lower (Kuhn et al., 2002). The MPM89 modification of Turner et al. (2009) produces a slight decrease ($<$0.1 K) however is only strictly applicable to the original MPM89 lines and the modified 22.235 GHz and the 183.31 GHz line width parameters produce local differences of around 0.7 K in the latter case. The Wentz and Meissner (2016) continuum, which is constrained by low frequency satellite observations, produces quite similer results to the latest MT-CKD. The highest frequency ICI channel would be strongly affected by the absence of the 658 GHz line in those studies that use the PWR98 lines, with a maximum error of about 1.5 K. There are some large differences around certain Koshelev et al. (2011) line centres, where the authors applied a pressure shift based on earlier measurements that wasn't included in the original line parameters specified by Rosenkranz (1998). Differences between the two versions of MT-CKD reach 0.5 K and the ICI channels around 248 and 664 GHz are affected by this. There are greater implications

at frequencies above 800 GHz but this is above the instruments range so not as critical.

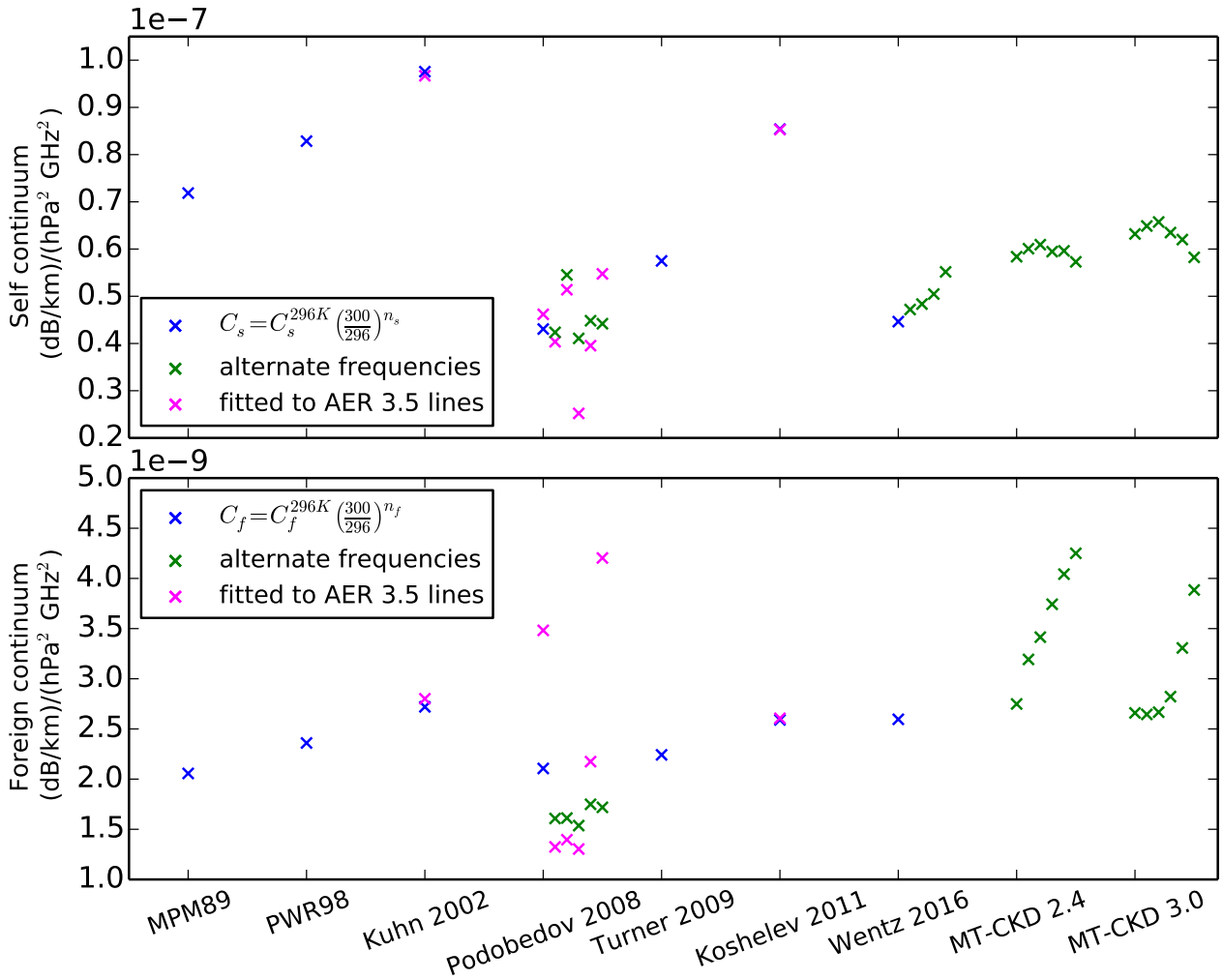

Figure 14: Continuum coefficients at a temperature of 296 K, which is an adjustment to all apart from MT-CKD from their nominal temperature of 300 K. Where possible, values have been re-regressed under the conditions of the original experiment to a common set of underlying lines, which is chosen to be AER 3.5 (magenta crosses). Some studies provide values derived at different frequencies (offset green crosses).

3.2.4 Re-regressing the continuum for alternate lines

In an attempt to remove the inconsistencies involved when comparing coefficients derived with different underlying lines a method of 're-regression' is employed to remove the influence of the original lines and replace them with a consistent set. In this case AER 3.5 lines are chosen as the baseline, in order to directly compare results with MT-CKD. This method was applied where the conditions of the original experiment were clearly documented and reproducable, which in practice was three of the studies. If this adjustment were sucessfull it is expected that the coefficient value would converge, and in particular move towards the range of values given by MT-CKD. This is not the case which indicates that the experiments are still not directly comparable, possibly due to the different temperatures, frequencies and their imperfect nature (including the nitrogen to

air adjustment). Re-regression for Koshelev et al. (2011) and Kuhn et al. (2002) has little modifying effect, as opposed to the results of Podobedov et al. (2008) even though the first two use PWR98 lines with a 750 GHz cut off for resonant absorption, which implies this is more similer to the AER lines than the HITRAN 2004 database with a cutoff. The results of this analysis re-enforce the recommendation that the continuum and the lines used to derive it should not be separated from each other.

3.2.5 Water vapour continuum summary

- There is no one continuum parameterisation that satisfies all of ICI's requirements from a theoretical point of view, in terms of appropriate experimental conditions.
- The manual adjustment of foreign broadening coefficients derived from laboratory experiments with pure N_2 for use in air employs a simple dividing factor of 1.12 which dominates uncertainties.
- Of the nine studies considered here, the continuum derived by Kuhn et al. (2002) absorbs most strongly across the 0–1000 GHz range and Podobedov et al. (2008) is the weakest below 200 GHz but strengthens at higher frequencies due to its strong foreign temperature exponent.
- The range of TOA brightness temperatures produced by these different combinations of lines and continua can be up to 0.9 $\pm$0.6 K in window regions.
- Based on the results of 're-regressing' certain continua for different lines it is advised that a particular continuum and its associated lines should not be separated.
- Continua derived using Rosenkranz (1998) lines are not recommended for use with ICI as (among others) the 658 GHz line is not included which has a non-negligible influence over channels 12 and 13.
- Turner et al. (2009) could be used to replace the MPM89 continuum as it essentially provides an update with real atmospheric constraints. However, as two of the lines in AMSUTRAN v1 (22.235 and 183.31 GHz) have been modified from the original Liebe (1989) values it is not strictly valid with the current line configuration, which is also true for the MPM89 continuum currently in use. Furthermore, section 3.1 recommends the use of a larger line database for ICI.
- Using the Wentz and Meissner (2016) continuum would necessitate reducing the number of water vapour lines even further to 15, however, it is re-assuring that results show that the only model constrained by satellite observations closely aligns with the latest version of MT-CKD.
- With these restrictions the only remaining option is the most recent MT-CKD (3.0) for use with AER 3.5 lines, which would have the added benefit of making the microwave consistent with the infrared. MT-CKD 3.0 does not differ greatly to the MPM89 continuum, and the total (lines plus continuum) absorption is similer to the control at ICI channels frequencies.
- MT-CKD is actively updated based on empirical constraints, and is likely to change by the end of 2019 at microwave/sub-millimetre frequencies (Eli Mlawer, personal communication April 2019).

4 Ozone

4.1 Ozone lines

Ozone is well known for its three fundamental vibration bands in the infrared at 9.066 (ν_1), 9.597 (ν_3) and 14.27 (ν_2) microns for the $^{16}O_3$ isotopologue, and ultraviolet absorption in the Harley, Huggins, Chappuis and Wulf bands (200 – >700 nm) which are utilised by satellite instruments to monitor ozone levels. The band of strong rotational transitions in the microwave and sub-millimetre has recieved less attention but it becomes more important with increasing frequency as transitions rise in intensity. Below 200 GHz the maximum impact on a satellite channel is around 0.3 K on certain 183 GHz channels (John and Buehler, 2004), however, greater contamination is likely at sub-mm frequencies. Ozone lines are sharp as they peak in the stratosphere so intensity is perhaps a more important parameter than those that describe broadening.

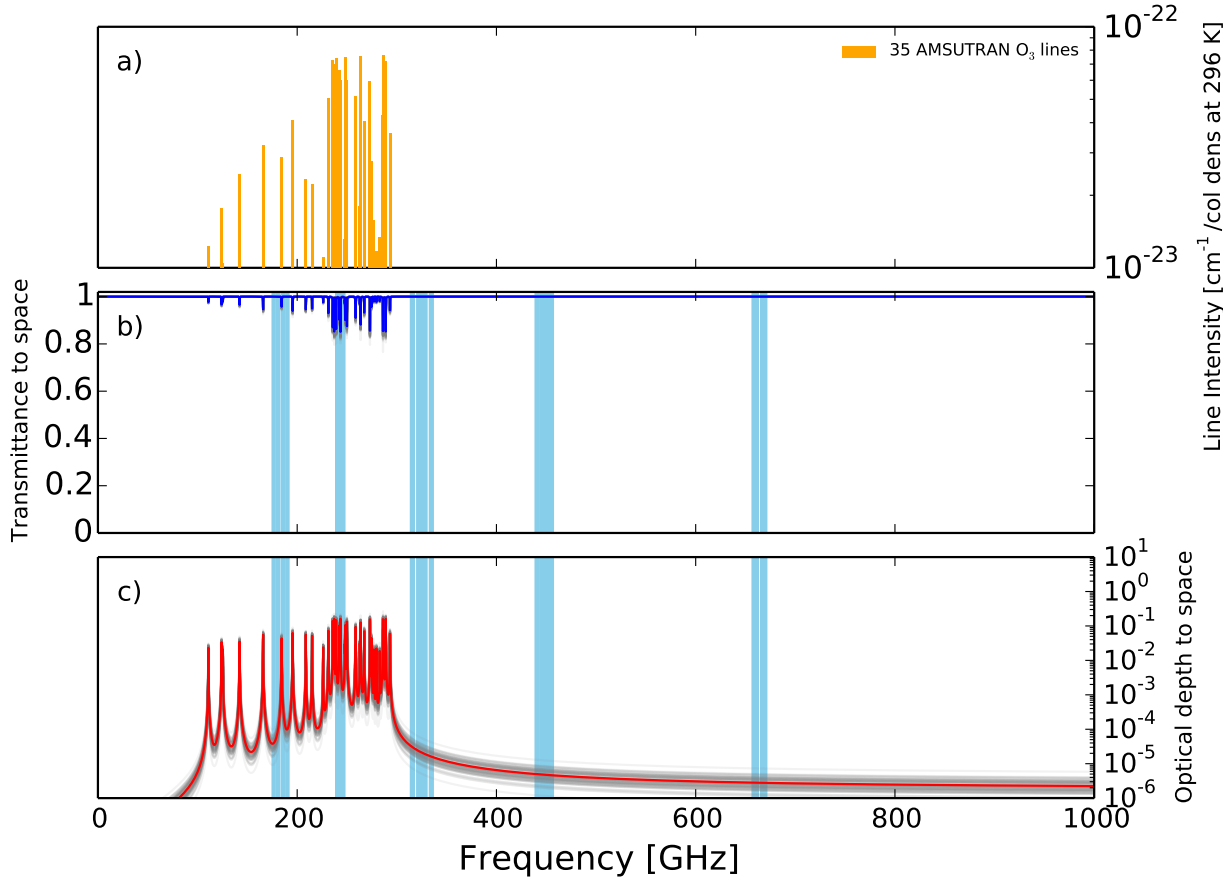

Figure 15: a) Location, log of intensity and to-scale halfwidth at 296 K of the 35 ozone lines in the v1 configuration of AMSUTRAN b) Surface-to-space transmittance for 83 diverse atmospheric profiles (grey lines) and their mean (blue line) for these ozone lines only. c) Surface-to-space optical depth, for 83 diverse atmospheric profiles (grey lines) and their mean (red line) for these ozone lines only. The passbands of ICI channels are shaded in sky blue.

In 2005 the 35 strongest ozone lines below 300 GHz were added to AMSUTRAN (Figure 15) in response to the potential bias reported by John and Buehler (2004), as an option to include their absorption with the

mixed gases. The line parameters are taken from the HITRAN 2000 catalogue (Rothman et al., 2003), and are adjusted to radio engineering units for consistency with the Liebe formulation for water vapour and oxygen. See Turner et al. (2019, Appendix A) for details of the conversion.

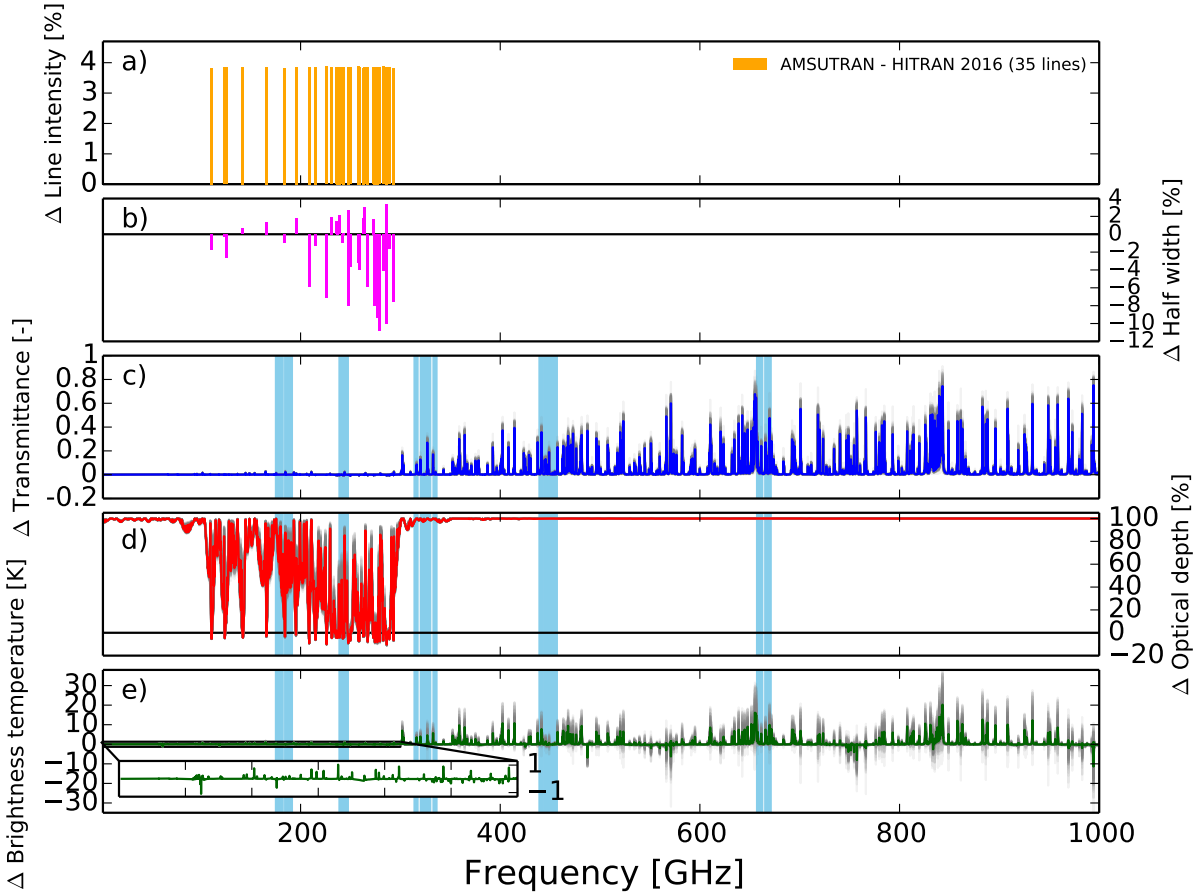

Figure 16: Differences between the v1 configuration of ozone in AMSUTRAN (35 lines below 300 GHz from HITRAN 2000) and the full HITRAN 2016 database. a) Percentage difference in line intensity at 296 K for the 35 lines included in AMSUTRAN v1. b) Percentage difference in total halfwidth. c) Ozone transmittance differences for 83 diverse atmospheric profiles (grey lines) and their mean (blue line). d) Percentage optical depth ozone differences for 83 diverse atmospheric profiles (grey lines) and their mean (red line). e) Brightness temperature differences for 83 diverse atmospheric profiles (grey lines) and their mean (green line) due to the change in ozone, zoomed in for the 0–300 GHz range. The passbands of ICI channels are shaded in sky blue.

4.1.1 HITRAN 2016

HITRAN line intensities for ozone were last modified in the microwave at the 2004 revision. Values for the principal isotopologue $^{16}O_3$ (99.2901 % abundance) and both isotopomers of the second most abundent isotopologue, $^{16}O^{16}O^{18}O$ (0.3982 % abundance) and $^{16}O^{18}O^{16}O$ (0.1991 % abundance), in the earlier 1996 revision were taken from Flaud et al. (1990b) but were scaled downwards in the 2004 version by dividing by 1.04 in line with the findings of Flaud et al. (2003). The validity of this scaling has recently been called into question by Birk et al. (2019) as the initial study centred on the infrared but the scaling was applied to all

wavelengths. Intensities for the less abundent remaining isotopologue $^{16}O^{16}O^{17}O/^{16}O^{17}O^{16}O$ are unchanged from the values given by Pickett et al. (1998).

The majority of air-broadened half-widths (γ_{air}) for rotational ozone in HITRAN 2016 are derived either from Flaud et al. (1990a) with polynomial expressions for J" scaled by 1.05 (2008, I.E. Gordon, private communication), or from Wagner et al. (2002) using values originally obtained for the ν_1/ν_2 or ν_3 bands. The temperature dependences of γ_{air} are either also from Wagner et al. (2002) or take the mean value of Gamache (1985). All values for self-broadened half width (γ_{self}) are based on the method of Smith (2001) described in Rothman et al. (2005) which have been subsequently modified (2004, M.A.H. Smith, NASA Langley Research Center, private communication).

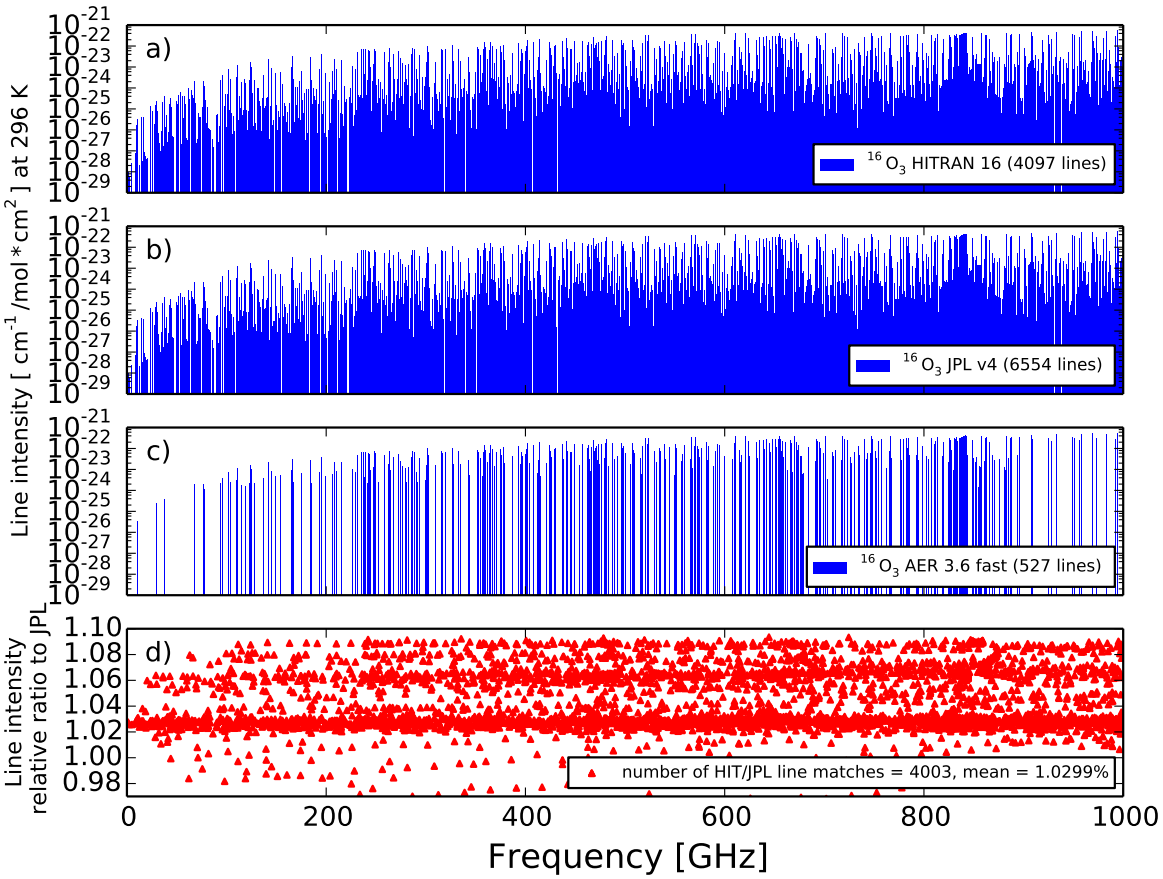

Figure 17: Line intensities for the principal isotopologue of ozone, $^{16}O_3$, provided in: a) HITRAN 2016, b) JPL version 4 (converted to HITRAN units and adjusted for partition function and temperature) and c) AER 'fast' lines. d) The relative intensity difference between HITRAN 2016 and JPL intensities for corresponding lines.

Figure 16 shows the differences between the 35 lines in AMSUTRAN v1 and those from the HITRAN 16 ozone catalogue across the whole spectral region, hence frequencies above 300 GHz solely display the effect of adding ozone where previously there was none. As the HITRAN 2000 lines predate the aforementioned

line intensity scaling the 4% reduction is apparent between versions (16a), whereas halfwidths have mostly increased in the later HITRAN by up to 11%, with contributions from both foreign and self-broadening components (16b). To improve the sub-mm it is obvious that ozone needs to be included beyond 300 GHz as leaving it out would result in errors of up to 40 K at individual frequencies and in particular the 664 GHz channels of ICI would be subject to significant error (16e).

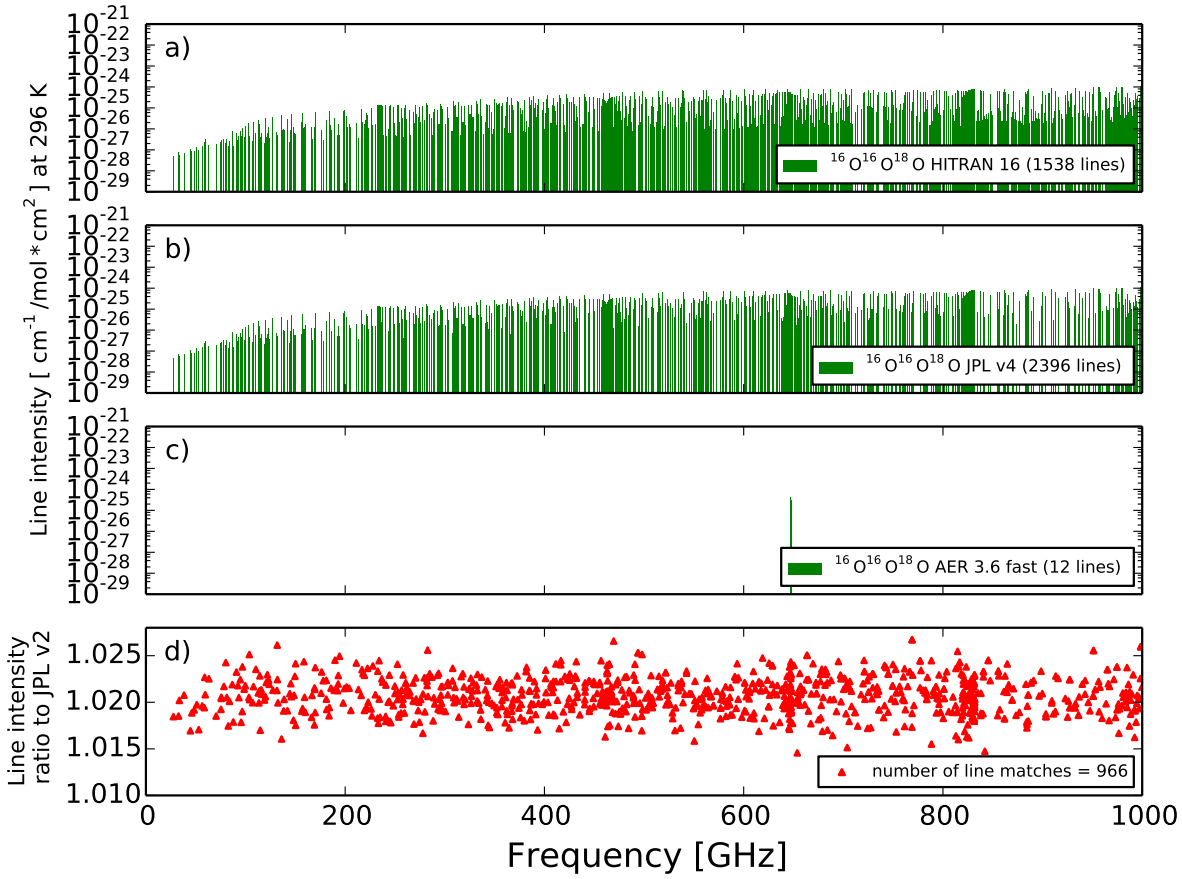

Figure 18: Line intensities for the second most abundent isotopomer of ozone ($^{16}O^{16}O^{18}O$) provided in: a) HITRAN 2016, b) JPL version 2 (converted to HITRAN units and adjusted for partition function and temperature), and c) AER 'fast' lines. d) The relative intensity difference between HITRAN 2016 and JPL intensities for corresponding lines.

4.1.2 JPL 2005 v4

Figure 17 shows the intensities and number of $^{16}O_3$ lines available up to 1000 GHz in HITRAN 2016, JPL version 4 and the AER 3.5 'fast' database, where line parameters follow those in HITRAN 2012 database. Rotational $^{16}O_3$ line intensities in the Jet Propulsion Laboratory (JPL) database (Pickett et al., 1998) were updated in November 2005 (JPL version 4) via the predictive calculation described in Birk et al. (2019). JPL values are converted to HITRAN units using the full temperature and partition function adjustment given in Rothman and Gordon (2006). Relative ratios of HITRAN 2016 intensities to each corresponding JPL v4 line,

where 4003 of the 6554 JPL lines are present in the HITRAN database, have a mean difference of difference of 2.99% (17d). The same procedure for AER lines is superfluous as its intensities are taken from HITRAN. Figure 17d essentially reproduces the HIT16 set of points in Birk et al. (2019, Figure 1) where the authors obtain an average relative difference of 4.0% which is 1% highter than the present analysis. The value of the Total Internal Partition Sum (TIPS) used for HITRAN at 296 K is given as 3483.71 by Gamache et al. (2017), however, Birk et al. (2019) use a slightly different TIPS value of 3473.0 which is taken from the Spectroscopy and Molecular Properties of Ozone (S&MPO) database (Babikov et al., 2014) and deviates from the Gamache et al. (2017) value by 0.3 %. When the analysis is repeated using the S&MPO TIPS value an average relative difference of 3.3% is obtained. It is suprising that Birk et al. (2019) achieve a precise 4.0% difference as the version 4 intensities have been modified from the original Flaud et al. (1990b) values upon which the HITRAN pre-scaled values are based.

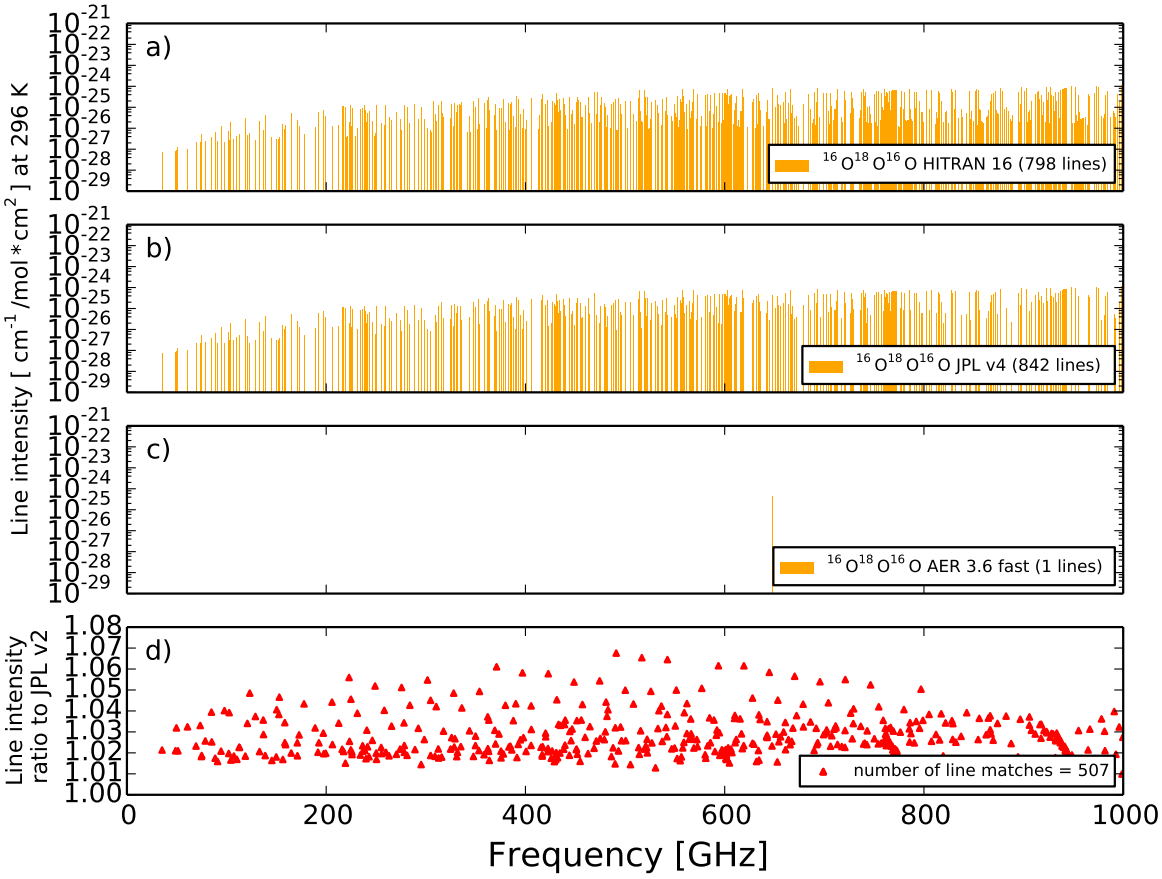

Figure 19: Line intensities for the third most abundent isotopomer of ozone (^{16}O^{18}O^{16}O) provided in: a) HITRAN 2016, b) JPL version 2 (converted to HITRAN units and adjusted for partition function and temperature), and c) AER 'fast' lines. d) The relative intensity difference between HITRAN 2016 and JPL intensities for corresponding lines.

Figures 18 and 19 show the same information as Figure 17 for the isotopomers ^{16}O^{16}O^{18}O and ^{16}O^{18}O^{16}O. This isotopologue has a less significant contribution as line intensities do not exceed magnitudes of 10^{-25}

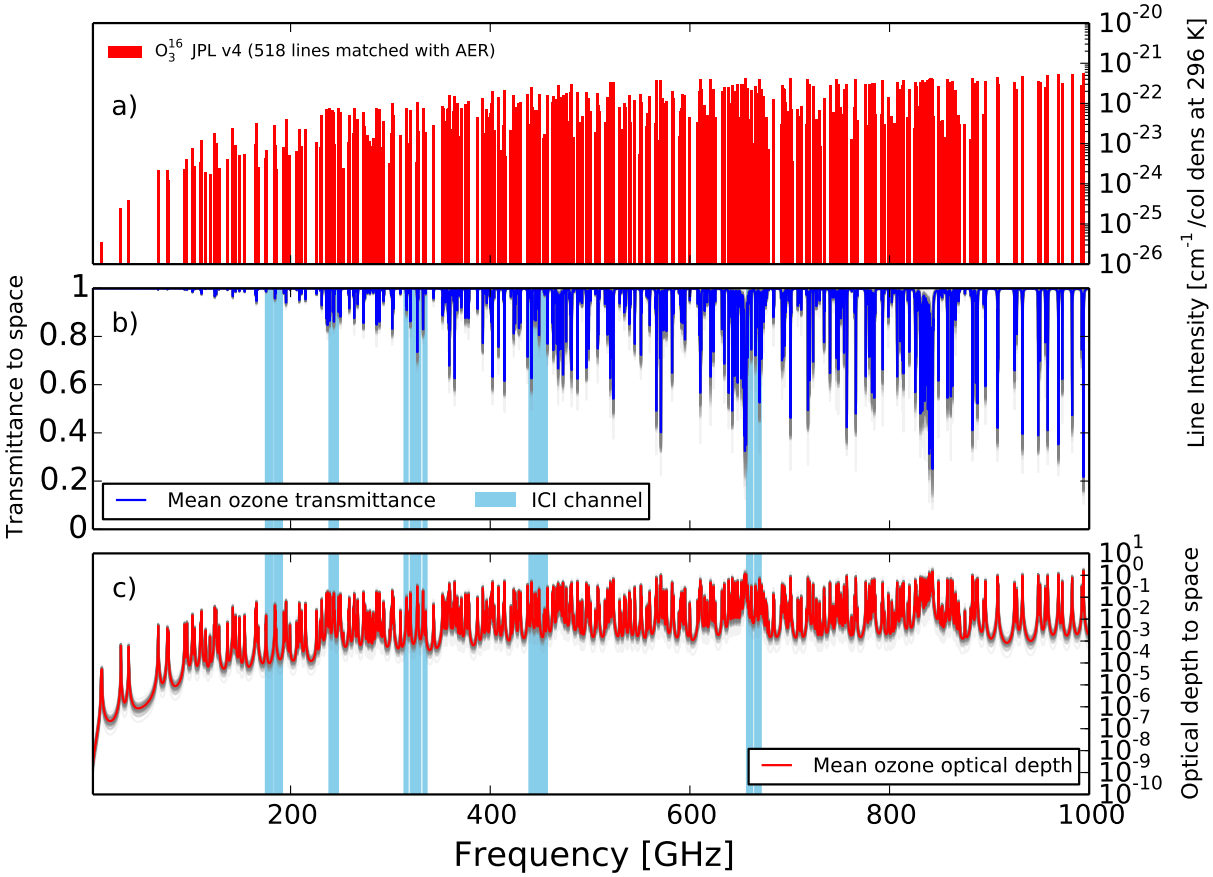

Figure 20: a) Location, log of intensity and to-scale halfwidth at 296 K of 518 ozone lines below 1000 GHz (653 between 1 and 1750 GHz) from JPL v4 sub-selected to those present in the AER 3.5 'fast' database. b) Surface-to-space transmittance and c) surface-to-space optical depth, for 83 diverse atmospheric profiles (grey lines) and their mean (bold line) for ozone only. The passbands of ICI channels are shaded in sky blue.

$\mathrm{cm}^{-1}/(\mathrm{mol\ cm}^2)$ in this region (whereas some $^{16}\mathrm{O}_3$ lines can reach $10^{-21}\ \mathrm{cm}^{-1}/(\mathrm{mol\ cm}^2)$). Only 13 lines are included in the AER 'fast' database which all centre at 647 GHz. Average reletive differences between HITRAN 2016 and JPL version 2 are 2.1 % and 2.2 % respectively, using the Gamache et al. (2017) TIPS values of 7465.7 and 3647.1 which are 0.11 % and 0.13 % higher than those given in S&MPO. When the latter values are used the differences are 3.1 % and 3.5 % respectively.

4.1.3 JPL 2005 with broadening parameters

Clearly, the inadvertently scaled HITRAN (and subsequently AER) line intensities should not be used in their present state. As the scaling method does not appear to be straight-forward it is not advisable to simply reverse the error by multiplying intensities by 1.04, instead the more recently derived intensities from the JPL catalogue can be used. As JPL does not provide broadening parameters in the online catalogue a new line list has been provided by JPL directly (2019, Iouli Gordon, Harvard & Smithsonian, personal communication) with the broadening parameters calculated following the standard HITRAN procedure from Wagner et al. (2002)

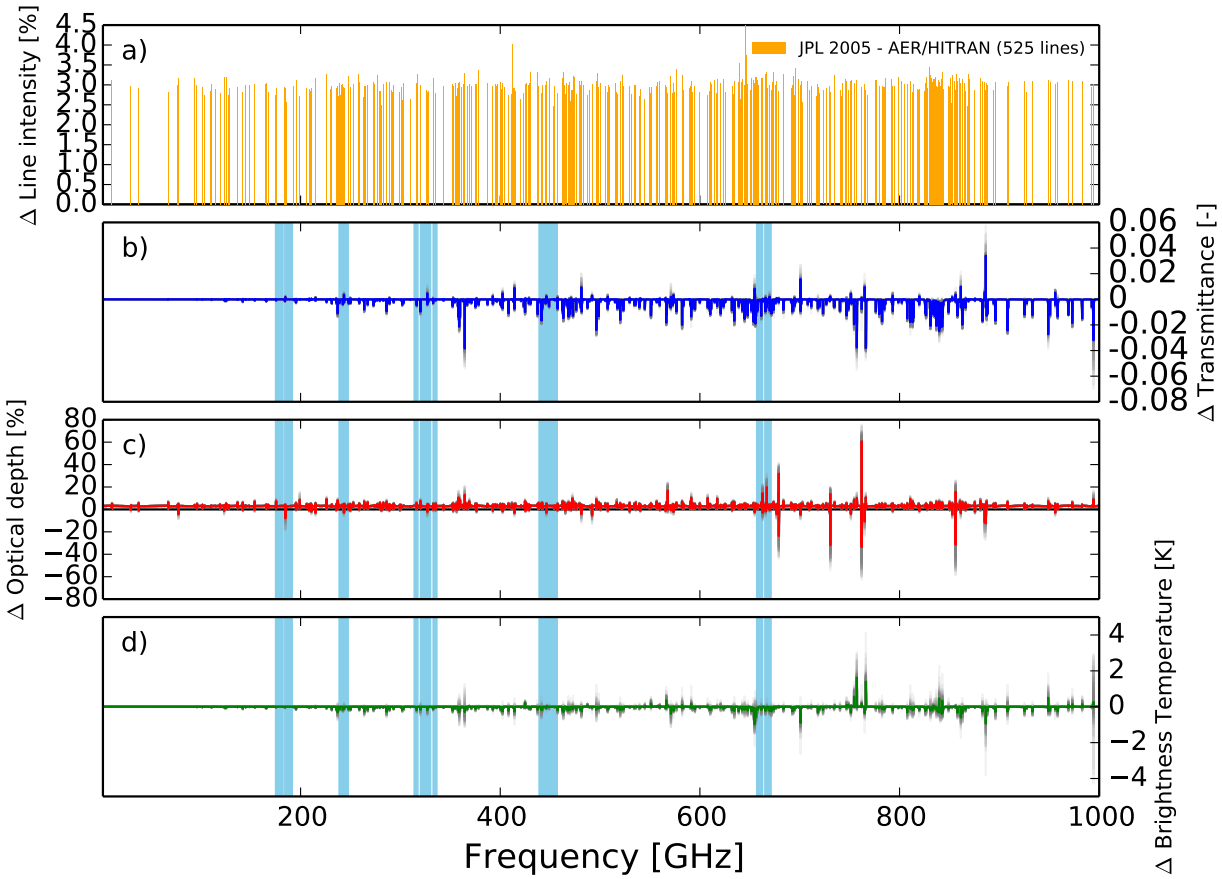

Figure 21: Differences between the AER 3.5 'fast' configuration of $^{16}O_3$ ozone lines and those from JPL 2005 version 4 database for corresponding lines. a) Percentage difference in line intensity. b) Difference in transmittance for 83 diverse atmospheric profiles (grey lines) and their mean (blue line) due to ozone only. c) Percentage optical depth differences for 83 diverse atmospheric profiles (grey lines) and their mean (red line) for ozone only; d) TOA brightness temperature differences for 83 diverse atmospheric profiles (grey lines) and their mean (green line). The passbands of ICI channels are shaded in sky blue.

with some adjustments for J=K values. The algorithm does not cover all possible lines therefore γ_{air} = 0.07 and γ_{self} = 0.085 are introduced in these cases. 518 out of the 527 $^{16}O_3$ lines below 1000 GHz in the AER 'fast' database are present in the new line list which accounts for 98.5% of the total sum of AER line intensities but only around 90% of HITRAN or JPL. The choice of TIPS should be reviewed, as it appears that the ozone values given in Gamache et al. (2017) could be in error, so the S&MPO value of 3473.0 is recommended. The resulting lines and transmittance and optical depth from this combination is shown in Figure 20. 653 lines are included in the calculation up to 1750 GHz to allow for the far wings of lines beneath the cut off threshold, however, as the halfwidth of ozone is so small there will be very little influence from these higher frequencies. There is also relatively little variation between profiles. The difference between this modified JPL catalogue and the original AER/HITRAN lines is shown in Figure 21 where panel a) clearly displays a difference in line intensity centering at 3%. Brightness temperatures in ICI channels for the most part are no more than 0.2 K different apart from at 664 GHz where there is a difference of up to 2 K on the lower frequency edge of channels

12 and 13. At higher frequencies (such as around 775 GHz) differences can reach up to 4 K for certain profiles.

4.1.4 Ozone lines summary

- Ozone cannot be ignored at sub-mm wavelengths due to the increasing intensity of line transitions, which is a more important parameter than broadening due to their sharp peaking in the stratosphere. Omission leads to monochromatic differences of up to 40 K at high freqeuncies.
- Ozone intensities at all wavelengths up to the infrared were scaled down by 1.04 % in HITRAN 2004 and have not been modified since. The justification for the scaling has recently been called into question for the microwave/sub-mm region by Birk et al. (2019).
- The present analysis shows a mean difference of around 3%, rather than the expected 4%, between JPL and HITRAN/AER line intensities for the principle isotopologue $^{16}O_3$.
- The Gamache et al. (2017) TIPS value for $^{16}O_3$ at 296 K, which is used by HITRAN is also thought to be in error and it is recommended to preferentially use the one provided in the S&MPO database.
- A new ozone line list based on 'correct' 2005 JPL values and subsetted for the AER 'fast' database has been created in the course of this work and is recommended for use.
- Differences between this new list and the un-modified AER lines can reach up to 4 K at high frequencies, but in general no more than 0.2 K in ICI channels.

5 Oxygen

5.1 Oxygen lines

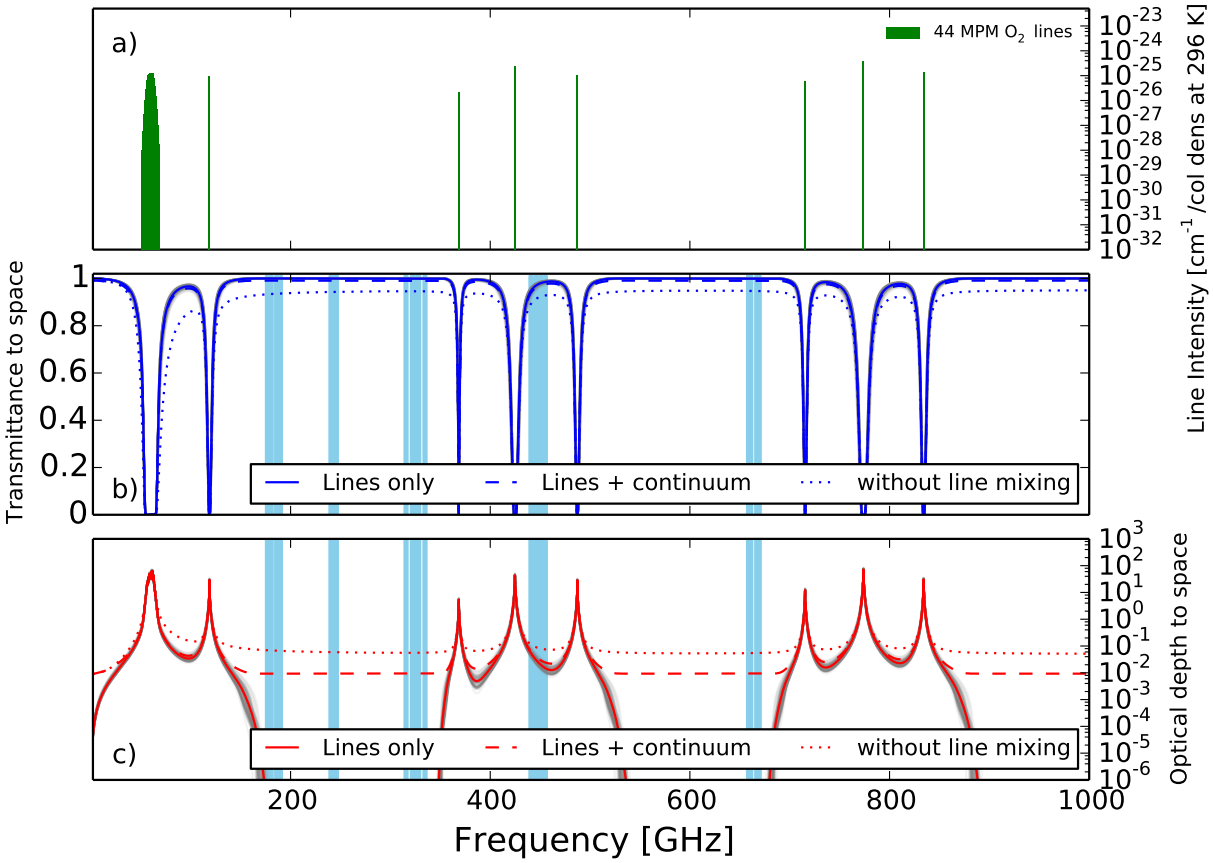

Figure 22: a) Location, log of intensity and to-scale halfwidth at 296 K of the 44 oxygen lines in the v1 configuration of AMSUTRAN. b) Surface-to-space transmittance and c) surface-to-space optical depth, for 83 diverse atmospheric profiles (grey lines) and their mean (bold line) for oxygen lines only, for oxygen lines and the oxygen continuum (dashed line) and both without the line mixing parameterisation (dotted line). The passbands of ICI channels are shaded in sky blue.

The 60-GHz oxygen band is of vital importance for temperature sounding by microwave satellite instruments due to the stratification of line intensities which provides information on the vertical temperature profile. The band comprises a series of fine structure transitions between sublevels caused by the splitting of the rotational levels (with rotational angular momentum N) through interaction with the electronic spin of the molecule. AMSUTRAN is confined to the lowest 19 levels which includes 37 fine structure transitions between 50 and 69 GHz. The transitions are weak yet the abundance of oxygen is large yielding line intensities that are comparable to water vapour. The close proximity of the lines in this complex give rise to non-negligible line mixing (overlap interference) which will affect absorption so that the line cannot be modelled as if it were isolated. This is included in the AMSUTRAN oxygen subroutine as a modification to the original VVW lineshape (Equation 3) via the line mixing parameter, δ_i. δ_i is a first-order function of pressure (Equation 6). The current values of a_5

and a_6 are given in Table 5 of Tretyakov et al. (2005) where all a_6 are the same as Liebe et al. (1992) and a_5 values are adjusted to be consistent with the δ_i parameters derived empirically for air (Tretyakov et al., 2005, Table 4).

The lower sub level of the $N = 1$ rotational state results in an isolated strong line outside of the 60-GHz band at 118.75 GHz, but the first true rotational transition doesn't occur until above 368 GHz. The MPM models include six of these higher frequency rotational lines. The positions and strengths of the lines included in AMSUTRAN v1 are shown in Figure 22a. The MPM models also include a parameterisation for non-resonant absorption by absorption (Liebe et al., 1992), which arises from the relaxation (Debye) spectrum of the magnetic moment of oxygen below 10 GHz, the contribution of which is shown in Figure 22c (dashed line). The non-resonant contribution is not discussed here further as it only contributes a small amount to the total absorption, but more information about it can be found in Turner et al. (2019, Section 6.3.1).

5.1.1 Line mixing

At the centre of the 60-GHz band line mixing acts to increase absorption between 56 and 63 GHz but has little to no effect on the transmittance which remains at zero (Figure 22b). However, it has a noticeable effect at higher frequencies, where transmittances are increased in the line wings by around 0.05 (5%) which perpetuates all the way up to 1000 GHz, a far larger difference than the spread due to the different atmospheric profiles (grey lines). It is interesting that parameters associated with a localised band of lines spanning 20 GHz at 60 GHz have such a far reaching influence that acts to decrease absorption. It should be noted that the line mixing parameterisation is empirically derived and so there is a certain amount of uncertainty in its formulation. It has also been shown in Tretyakov et al. (2005) that experimental values in this band systematically deviated from the first order predictions derived. Its nature is such that values of negative absorption are possible, which the MPM formulisation resets to zero, as demonstrated by the zero optical depth regions between the three bands of oxygen lines in Figure 22c. A subsequent study by Makarov et al. (2011) developed the MPM line mixing approach to a second order function of pressure which the authors found to reduce residual errors from observations to within 2% or less within the 60 GHz band, however its performance at higher frequencies is unknown. The extended lineshape in this case takes the form:

$$F(\nu) = \frac{\nu}{\nu_i}\left[\frac{\gamma_i(1+g_iP^2)+\delta_i(\nu-\nu_i-\delta\nu_iP^2)}{(\nu-\nu_i-\delta\nu_iP^2)^2+\gamma_i^2}+\frac{\gamma_i(1+g_iP^2)-\delta_i(\nu+\nu_i+\delta\nu_iP^2)}{(\nu+\nu_i+\delta\nu_iP^2)^2+\gamma_i^2}\right] \tag{12}$$

where g_i and $\delta\nu_i$ are second order mixing coefficients. g_i is associated with mixing line intensities and $\delta\nu_i$ is associated with mixing line central frequencies. More recent studies derive a new model for mixing known as the Energy Corrected Sudden (ECS) model Makarov et al. (2013, 2018). The applicability of these new parameterisations in the context of ICI are discussed later in this section.

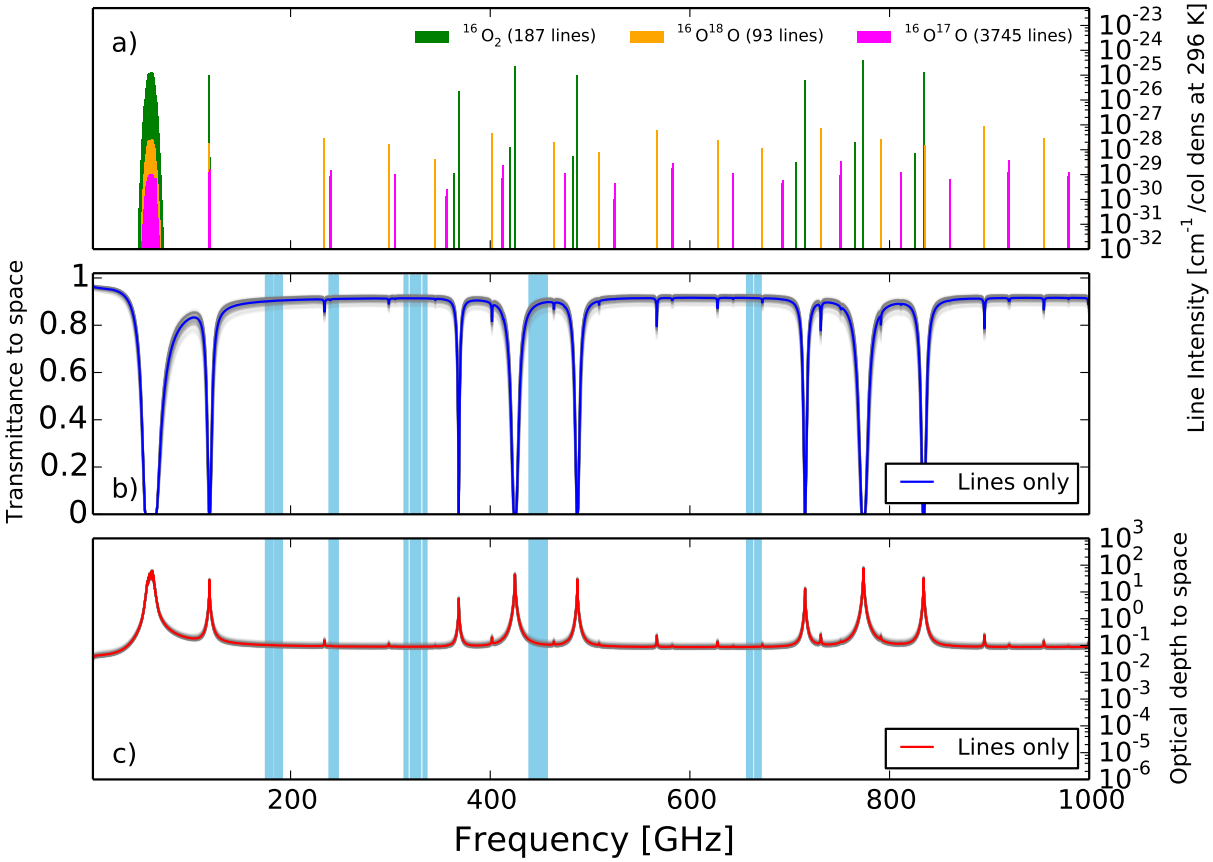

Figure 23: a) Location, log of intensity and to-scale halfwidth at 296 K of the 4025 oxygen lines in HITRAN 2016. b) Surface-to-space transmittance and c) surface-to-space optical depth, for 83 diverse atmospheric profiles (grey lines) and their mean (bold line) for oxygen lines only, with no line mixing. The passbands of ICI channels are shaded in sky blue.

5.1.2 HITRAN O_2

Figure 23a shows the position and intensities of the 4025 O_2 lines available in the HITRAN 2016 line catalogue below 1000 GHz for the first three isotopologues of oxygen, 93% of which are the from the least abundant $^{16}O^{17}O$ molecule. Intensities and halfwidths are calculated from a semi-empirical model described in Mackie et al. (2011, not yet published) and were updated last in the HITRAN 2012 revision, (Rothman et al., 2013) briefly describes the model. The air and self-broadened half-widths are derived based on measurements from Tretyakov et al. (2005) (for 44 lines) and Golubiatnikov and Krupnov (2003). Line positions were updated in the HITRAN 2016 revision from Yu et al. (2014) using a 'Dunham fit' method with new observations. Based on measurements from Drouin (2007), temperature dependencies for the air-broadened half-widths was set to one of three values, 0.97, 0.86 or 0.72 depending on the lines value of N. Line mixing coefficients are not explicitly provided in the HITRAN database, however, they are included in the derivation of the half width parameters for the oxygen A-band around 762 nm.

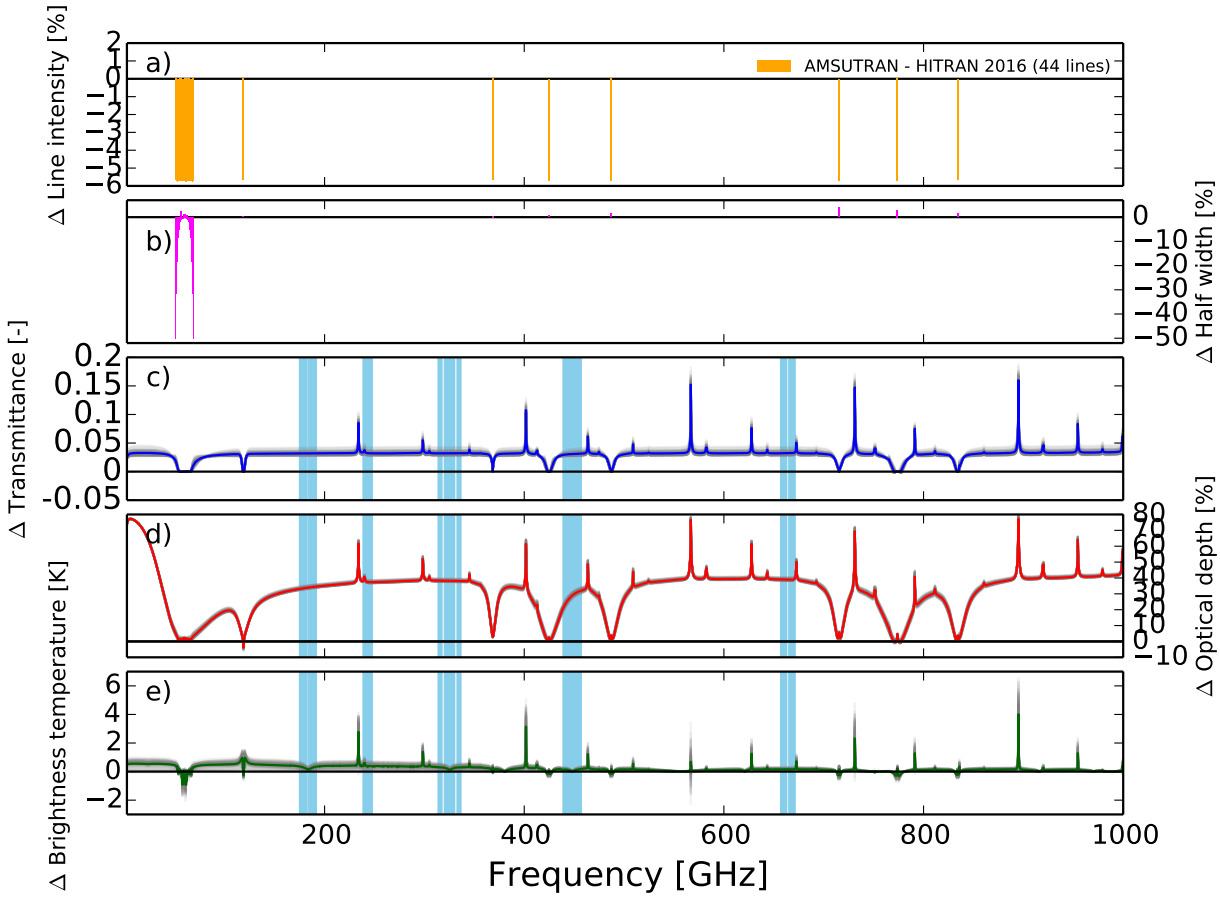

Figure 24: Differences between the v1 configuration of oxygen in AMSUTRAN and the full HITRAN 2016 database. Line mixing has been omitted from AMSUTRAN v1 for consistency with HITRAN ($\delta_i = 0$). a) Percentage difference in line intensity at 296 K for the 44 lines included in AMSUTRAN v1. b) Percentage difference in total halfwidth. c) Oxygen transmittance differences for 83 diverse atmospheric profiles (grey lines) and their mean (blue line). d) Percentage oxygen optical depth differences for 83 diverse atmospheric profiles (grey lines) and their mean (red line). e) Brightness temperature differences for 83 diverse atmospheric profiles (grey lines) and their mean (green line) due to the change in oxygen. The passbands of ICI channels are shaded in sky blue.

HITRAN values for O_2 line intensities are consistently larger than AMSUTRANv1 values by nearly 6% (Figure 24a), and total halfwidths are up to 50% larger in the outer lines of the 60-GHz band, however the inner lines and those at higher frequencies are generally less than 1% smaller (Figure 24b). The latter could in part be due to the differing algorithms for specifying the halfwidth. The MPM formula (Equation 5) does not explicitly include any dependency on self-broadening (which assumes the foreign and self-broadening half-widths are the same) and the large differences coincide with when these values deviate from one another in HITRAN. In order to compare line-by-line output from HITRAN and AMSUTRAN v1 it is necessary to omit line mixing from AMSUTRAN calculations, otherwise this will dominate differences. Away from line centres there is a constant reduction of transmittance of around 0.04 across all frequencies and around a 40% increase in optical depth (Figure 24c–d), which are likely to be due to the aforementioned MPM formulation of the halfwidth, which also includes an explicit dependency on water vapour and the slightly higher half-width temperature dependency

of 0.8 in MPM versus 0.72 in HITRAN (apart from a couple of values of 0.97). These broad features have a greater effect at frequencies below 60 GHz where the spectrum is less opaque, and HITRAN produces values up to 1 K lower, reducing to around 0.1 K above 400 GHz (Figure 24e).

Signals of the $^{16}O^{18}O$ isotopologue present in the HITRAN line list are clearly visible in the residual quantities in Figure 24, where the extra absorption is responsible for a brightness temperature reduction of up to 6 K (at 895 GHz). While none of the more strongly absorbing lines lie directly within the passbands of ICI channels, the 672.5 GHz line which has a 1 K effect at its peak grazes the upper edge of channels 12-13 centred at 664 GHz, however as oxygen lines are very sharp it is unlikely to affect the channels. Similarly the 233.95 GHz is in close proximity to channels 4–5 around 242 GHz, however there is a 5 GHz gap between them. Somewhat more worrying is the $^{16}O^{17}O$ line at 240.26 GHz which is just inside the lower frequency passband of these channels and though the perturbation of the line on brightness temperatures is small when deducted from the baseline difference, perhaps up to 0.2 K, this is something that should be taken into consideration.

5.1.3 Zeeman effect

In addition to the overlapping effects of oxygen lines at low altitudes due to pressure broadening, at high altitudes its behavior is further complicated due to Doppler broadening and the splitting of oxygen lines into several smaller ones by the Zeeman effect in the presence of a geomagnetic field (Zeeman, 1896). One of the consequences of this is that the line has a wider range of influence than if it were not split. Due to the complex nature of Zeeman splitting, a separate version of AMSUTRAN has been developed to include its effects for existing satellite instruments with high peaking channels in the 60-GHz band, i.e. SSMIS, AMSU-A and ATMS. This version of AMSUTRAN applies the widely-used coherency matrix method of Lenoir (1967), which treats oxygen as a 'Hund case (b)' molecule, and follows the Rosenkranz and Staelin (1988) formulation of the line-by-line model developed by Rosenkranz to incorporate both Doppler broadening and Zeeman splitting into the spectral calculation. Figure 25 shows an example of the Zeeman split transmittances calculated by AMSUTRAN for various satellite viewing geometries. In general the extent of the perturbation does not exceed 2 MHz from the line centre, yet the difference in measured brightness temperature can be several kelvin. Therefore there are potential implications for ICI, as the true behavior could extend the influence of the $^{16}O^{18}O$ 672.5 GHz line or the $^{16}O^{17}O$ 240.26 GHz line into the channel passbands if they peaked high enough in the atmosphere, but as they produce small residual signals this is unlikely. Currently AMSUTRAN only calculates the Zeeman effect for 34 lines in the spin rotation band, 33 between 51 and 68 GHz and the 118.75 GHz line, and the current treatment is sufficient for these transitions. However, the Hund case (b) approximation becomes problematic for the higher frequency transitions and it becomes necessary to include the off-diagonal elements of the fine structure Hamiltonian and higher order Zeeman interactions (Drouin et al., 2010). The recent work of Larsson et al. (2019) presents updated coefficients using these detailed calculations, which could provide scope for future improvement in this respect.

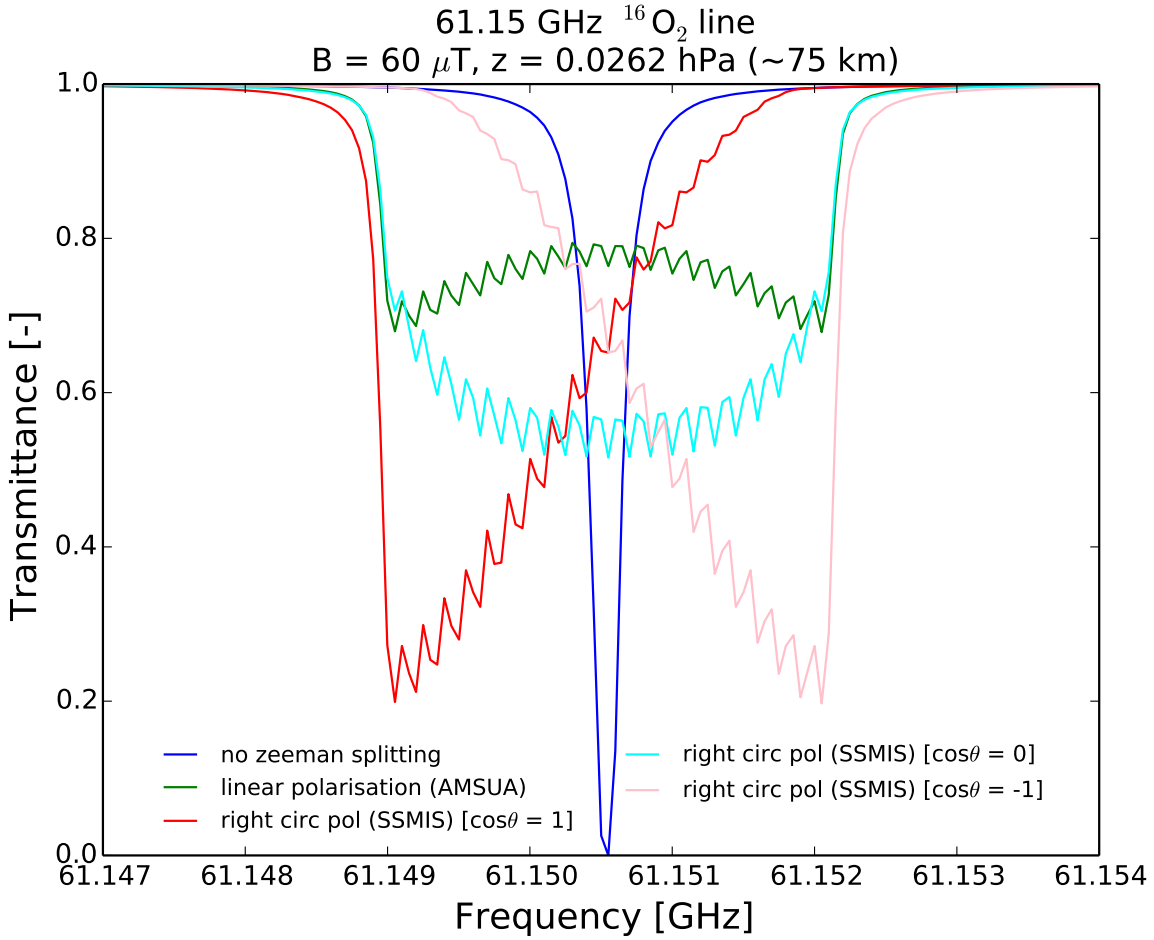

Figure 25: Zeeman affected transmittance spectrum from 0.0262 hPa (75 km) to space in the vicinity of the 9+ $^{16}O_2$ line at 61.15 GHz with the application of a magnetic field of 60 μT and receiver geometry representing either linear polarisation, like AMSU-A (green line), or right circular polarisation, like SSMIS where the geomagnetic field is either perpendicular to the viewing path (cyan line), or parallel to it (red and purple lines). θ is the angle between the magnetic field and viewing path. The un-split oxygen line is shown for reference (blue line).

5.1.4 Oxygen lines summary

- Line mixing implemented in the 60 GHz oxygen band has a proportionally greater effect in the line wings. The MPM formulation used in AMSUTRAN, which only includes first order terms, acts to decrease absorption by a relatively constant amount of 5% (transmittance) up to and beyond 1000 GHz. The inclusion of the MPM92 non-resonant oxygen formulation partly compensates for this reduction ensuring that there is always non-zero oxygen absorption between bands of lines.

- Recent work has sought to improve the parameterisation of line mixing by either retaining the MPM formulation and incorporating higher order terms, or deriving a new more physically based model (ECS), but as no clear improvement has been presented for the far-wings of the 60-GHz oxygen complex, which is the relevant region for ICI channels, adopting a new scheme or set of coefficients is not recommended for this purpose.

- There are systematically larger line intensities of just under 6% in HITRAN with respect to AMSUTRAN v1 and up to 50% larger total halfwidths, the latter in part due to the non-separation between air and self broadening in the MPM formula for halfwidth.
- In the absence of line mixing there is still less absorption overall with the AMSUTRAN oxygen scheme. The maximum difference in brightness temperatures away from line centres is 1 K at lower frequencies where the atmosphere is less opaque. There are larger differences of up to 2 K around the 118 GHz line and the outer lines of the 60 GHz oxygen band.
- Adding $^{16}O^{18}O$ lines is significant in the immediate vicinity of the line yielding reductions of up to 6 K. While ICI channels are clear from strong lines there is a slight risk of contamination from the 672.5 GHz line, which sits on the higher frequency edge of channels 12/13, and more so from the $^{16}O^{17}O$ 240.26 GHz line, which is just inside the lower frequency passband of channels 4/5. This line perturbs brightness temperatures by 0.2 K at its peak.
- Incorporating additional lines into the oxygen scheme would necessitate either replacing all lines and implementing a suitable line mixing routine, or mixing two different line absorption algorithms for the same molecule, as MPM-like parameters are only available for the existing 44 oxygen lines.
- High peaking oxygen lines are subject to splitting in the presence of a magnetic field, which broadens their influence by around 2 MHz either side of the line centre. ICI channels are unlikely to be affected as the two lines mentioned in the previous point are not subject to Zeeman splitting because their signals are not strong enough to suggest high peaking.

6 Sensitivity of ICI channels to new spectroscopy

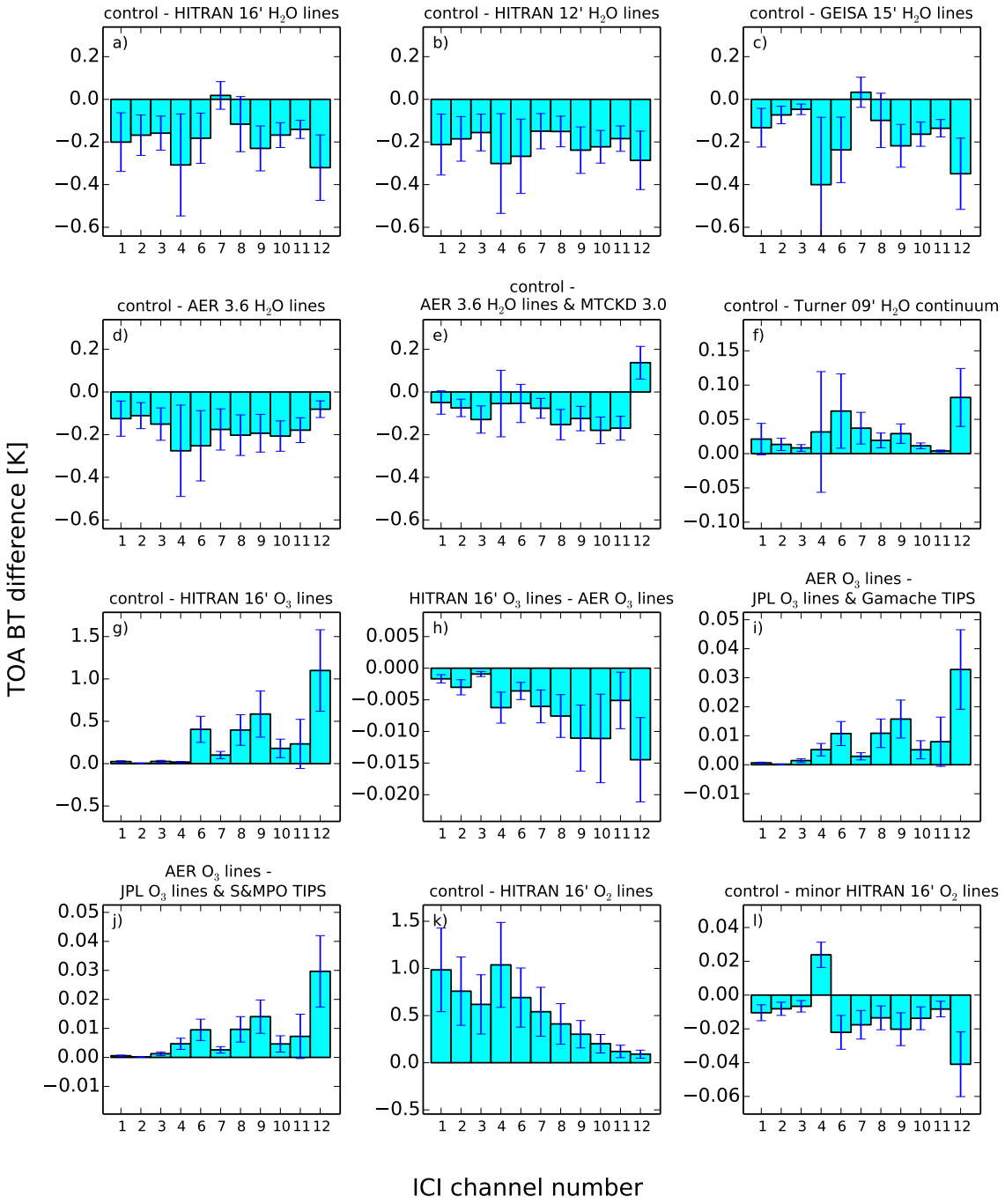

Figure 26: Sensitivity tests of isolated spectroscopic changes (labeled above each panel) in ICI channels. Bars are the mean difference over 83 atmospheric profiles and error bars are the standard deviation. Averaged transmittances are calculated from the grid of monochromatic transmittances specified over the two passbands of each channel, the details of which are given in Table 1. Channels 5 and 13 have been omitted as the only difference between them is their polarisation, hence they produce the same results as channels 4 and 12 (respectively). Control is the AMSUTRAN v1 spectroscopic configuration.

Figure 26 displays the range of sensitivities of ICI channels in response to applying each of a distilled list of the

spectroscopic changes detailed in previous sections, with all other aspects unchanged. Panels a–d show the effects due to H_2O line spectroscopy substitutions, where each new configuration replaces the 30 AMSUTRAN v1 lines with those from a different, larger, database. AMSUTRAN v1 produces very strong H_2O line absorption, and for each of the five lines that directly affect these channels has the highest line intensity of all sources investigated (Table 3), hence use of the larger databases would produce an overall increase in brightness temperature (less absorption = lower altitude of emission = higher brightness temperature). A particularly strong sensitivity to air-broadened half-width is seen in channels 12/13 (664 GHz), which is affected by the 556.94 and 752.03 GHz lines, for which GEISA 15‘ and AER 3.5 list nearly identical parameters, with the exception of air-broadened half-widths for which AER’s are 5-6% higher, resulting in a difference of around 0.3 K between them. Additionally, channel 7 which is the middle of the three 325.25 GHz channels (325.25 $\pm$3.5 GHz) is significantly affected by the recent increase in air-broadened half-width from 0.0944 to 0.1002 cm^{-1}/atm, which was applied in both the HITRAN 16‘ and GEISA 15‘ databases, to the extent that it over-compensates for the higher AMSUTRAN v1 line intensity producing a lower mean brightness temperature. Interestingly, this recent change reverts to a value from a study published over 50 years ago (Ryadov and Furashov, 1966). Panel e shows the effect of combining the AER line substitution with its corresponding continuum: MT-CKD (whereas the prior panels retain the existing one from MPM89), which reduces the differences overall to no more than 0.2 K. This reduction is to be expected because in an ideal world the total H_2O absorption should be equal no matter the experiment, though in practical terms this is never quite the case. Alternatively retaining the AMSUTRAN v1 lines and modifying the MPM89 continuum with the percentage adjustments suggested by Turner et al. (2009) perturbs the TOA brightness temperature by a maximum of about 0.13 K, but in the opposite direction to the total effect of AER H_2O spectroscopy, strengthening the absorption.

Turning to O_3 line absorption, panel g first of all shows the necessity of adding ozone beyond 300 GHz, as it’s omission would lead to errors of up to 1.1 $\pm$0.5 K in channels 12/13. However, below 300 GHz the difference between the 35 HITRAN 00‘ lines presently installed in AMSUTRAN, and the complete database of HITRAN 16‘ lines (6432 lines between 0 and 1000 GHz) is not more than 0.05 K. The difference when using the AER ’fast’ database, which retains only 540 of the most significant lines (approximately 8%) at a fraction of the computational expense, is minimal: not exceeding 0.02 K (panel h). Panel i displays the effect of reverting from the incorrectly scaled O_3 line intensities, unchanged since they were applied in HITRAN 04‘, to the JPL 05‘ intensities provided by I. Gordon (2019) as detailed in section 4.1.3, which has a maximum effect of nearly 0.05 K (in the 664 GHz channels) and acts in a way to increase absorption. When the 296 K TIPS value from the S&MPO database is used (panel j), as recommended by Birk et al. (2019), there is only a slight reduction (0.005 K) with respect to using the existing value in HITRAN 16‘ provided by Gamache et al. (2017).

The final two panels address the question of O_2 line absorption, where first the current configuration of 44 oxygen lines is completely replaced by those from HITRAN 16‘ (4025 lines between 0 and 1000 GHz), the latter without line mixing or a continuum as this is all that is possible at this stage (panel k). The large differences of up to 1 $\pm$0.5 K are primarily due to the absence of line mixing. This is particularly evident when comparing with panel l, which is the perturbation purely from the addition of the remaining oxygen lines above 200 GHz (i.e. omitting the six lines already present), and where differences stay below 0.04 $\pm$0.02 K. There is a possibility

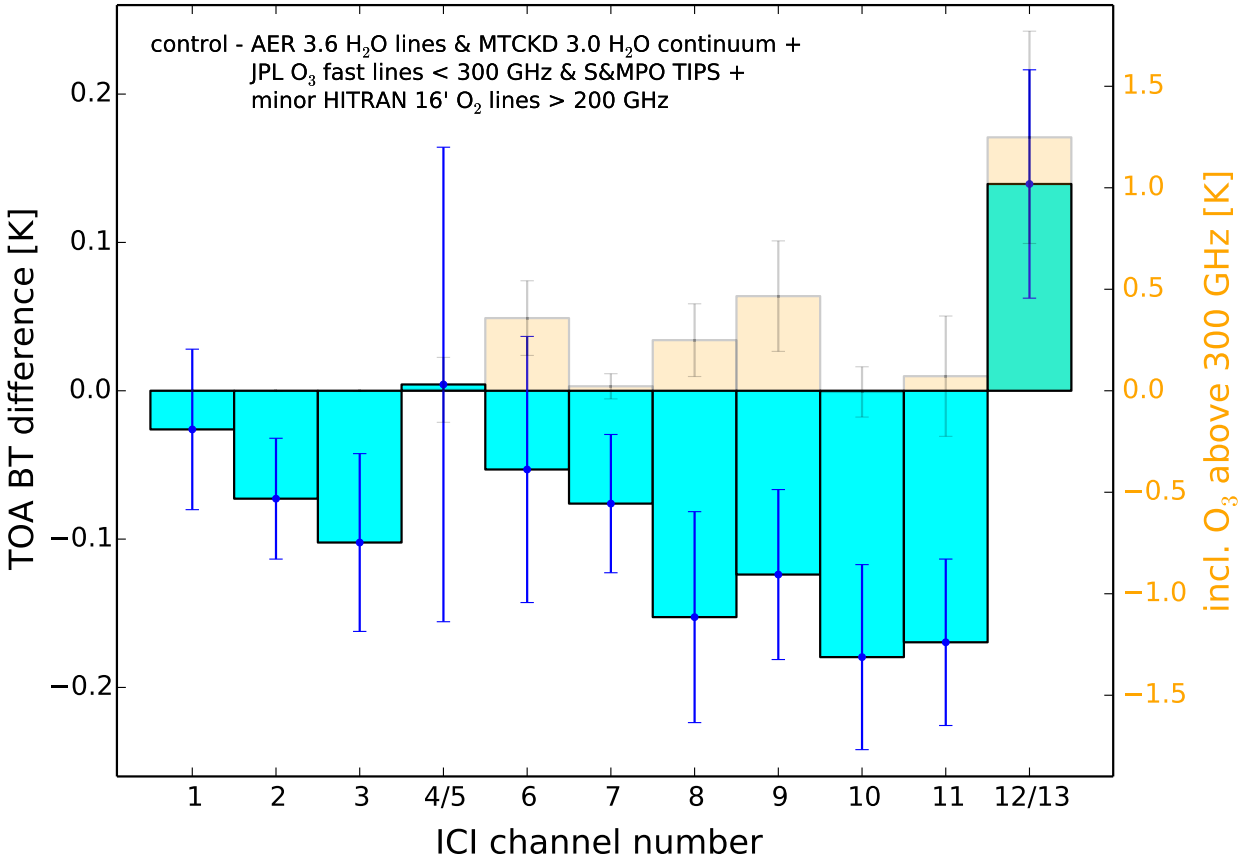

Figure 27: Same format as Figure 26 but the total TOA brightness temperature difference between the configuration with all recommended spectroscopic changes and the control configuration. Including ozone lines in the new configuration beyond 300 GHz has been separated out (orange bars, right hand axis).

that the measurement of the six strong higher frequency lines could encompass the effects of surrounding minor lines, in which case to add them again would be a duplication, but as this is something which cannot be confirmed it must be assumed that the lines have been measured in isolation and thus it is more accurate to include them.

The effect of replacing the current configuration with that recommended through the course of this work is shown in Figure 27, where the total difference including the addition of ozone beyond 300 GHz (orange bars) is shown alongside the total of all other changes (cyan bars), as the former is an order of magnitude larger than the latter. There is obviously going to be a large effect in all channels apart from 1–3 around 183.31 GHz due to the extra absorption, which reaches up to 1.25 $\pm$0.6 K in channels 12/13, but for every other channel this is partly moderated by a decrease due to the change in water vapour parameters and the addition of minor oxygen lines above 200 GHz. For channels 4/5 the combination of changes cancels to nearly zero in the mean, however the standard deviation over all profiles can be as large as the mean in other channels. By fortuitous compensation, channels 7 and 10 in the middle of the 325 and 448 GHz band of channels, respectively,

would not experience any change with the recommended changes on average, in comparison with if they had not been modified at all. Channels 1–3 all experience a total decrease in absorption (increase in brightness temperature), that becomes larger closer to the line centre (of up to 0.1 $\pm$0.06 K) due primarily to the $\sim$2% decrease in AER line intensity which was modified as a result of the in-situ atmospheric campaigns described in Mlawer et al. (2019), and which the corresponding $\sim$3% increase in air-broadened half-width is not enough to compensate.

6.1 ICI channel summary

- All ICI channels experience an increase in brightness temperature with the installation of H_2O spectroscopy from larger line databases (with the small exception of channel 7), which is only partly compensated by using a corresponding water vapour continuum, such as MT-CKD, Differences when using the combined H_2O spectroscopy from AER are up to 0.2 K higher with respect to the control configuration (this is a decrease in channels 12/13).
- The addition of O_3 lines beyond 300 GHz, where previously there was none, overwhelms all other spectroscopic changes, indicating brightness temperature would be up to 1.6 K too high if it were left unchanged.
- Using the corrected JPL 05‘ line intensities and S&MPO TIPS value at 296 K adds to the absorption by up to 0.04 K, whereas reducing the number of O_3 lines to a manageable amount, whilst still retaining almost all impacts, reduces it by up to 0.02 K.
- Adding minor oxygen lines beyond 200 GHz perturbs brightness temperatures by up to 0.06 K.
- As a result of this work, the spectroscopic changes recommended to be applied to AMSUTRAN, for the purposes of ICI, are:
  - Replace the 30 MPM H_2O lines and the MPM89 water vapour continuum with the ’fast’ database of AER H_2O lines (v3.5) up to the line cutoff (750 GHz) beyond 1000 GHz, and the corresponding water vapour continuum MT-CKD 3.0.
  - Replace the 35 HITRAN 00‘ O_3 lines with all those from the AER O_3 ’fast’ database up to the line cutoff (750 GHz) beyond 1000 GHz, but use the corresponding line parameters from JPL 05‘.
  - Add remaining HITRAN 16‘ O_2 lines above 200 GHz up to the line cutoff (750 GHz) beyond 1000 GHz, whilst retaining the existing 44 Tretyakov et al. (2005) lines, mixing and continuum parameterisations already implemented in AMSUTRAN.
- Omitting the inclusion of ozone, the combined effect of all recommended changes does not exceed 0.23 K. In channels 6–11 this change is an increase that mitigates the extra ozone absorption somewhat, however in ‘window‘ channels 4–5 and 12–13 it is a decrease that adds to it.
- The 183.31 GHz channels (1–3) would experience an average reduction of brightness temperature of up to 0.1 $\pm$0.06 K under the new regime, which is almost entirely due to the lower line intensity provided in the AER database.

7 RTTOV validation

Figure 28 shows that differences between AMSUTRAN and RTTOV are generally low for the v1 spectroscopic configuration; below 0.02 K in the mean and 0.1 K in the standard deviation, but with a maximum difference of 0.4 K in channel 11 (448.0 $\pm$1.4 GHz), using the dependent profile set.

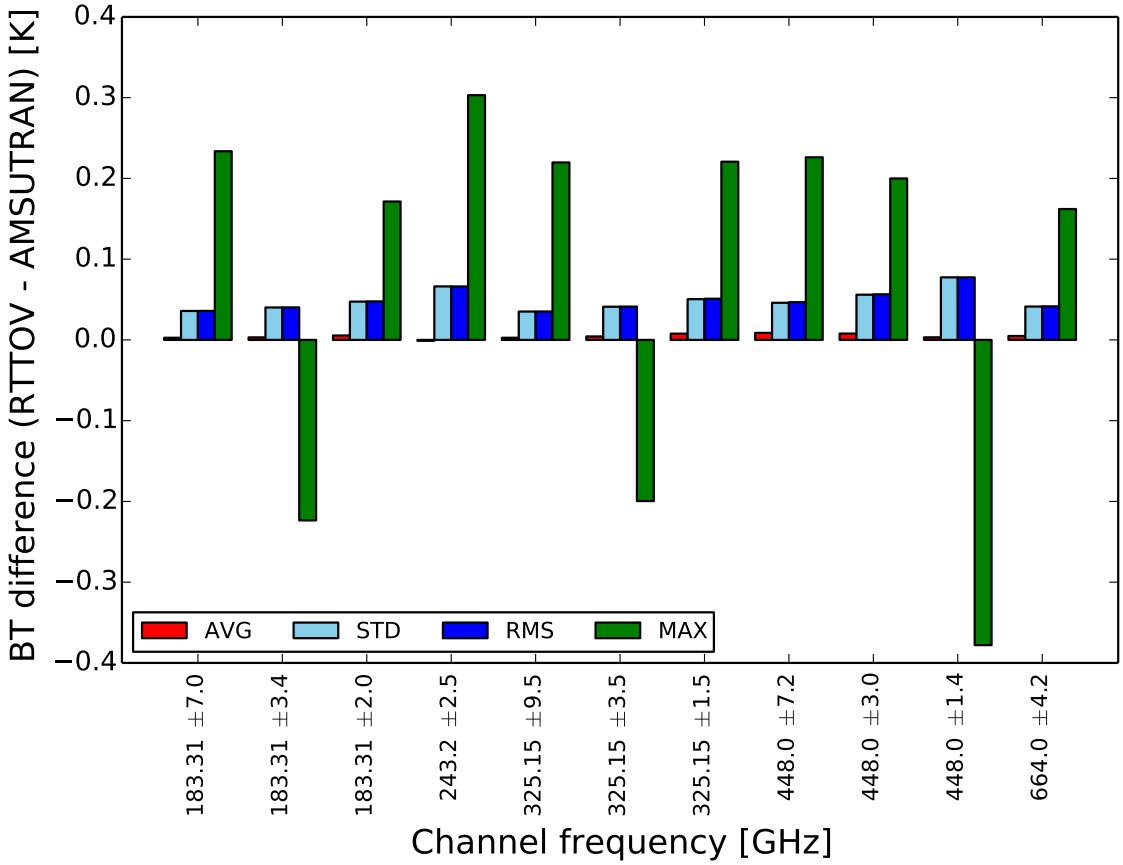

Figure 28: Validation plot of the difference in TOA brightness temperatures between channel integrated radiances from AMSUTRAN, and radiances calculated with RTTOV coefficients and predictors, for ICI channels. The spectroscopic configuration is the v1 control from section 2.1. Ozone is included up to 300 GHz in the mixed gases. Channels 5 (243.2 $\pm$2.5 GHz) and 13 (664.0 $\pm$4.2 GHz) have been omitted as they produce the same results as channels 4 and 12, respectively. The profiles validated are the 83 profile, 54 level, 'dependent' set which is used to calculate all coefficients, over which AVG is the mean, STD is the standard deviation, RMS is the root mean squared error, and MAX is the maximum difference between AMSUTRAN and RTTOV.

The pattern of biases are typical of those seen in the higher frequency water vapour channels and are similar in magnitude to the 183 GHz channels of ATMS (Figure 1). Differences are due to a combination of the error in the optical depth regression scheme, where predictors and coefficients don't completely reproduce the optical depths (or transmittances) produced by AMSUTRAN, and the error in reducing a polychromatic channel to a monochromatic central frequency. The latter is found to be negligible for these channels with less than a μK lost between averaged line-by-line radiances and radiances calculated at the central frequency using averaged transmittances over the channel.

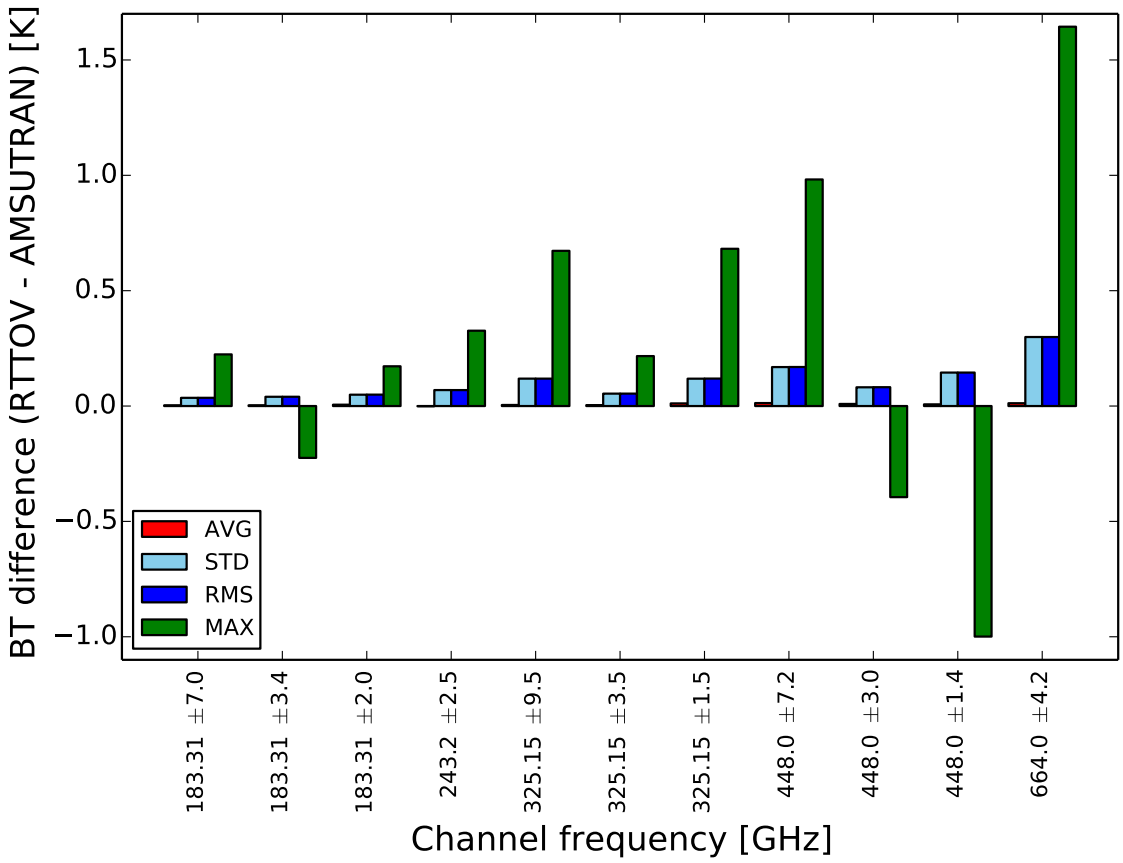

Figure 29: Same as Figure 28, apart from spectroscopic configuration is the one recommended in the course of this work, which is shown in Figure 27. Ozone is included up to 1000 GHz in the mixed gases. The profile database used is the 83 profile, 54 level, 'dependent' set which is the standard set used to calculated all coefficients.

Figure 29 is the same validation applied to RTTOV and AMSUTRAN output that adopt the recommended configuration of spectroscopy for ICI. At first glance statistics are much worse above 300 GHz resulting from the addition of ozone, which is treated as a well-mixed gas. The variability between profiles is too great for a fixed gas treatment at these frequencies, and hence separate predictors are required to prevent inconsistencies between RTTOV and AMSUTRAN of up to 1.7 K (channel 12/13: 664.0 $\pm$4.2 GHz). This has been implemented in Figure 30, heavily reducing these strong biases, shifting the maximum difference to channel 1 (183.31 $\pm$7.0 GHz) with a value of 0.23 K, suggesting the ozone predictors perform well. The recommended configuration calculated in this manner overall performs better than the control, excepting a slight degradation in the 448 GHz channels (but with lower maximum biases).

One final test of the prediction scheme is its robustness to different atmospheric profiles, as might be provided by a user. For this an independent set of 52 profiles is employed, that was not involved in the creation of the coefficient file, unlike the dependent 83 profile set. Both of these sets are shown in Appendix A. The profiles are interpolated to 54 levels in order for RTTOV to compute radiative transfer on coefficient levels. This is shown in Figure 31 and, as expected, biases are higher in magnitude, by approximately double, but slightly

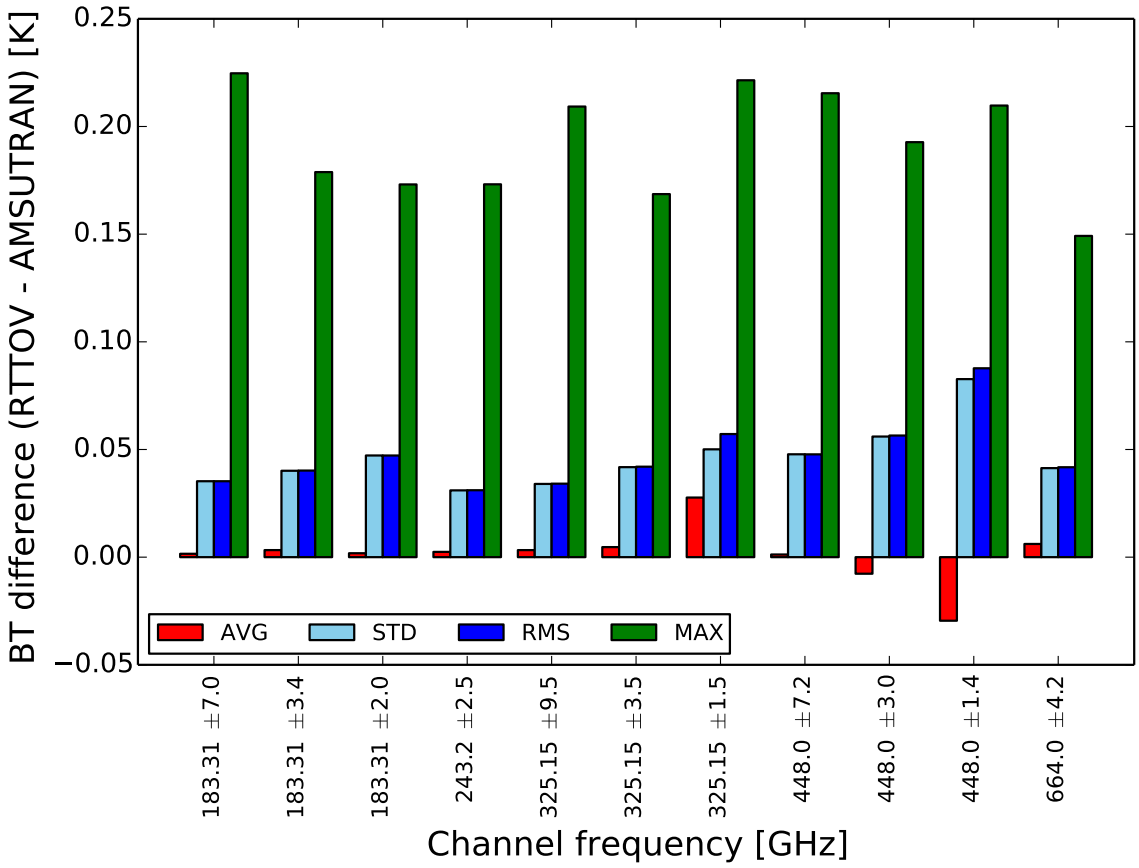

Figure 30: Same as Figure 29, apart from ozone is included as a variable gas (separate predictors) The spectroscopic configuration is the one recommended in the course of this work, which is shown in Figure 27. The profile database used is the 83 profile, 54 level, 'dependent' set which is the standard set used to calculated all coefficients.

less so for standard deviation and rmse. Maximum biases on the whole reduce, suggesting the profile set does not contain as extreme values as the dependent one. Mean biases are still well within acceptable ranges.

7.1 RTTOV validation summary

- Ozone must be treated as a variable gas by RTTOV to enable separate predictors to properly account for its variability.
- The recommended spectroscopic configuration improves upon the controls performance of RTTOV against AMSUTRAN by reducing the larger maximum bias values, with mean biases not exceeding 0.03 K and standard deviations not exceeding 0.1 K
- Independent verification of this configuration against a completely separate profile set yields mean biases not exceeding 0.05 K and standard deviations not exceeding 0.18 K.

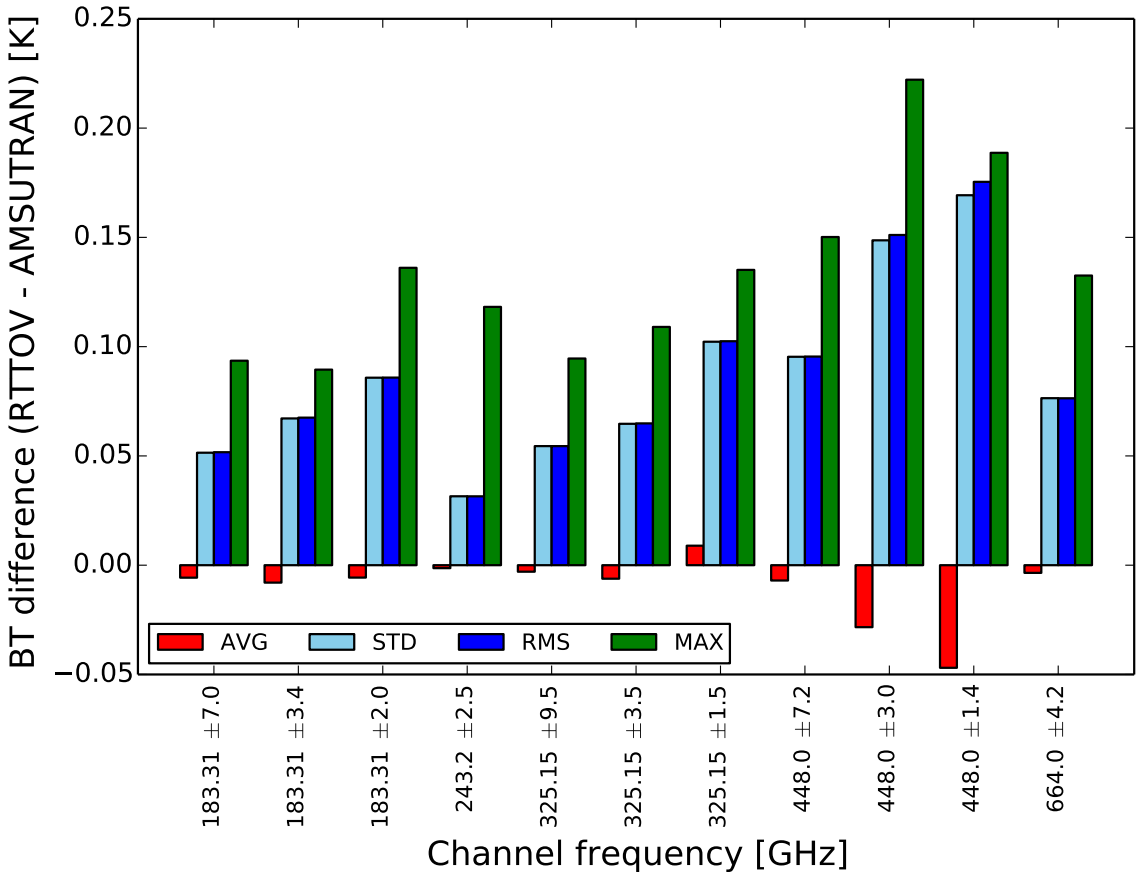

Figure 31: Same as Figure 30, apart from the profile database used is the 52 profile, 101 level, 'independent' set which has been interpolated to the 54 coefficient levels as is the procedure within RTTOV. The spectroscopic configuration is the one recommended in the course of this work, which is shown in Figure 27. Ozone is included as a variable gas (separate predictors).

8 Conclusion and Discussion

A thorough review of the potential options available to upgrade spectroscopy in the microwave precursor model to RTTOV, AMSUTRAN, has been performed with a focus on the sub-millimetre channels of the forthcoming ICI satellite instrument. This has yielded several recommendations for spectroscopic improvements from a theoretical point of view. The most impactful of which is less of an improvement than an addition, of ozone above 300 GHz where before it was absent, increasing simulated channel absorption by up to 1.5 K in equivalent brightness temperature effects. Similarly, it is recommended that minor oxygen lines should be added above 200 GHz as some encroach upon ICI channels but the effects are much smaller. As ICI primarily utilises spectral regions where water vapour absorption dominates, a wide breadth of options were investigated to improve upon the current MPM89 configuration, before finally settling on AER parameters. This substitution has, on average, a 0.15 K effect on brightness temperatures, a magnitude equivalent to the standard deviation of error in the RTTOV optical depth regression scheme. The only parts of the current spectroscopy that would remain with the new scheme are the 44 oxygen lines and the dry continua, with all other aspects modified.

The effect of applying these recommendations have been shown with respect to the current spectroscopy in AMSUTRAN (v1) as control, however, the latter should be taken as a baseline and not a benchmark, as it shows no more than the shift in results that would occur if the change were applied. This has no empirical consequence beyond 200 GHz as no instrument has been subject to the existing spectroscopy in this region. The question remains as to whether other microwave instruments should adopt the recommended spectroscopy, which is beyond the scope of Part One and is discussed in Part Two of this report (forthcoming). In some ICI channels the combination of changes cancels out, i.e. if no adjustments were made ICI channels 7 and 10 would produce the same results as with the recommended configuration, but channels 12 and 13 could be in error by up to 1.5 K.

An important lesson learnt is that care must be taken when combining spectroscopy from different sources that the resulting configuration does not conflict and potentially produce wrong results. Where more than one option is available for a particular parameter it is not simply the case that any can be applied in isolation without considering the rest of the model setup. All the aspects of the original MPM89 model were measured in completeness using the same experimental techniques, and it is possible that replacing one aspect could throw off the balance with the remaining model. This is shown most obviously in the case of separating the lines and continuum of water vapour but it could be imagined that an inter-species conflict would exist also. It may additionally be the case that adding extra spectroscopy to the existing configuration, such as missing lines, could result in the total absorption being overestimated, if, for example, the effects of these lines were somehow already accounted for in the parameters of existing lines (i.e. the strengths of MPM89 water vapour lines are consistently higher than the equivalent values from larger line databases). It is hoped this would not be the case, but as the parameters depend so much on the experimental conditions the only real way to test this is a systematic analysis against observations, necessitating a follow on project.

When dealing with discrete, well-separated parts of the spectrum, such as those measured by satellite channels, the requirement of synergy can realistically be relaxed if judged appropriate. This is the reason why, in the past, AMSUTRAN has followed a path of individual modifications in response to the needs of satellite instruments. One example being updated values for the half-width parameters of the heavily utilised 22.235 and 183.31 GHz water vapour lines, where it was decided that the impact of improving the absorption in the direct vicinity of these lines was more important than a conflict with their existing intensity values, and the water vapour continuum, the latter of which plays a minor role in comparison. Following this logic, it would be unwise to neglect adding a minor line in the near vicinity of ICI channels that could be making its presence known in the measurements, even if it means mixing two different algorithms, such as is the case with oxygen lines, as there is comparatively little effect on the rest of the spectrum. A key advantage of moving to AER lines and the MT-CKD continuum for water vapour is that inconsistencies in the existing configuration will be removed.

Finally it is reasonable to conclude that many improvements in the sub-millimetre will not be constrained by best experimental techniques but by limited choices. The number of options for lines and continuum are not inexhaustible in this region and no one configuration stands out as completely suiting the needs of ICI. For example as the derivation of water vapour continuum is tied to the lines both must be judged appropriate which

is difficult as most line parameters have been refined since the original continuum experiments were carried out. The recommended AER combination has the advantage of regular synergistic refinement of both these components with dedicated in-situ campaigns, but these have not yet focused explicitly on the sub-millimetre region. There is a pressing need for more sub-millimetre measurements to be made, both within the laboratory and in the real atmosphere, as it is becoming increasingly utilised by the atmospheric community and is likely to be more so in the future.

Appendices

A Profile datasets

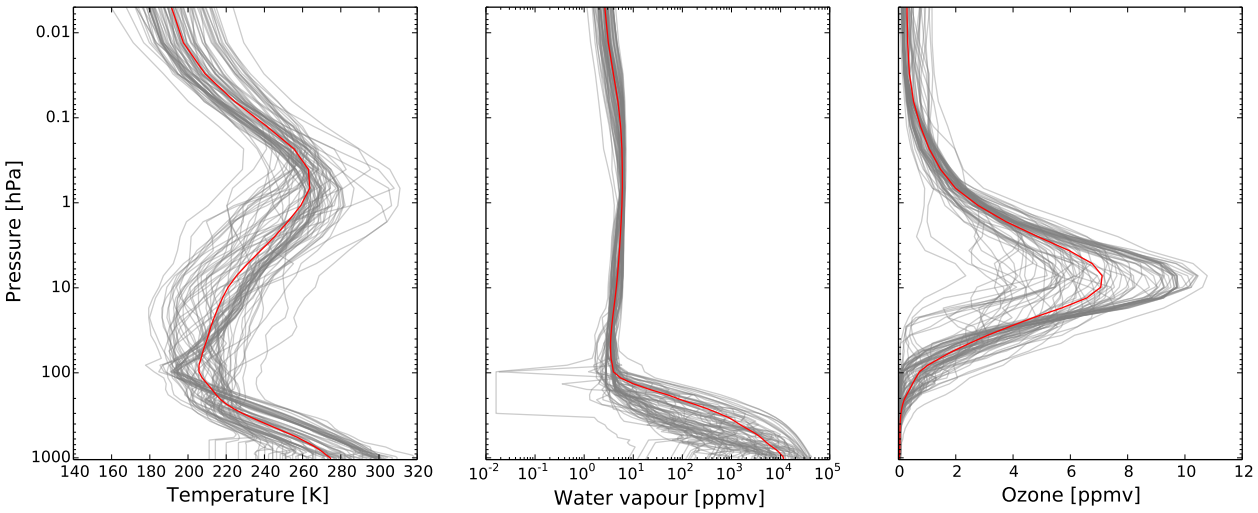

Figure 32: Atmospheric variables in the 83 profile, 54 level 'dependent' profile set that is used to create RTTOV coefficients. The mean profile is shown in red.

A set of 83 profiles covering a diverse range of global atmospheric conditions is used for generating the transmittances that subsequently produce the fast model coefficients (Matricardi, 2008). These were selected from a large database of profiles on 91 levels generated by the experimental suite (cycle 30R2) of the ECMWF forecasting system, as described in Chevallier et al. (2006). The 81st, 82nd and 83rd profiles are the minimum, maximum and mean, respectively, of the initial database. For use in AMSUTRAN the profiles have been interpolated to 54 levels between 0.005 and 1050 hPa, which has been shown by Saunders et al. (2013) to be a good compromise to reduce the burden of computation, whilst the levels have been chosen to provide adequate representation throughout the atmosphere and a smooth profile of pressure differences, this last being a requirement for RTTOV. The profiles consist of level values of total pressure in hPa, temperature in K, volume mixing ratio (vmr) of water vapour in parts per million by volume, and the same for ozone, see Figure 32. Additionally, a separate set of 52 profiles on 101 levels has been compiled using the same initial envelope

of profiles, in order to provide an independent test of the coefficient file (Figure 33).

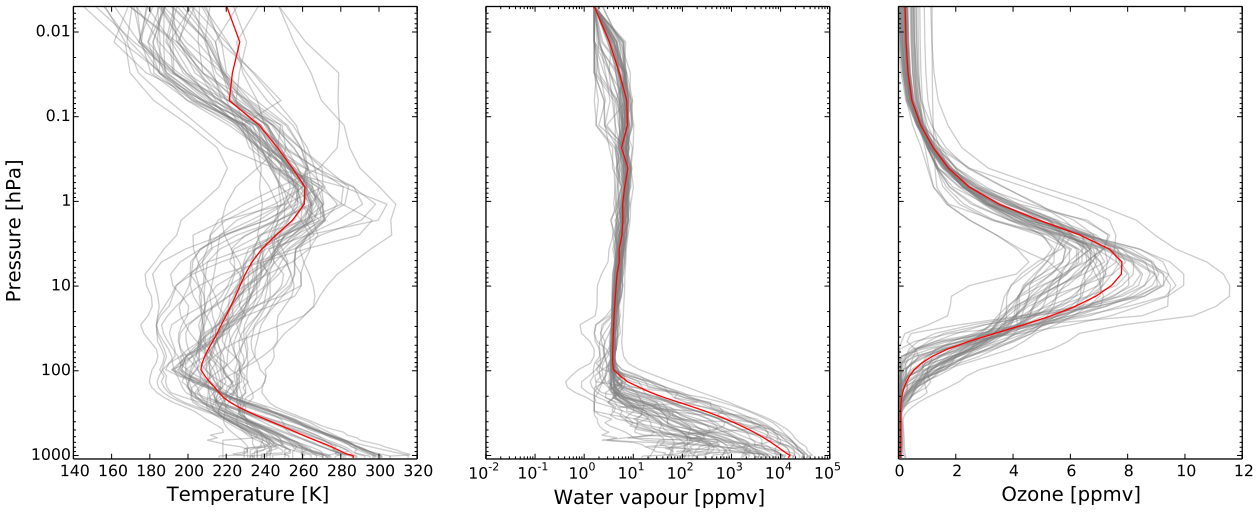

Figure 33: Atmospheric variables in the 52 profile, 101 level 'independent' profile set that has been interpolated to 54 levels for use with RTTOV coefficients. The mean profile is shown in red.

References

Armante, R., Scott, N., Crevoisier, C., Capelle, V., Crepeau, L., Jacquinet, N., and Chédin, A. (2016). Evaluation of spectroscopic databases through radiative transfer simulations compared to observations. Application to the validation of GEISA 2015 with IASI and TCCON. *Journal of Molecular Spectroscopy*, 327:180–192.

Auligné, T., McNally, A., and Dee, D. (2007). Adaptive bias correction for satellite data in a numerical weather prediction system. *Quarterly Journal of the Royal Meteorological Society*, 133(624):631–642.

Babikov, Y. L., Mikhailenko, S. N., Barbe, A., and Tyuterev, V. G. (2014). S&MPO–an information system for ozone spectroscopy on the WEB. *Journal of Quantitative Spectroscopy and Radiative Transfer*, 145:169–196.

Bauer, A., Godon, M., Carlier, J., and Ma, Q. (1995). Water vapor absorption in the atmospheric window at 239 GHz. *Journal of Quantitative Spectroscopy and Radiative Transfer*, 53(4):411–423.

Bauer, A., Godon, M., Carlier, J., Ma, Q., and Tipping, R. (1993). Absorption by H_O and H_2O-N_2 mixtures at 153 GHz. *Journal of Quantitative Spectroscopy and Radiative Transfer*, 50(5):463–475.

Bergadá, M., Labriola, M., González, R., Palacios, M., Marote, D., Andrés, A., García, J., Sánchez-Pascuala, D., Ordóñez, L., Rodríguez, M., et al. (2016). The Ice Cloud Imager (ICI) preliminary design and performance. In *Microwave Radiometry and Remote Sensing of the Environment (MicroRad), 2016 14th Specialist Meeting on*, pages 27–31. IEEE.

Birk, M. and Wagner, G. (2012). n averaged as a function of J" for J" = 0 to 13 from: Temperature-dependent air broadening of water in the 1250–1750 cm^{-1} range. *Journal of Quantitative Spectroscopy and Radiative Transfer*, 113(11):889–928.

Birk, M., Wagner, G., Gordon, I. E., and Drouin, B. J. (2019). Ozone intensities in the rotational bands. *Journal of Quantitative Spectroscopy and Radiative Transfer*, 226:60–65.

Cameron, J. and Bell, W. (2016). The testing and planned implementation of variational bias correction (VarBC) at the Met Office. *Proc. of the Twentieth International TOVS Study Conference, Wisconsin, USA*.

Cazzoli, G., Puzzarini, C., Buffa, G., and Tarrini, O. (2008). Pressure-broadening in the THz frequency region: the 1.113 THz line of water. *Journal of Quantitative Spectroscopy and Radiative Transfer*, 109(9):1563–1574.

Chevallier, F., Di Michele, S., and McNally, A. P. (2006). *Diverse profile datasets from the ECMWF 91-level short-range forecasts*. European Centre for Medium-Range Weather Forecasts.

Clough, S., Kneizys, F., and Davies, R. (1989). Line shape and the water vapor continuum. *Atmospheric research*, 23(3-4):229–241.

Clough, S., Shephard, M., Mlawer, E., Delamere, J., Iacono, M., Cady-Pereira, K., Boukabara, S., and Brown, P. (2005). Atmospheric radiative transfer modeling: a summary of the AER codes. *Journal of Quantitative Spectroscopy and Radiative Transfer*, 91(2):233–244.

Coudert, L., Martin-Drumel, M.-A., and Pirali, O. (2014). Analysis of the high-resolution water spectrum up to the Second Triad and to J = 30. *Journal of Molecular Spectroscopy*, 303:36–41.

Coudert, L. H. (1999). Line frequency and line intensity analyses of water vapour. *Molecular Physics*, 96(6):941–954.

Drouin, B. J. (2007). Temperature dependent pressure induced linewidths of o$_2$16 and 18o16o transitions in nitrogen, oxygen and air. *Journal of Quantitative Spectroscopy and Radiative Transfer*, 105(3):450–458.

Drouin, B. J., Yu, S., Miller, C. E., Müller, H. S., Lewen, F., Brünken, S., and Habara, H. (2010). Terahertz spectroscopy of oxygen, O_2, in its 3Σ- g and 1Δ electronic states: THz Spectroscopy of O_2. *Journal of Quantitative Spectroscopy and Radiative Transfer*, 111(9):1167–1173.

Flaud, J., Wagner, G., Birk, M., Camy-Peyret, C., Claveau, C., De Backer-Barilly, M., Barbe, A., and Piccolo, C. (2003). Ozone absorption around 10 μm. *Journal of Geophysical Research: Atmospheres*, 108(D9).

Flaud, J.-M., Camy-Peyret, C., Rinsland, C. P., Devi, V. M., Smith, M. A. H., and Goldman, A. (1990a). Improved line parameters for ozone bands in the 10-μm spectral region. *Applied optics*, 29(25):3667–3671.

Flaud, J.-M., Camy-Peyret, C., Rinsland, C. P., Smith, M. A. H., and Devi, V. M. (1990b). Atlas of ozone spectral parameters from microwave to medium infrared.

Fox, S., Lee, C., Moyna, B., Philipp, M., Rule, I., Rogers, S., King, R., Oldfield, M., Rea, S., Henry, M., et al. (2017a). ISMAR: an airborne submillimetre radiometer. *Atmospheric Measurement Techniques*, 10(2):477–490.

Fox, S., Turner, E., Newman, S., and Harlow, C. (2017b). Evaluation of clear-sky spectroscopy using ISMAR and MARSS. *Met Office milestone report*.

Frisk, U., Hagström, M., Ala-Laurinaho, J., Andersson, S., Berges, J.-C., Chabaud, J.-P., Dahlgren, M., Emrich, A., Florén, H.-G., Florin, G., et al. (2003). The Odin satellite-I. Radiometer design and test. *Astronomy & Astrophysics*, 402(3):L27–L34.

Froidevaux, L., Livesey, N. J., Read, W. G., Jiang, Y. B., Jimenez, C., Filipiak, M. J., Schwartz, M. J., Santee, M. L., Pumphrey, H. C., Jiang, J. H., et al. (2006). Early validation analyses of atmospheric profiles from EOS MLS on the Aura satellite.

Gamache, R. R. (1985). Temperature dependence of n_2-broadened halfwidths of ozone. *Journal of Molecular Spectroscopy*, 114(1):31–41.

Gamache, R. R. and Hartmann, J.-M. (2004). An intercomparison of measured pressure-broadening and pressure-shifting parameters of water vapor. *Canadian journal of chemistry*, 82(6):1013–1027.

Gamache, R. R. and Laraia, A. L. (2009). N_2-, O_2-, and air-broadened half-widths, their temperature dependence, and line shifts for the rotation band of $H_2^{16}O$. *Journal of Molecular Spectroscopy*, 257(2):116–127.

Gamache, R. R., Roller, C., Lopes, E., Gordon, I. E., Rothman, L. S., Polyansky, O. L., Zobov, N. F., Kyuberis, A. A., Tennyson, J., Yurchenko, S. N., et al. (2017). Total internal partition sums for 166 isotopologues of 51 molecules important in planetary atmospheres: Application to HITRAN2016 and beyond. *Journal of Quantitative Spectroscopy and Radiative Transfer*, 203:70–87.

Godon, M., Carlier, J., and Bauer, A. (1992). Laboratory studies of water vapor absorption in the atmospheric window at 213 GHz. *Journal of Quantitative Spectroscopy and Radiative Transfer*, 47(4):275–285.

Golubiatnikov, G. Y. and Krupnov, A. (2003). Microwave study of the rotational spectrum of oxygen molecule in the range up to 1.12 THz. *Journal of Molecular Spectroscopy*, 217(2):282–287.

Gordon, I. E., Rothman, L. S., Gamache, R. R., Jacquemart, D., Boone, C., Bernath, P. F., Shephard, M. W., Delamere, J. S., and Clough, S. A. (2007). Current updates of the water-vapor line list in HITRAN: A new 'Diet' for air-broadened half-widths. *Journal of Quantitative Spectroscopy and Radiative Transfer*, 108(3):389–402.

Gordon, I. E., Rothman, L. S., Hill, C., Kochanov, R. V., Tan, Y., Bernath, P. F., Birk, M., Boudon, V., Campargue, A., Chance, K., et al. (2017). The HITRAN 2016 molecular spectroscopic database. *Journal of Quantitative Spectroscopy and Radiative Transfer*, 203:3–69.

Harris, B. and Kelly, G. (2001). A satellite radiance-bias correction scheme for data assimilation. *Quarterly Journal of the Royal Meteorological Society*, 127(574):1453–1468.

Hewison, T. J., Cimini, D., Martin, L., Gaffard, C., and Nash, J. (2006). Validating clear air absorption models using ground-based microwave radiometers and vice-versa. *Meteorologische Zeitschrift*, 15(1):27–36.

Jacquemart, D., Gamache, R., and Rothman, L. S. (2005). Use of the semi-empirical coefficients of section 4.2.1: Semi-empirical calculation of air-broadened half-widths and air pressure-induced frequency shifts of water-vapor absorption lines. *Journal of Quantitative Spectroscopy and Radiative Transfer*, 96(2):205–239.

Jacquinet-Husson, N., Armante, R., Scott, N., Chédin, A., Crépeau, L., Boutammine, C., Bouhdaoui, A., Crevoisier, C., Capelle, V., Boonne, C., et al. (2016). The 2015 edition of the GEISA spectroscopic database. *Journal of Molecular Spectroscopy*, 327:31–72.

John, V. and Buehler, S. (2004). The impact of ozone lines on AMSU-B radiances. *Geophysical research letters*, 31(21).

Kikuchi, K.-i., Nishibori, T., Ochiai, S., Ozeki, H., Irimajiri, Y., Kasai, Y., Koike, M., Manabe, T., Mizukoshi, K., Murayama, Y., et al. (2010). Overview and early results of the Superconducting Submillimeter-Wave Limb-Emission Sounder (SMILES). *Journal of Geophysical Research: Atmospheres*, 115(D23).

Kim, E., Lyu, C.-H. J., Anderson, K., Vincent Leslie, R., and Blackwell, W. J. (2014). S-NPP ATMS instrument prelaunch and on-orbit performance evaluation. *Journal of Geophysical Research: Atmospheres*, 119(9):5653–5670.

Koshelev, M., Serov, E., Parshin, V., and Tretyakov, M. Y. (2011). Millimeter wave continuum absorption in moist nitrogen at temperatures 261–328 K. *Journal of Quantitative Spectroscopy and Radiative Transfer*, 112(17):2704–2712.

Kuhn, T., Bauer, A., Godon, M., Buehler, S., and Künzi, K. (2002). Water vapor continuum: absorption measurements at 350 GHz and model calculations. *Journal of Quantitative Spectroscopy and Radiative Transfer*, 74(5):545–562.

Lanquetin, R., Coudert, L., and Camy-Peyret, C. (2001). High-lying rotational levels of water: an analysis of the energy levels of the five first vibrational states. *Journal of molecular spectroscopy*, 206(1):83–103.

Larsson, R., Lankhaar, B., and Eriksson, P. (2019). Updated Zeeman effect splitting coefficients for molecular oxygen in planetary applications. *Journal of Quantitative Spectroscopy and Radiative Transfer*, 224:431–438.

Lenoir, W. B. (1967). Propagation of partially polarized waves in a slightly anisotropic medium. *Journal of Applied Physics*, 38(13):5283–5290.

Liebe, H., Hufford, G., and Cotton, M. (1993). Propagation modeling of moist air and suspended water/ice particles at frequencies below 1000 GHz. In *In AGARD, Atmospheric Propagation Effects Through Natural and Man-Made Obscurants for Visible to MM-Wave Radiation 11 p (SEE N94-30495 08-32)*.

Liebe, H., Rosenkranz, P., and Hufford, G. (1992). Atmospheric 60 GHz oxygen spectrum: New laboratory measurements and line parameters. *Journal of Quantitative Spectroscopy and Radiative Transfer*, 48(5-6):629–643.

Liebe, H. J. (1989). MPM–An atmospheric millimeter-wave propagation model. *International Journal of Infrared and Millimeter Waves*, 10(6):631–650.

Liebe, H. J. and Layton, D. H. (1987). *Millimeter-wave properties of the atmosphere: Laboratory studies and propagation modeling*. US Department of Commerce, National Telecommunications and Information Administration.

Liljegren, J. C., Boukabara, S. A., Cady-Pereira, K., and Clough, S. A. (2005). The effect of the half-width of the 22 GHz water vapor line on retrievals of temperature and water vapor profiles with a twelve-channel microwave radiometer. *IEEE Trans. Geosci. Remote Sens*, 43(5):1102–1108.

Lodi, L., Tennyson, J., and Polyansky, O. L. (2011). A global, high accuracy ab initio dipole moment surface for the electronic ground state of the water molecule. *The Journal of chemical physics*, 135(3):034113.

Mackie, C., Gordon, I., Rothman, L., Leshchishina, O., Kassi, S., Campargue, A., et al. (2011). Revision of spectral parameters for the bands of oxygen that involve ground x 3 σ g à and first excited a 1 δ g electronic states (in preparation). *J Quant Spectrosc Radiat Transfer*.

Makarov, D., Tretyakov, M. Y., and Boulet, C. (2013). Line mixing in the 60-GHz atmospheric oxygen band: Comparison of the MPM and ECS model. *Journal of Quantitative Spectroscopy and Radiative Transfer*, 124:1–10.

Makarov, D., Tretyakov, M. Y., and Rosenkranz, P. (2011). 60-GHz oxygen band: Precise experimental profiles and extended absorption modeling in a wide temperature range. *Journal of Quantitative Spectroscopy and Radiative Transfer*, 112(9):1420–1428.

Makarov, D., Vilkov, I., Koshelev, M., Aderkina, A., and Tretyakov, M. Y. (2018). Collisional Coupling of the Molecular Oxygen 16 O_2 Fine-Structure Lines Under Low Pressures. *Radiophysics and Quantum Electronics*, 60(10):808–823.

Martin, M., Coudert, L., Pirali, O., and Balcon, O. (2013). Positions and intensities of water vapor transitions in 0–6000 cm à 1 region. *J Chem Phys*.

Matricardi, M. (2008). *The generation of RTTOV regression coefficients for IASI and AIRS using a new profile training set and a new line-by-line database*. European Centre for Medium-Range Weather Forecasts.

McClatchey, R. A., Benedict, W., Clough, S. A., Burch, D., and Calfee, R. F. (1973). AFCRL atmospheric absorption line parameters compilation. Technical report, Air Force Cambridge Research Labs HANSCOM AFB MA.

Mlawer, E., Turner, D., Paine, S., Palchetti, L., Bianchini, G., Payne, V., Cady-Pereira, K., Pernak, R., Alvarado, M., Gombos, D., et al. (2019). Analysis of water vapor absorption in the far-infrared and submillimeter regions using surface radiometric measurements from extremely dry locations. *Journal of Geophysical Research: Atmospheres*.

Mlawer, E. J., Payne, V. H., Moncet, J.-L., Delamere, J. S., Alvarado, M. J., and Tobin, D. C. (2012). Development and recent evaluation of the MT_CKD model of continuum absorption. *Philosophical Transactions of the Royal Society A: Mathematical, Physical and Engineering Sciences*, 370(1968):2520–2556.

Pardo, J. R., Cernicharo, J., and Serabyn, E. (2001). Atmospheric transmission at microwaves (ATM): an improved model for millimeter/submillimeter applications. *IEEE Transactions on antennas and propagation*, 49(12):1683–1694.

Payne, V. H., Delamere, J. S., Cady-Pereira, K. E., Gamache, R. R., Moncet, J.-L., Mlawer, E. J., and Clough, S. A. (2008). Air-broadened half-widths of the 22 and 183 GHz water-vapor lines. *IEEE Transactions on Geoscience and Remote Sensing*, 46(11):3601–3617.

Payne, V. H., Mlawer, E. J., Cady-Pereira, K. E., and Moncet, J.-L. (2011). Water vapor continuum absorption in the microwave. *IEEE Transactions on Geoscience and Remote Sensing*, 49(6):2194–2208.

Pickett, H., Poynter, R., Cohen, E., Delitsky, M., Pearson, J., and Müller, H. (1998). Submillimeter, millimeter, and microwave spectral line catalog. *Journal of Quantitative Spectroscopy and Radiative Transfer*, 60(5):883–890.

Podobedov, V., Plusquellic, D., Siegrist, K., Fraser, G., Ma, Q., and Tipping, R. (2008). New measurements of the water vapor continuum in the region from 0.3 to 2.7 THz. *Journal of Quantitative Spectroscopy and Radiative Transfer*, 109(3):458–467.

Robert, D. and Bonamy, J. (1979). Short range force effects in semiclassical molecular line broadening calculations. *Journal de Physique*, 40(10):923–943.

Rosenkranz, P. (1988). Interference coefficients for overlapping oxygen lines in air. *Journal of Quantitative Spectroscopy and Radiative Transfer*, 39(4):287–297.

Rosenkranz, P. W. (1998). Water vapor microwave continuum absorption: A comparison of measurements and models. *Radio Science*, 33(4):919–928.

Rosenkranz, P. W. and Staelin, D. H. (1988). Polarized thermal microwave emission from oxygen in the mesosphere. *Radio Science*, 23(5):721–729.

Rothman, L., Barbe, A., Benner, D. C., Brown, L., Camy-Peyret, C., Carleer, M., Chance, K., Clerbaux, C., Dana, V., Devi, V. M., et al. (2003). The HITRAN molecular spectroscopic database: edition of 2000 including updates through 2001. *Journal of Quantitative Spectroscopy and Radiative Transfer*, 82(1-4):5–44.

Rothman, L. S. and Gordon, I. (2006). Steps for Converting Intensities from the JPL (or CDMS) Catalog to HITRAN Intensities.

Rothman, L. S., Gordon, I. E., Babikov, Y., Barbe, A., Benner, D. C., Bernath, P. F., Birk, M., Bizzocchi, L., Boudon, V., Brown, L. R., et al. (2013). The HITRAN2012 molecular spectroscopic database. *Journal of Quantitative Spectroscopy and Radiative Transfer*, 130:4–50.

Rothman, L. S., Jacquemart, D., Barbe, A., Benner, D. C., Birk, M., Brown, L., Carleer, M., Chackerian Jr, C., Chance, K., Coudert, L. e. a., et al. (2005). The HITRAN 2004 molecular spectroscopic database. *Journal of Quantitative Spectroscopy and Radiative Transfer*, 96(2):139–204.

Rubens, H. and Aschkinass, E. (1898). Observations on the absorption and emission of aqueous vapor and carbon dioxide in the infra-red spectrum. *The Astrophysical Journal*, 8:176.

Ryadov, V. Y. and Furashov, N. (1966). The width of the water vapor absorption line λ= 0.92 mm. *Radiophysics and Quantum Electronics*, 9(6):621–623.

Saunders, R., Hocking, J., Rundle, D., Rayer, P., Matricardi, M., Geer, A., Cristina, L., Brunel, P., and Vidot, J. (2013). RTTOV-11 science and validation report; EUMETSAT NWP SAF. Technical report, NWPSAF-MO-TV-32.

Saunders, R., Hocking, J., Turner, E., Rayer, P., Rundle, D., Brunel, P., Vidot, J., Roquet, P., Matricardi, M., Geer, A., et al. (2018). An update on the RTTOV fast radiative transfer model (currently at version 12). *Geoscientific Model Development*, 11(7):2717–2737.

Serov, E., Koshelev, M., Odintsova, T., Parshin, V., and Tretyakov, M. Y. (2014). Rotationally resolved water dimer spectra in atmospheric air and pure water vapour in the 188–258 GHz range. *Physical Chemistry Chemical Physics*, 16(47):26221–26233.

Serov, E., Odintsova, T., Tretyakov, M. Y., and Semenov, V. (2017). On the origin of the water vapor continuum absorption within rotational and fundamental vibrational bands. *Journal of Quantitative Spectroscopy and Radiative Transfer*, 193:1–12.

Shine, K. P., Ptashnik, I. V., and Rädel, G. (2012). The water vapour continuum: brief history and recent developments. *Surveys in Geophysics*, 33(3-4):535–555.

Slocum, D. M., Slingerland, E. J., Giles, R. H., and Goyette, T. M. (2013). Atmospheric absorption of terahertz radiation and water vapor continuum effects. *Journal of Quantitative Spectroscopy and Radiative Transfer*, 127:49–63.

Smith, M. (2001). Characterization of line broadening and shift parameters of ozone for spectroscopic databases. *56th International symposium on molecular spectroscopy, Ohio State University, June 11–15*, page Paper ME03.

Thomas, B., Brandt, M., Walber, A., Gibson, H., Philipp, M., Sonnabend, G., Benzazaa, M., Gonzalez, R., Bergada, M., Martinez, J., et al. (2014). Millimeter & sub-millimeter wave radiometer instruments for the next generation of polar orbiting meteorological satellites-MetOp-SG. In *Infrared, Millimeter, and Terahertz waves (IRMMW-THz), 2014 39th International Conference on*, pages 1–3. IEEE.

Tretyakov, M. Y., Koshelev, M., Dorovskikh, V., Makarov, D., and Rosenkranz, P. (2005). 60-GHz oxygen band: precise broadening and central frequencies of fine-structure lines, absolute absorption profile at atmospheric pressure, and revision of mixing coefficients. *Journal of Molecular Spectroscopy*, 231(1):1–14.

Tretyakov, M. Y., Serov, E., Koshelev, M., Parshin, V., and Krupnov, A. (2013). Water dimer rotationally resolved millimeter-wave spectrum observation at room temperature. *Physical Review Letters*, 110(9):093001.

Turner, D., Mlawer, E., Bianchini, G., Cadeddu, M., Crewell, S., Delamere, J., Knuteson, R., Maschwitz, G., Mlynczak, M., Paine, S., et al. (2012). Ground-based high spectral resolution observations of the entire terrestrial spectrum under extremely dry conditions. *Geophysical Research Letters*, 39(10).

Turner, D. D., Cadeddu, M. P., Lohnert, U., Crewell, S., and Vogelmann, A. M. (2009). Modifications to the water vapor continuum in the microwave suggested by ground-based 150-GHz observations. *IEEE Transactions on Geoscience and Remote Sensing*, 47(10):3326–3337.

Turner, E., Rayer, P., and Saunders, R. (2019). AMSUTRAN: A microwave transmittance code for satellite remote sensing. *Journal of Quantitative Spectroscopy and Radiative Transfer*.

Turner, E. C., Withington, S., Newnham, D. A., Wadhams, P., Jones, A. E., and Clancy, R. (2016). Simulation of submillimetre atmospheric spectra for characterising potential ground-based remote sensing observations. *Atmospheric Measurement Techniques*, 9(11):5461–5485.

Van Vleck, J. H. and Weisskopf, V. F. (1945). On the shape of collision-broadened lines. *Reviews of Modern Physics*, 17(2-3):227.

Wagner, G., Birk, M., Schreier, F., and Flaud, J.-M. (2002). Spectroscopic database for ozone in the fundamental spectral regions. *Journal of Geophysical Research: Atmospheres*, 107(D22):ACH–10.

Wang, D., Prigent, C., Aires, F., and Jimenez, C. (2017). A statistical retrieval of cloud parameters for the millimeter wave Ice Cloud Imager on board MetOp-SG. *IEEE Access*, 5:4057–4076.

Wentz, F. J. and Meissner, T. (2016). Atmospheric absorption model for dry air and water vapor at microwave frequencies below 100 GHz derived from spaceborne radiometer observations. *Radio Science*, 51(5):381–391.

Yang, Y., Mandehgar, M., and Grischkowsky, D. (2014). Determination of the water vapor continuum absorption by THz-TDS and Molecular Response Theory. *Optics Express*, 22(4):4388–4403.

Yu, S., Drouin, B. J., and Miller, C. E. (2014). High resolution spectral analysis of oxygen. IV. Energy levels, partition sums, band constants, RKR potentials, Franck-Condon factors involving the X 3 Σ g-, a 1Δ g and b 1 Σ g+ states. *The Journal of chemical physics*, 141(17):174302.

Zeeman, P. (1896). On the Influence of Magnetism on the Nature of the Light Emitted by a Substance (Part I). *Communications from the Physical Laboratory at the University of Leiden*, 33:1–8.